Title
The Science and Technology of Automatable Droplet Lipid Bilayer Platforms

Author
Portonovo, Shiva A.

Publication Date
2012

Peer reviewed|Thesis/dissertation

UNIVERSITY OF CALIFORNIA

Los Angeles

The Science and Technology of Automatable Droplet Lipid Bilayer Platforms

A dissertation submitted in partial satisfaction of the
requirements for the degree Doctor of Philosophy
in Biomedical Engineering

by

Shiva A. Portonovo

2012

ABSTRACT OF THE DISSERTATION

The Science and Technology of Automatable Droplet Lipid Bilayer Platforms

by

Shiva A. Portonovo

Doctor of Philosophy in Biomedical Engineering

University of California, Los Angeles, 2012

Professor Jacob J. Schmidt, Chair

Droplet lipid bilayers have been shown to be robust platforms for studying membrane proteins in a highly controlled environment. They are stable and can be formed using automated fluid handling techniques. Measuring membrane protein activity and compound transport through droplet lipid bilayers, however, is labor intensive, and most often requires technicians to manually insert electrodes into small volume droplets. This problem prevents droplet lipid bilayers from being employed in high-throughput measurement platforms. Solutions employing the integration of droplet lipid bilayer formation and measurement are developed in this work. Refinements allowing for simplified control over the size of droplet lipid bilayers for consistent measurements across arrays of bilayers formed in parallel are discussed. The development of a measurement chamber that allows for continuous solution perfusion of intact droplet lipid bilayers is also discussed. These new techniques for forming and measuring droplet lipid bilayers

are tested by measuring the drug dose-dependence of activity from ensembles of human ether-a-go-go related gene encoded ion channel (hERG) reconstituted into droplet lipid bilayers. Finally, an automated microfluidic platform allowing for the optical measurement of passive drug permeation through droplet lipid bilayers is developed and discussed. The methods produced in this work indicate that automated formation and measurement of droplet lipid bilayers is feasible. In doing so, they provide the potential to greatly expand the applications of artificial lipid bilayer research.

The dissertation of Shiva A. Portonovo is approved.

Dino DiCarlo

Harold G. Monbouquette

Giovanni Zocchi

Jacob J. Schmidt, Committee Chair

University of California, Los Angeles

2012

TABLE OF CONTENTS

List of Figures

List of Tables

List of Symbols and Abbreviations

α-HL: alpha-hemolysin
AchR: acetylcholine receptor
AD: acceptor droplet
Ag/AgCl: silver-silver chloride
$CaCl_2$: calcium cholride
CCD: charge coupled device
CM: contacting monolayer
CNC: computer numeric controlled
CO_2: carbon dioxide
DD: donor droplet
DI: deionized (water)
DMSO: dimethyl sulfoxide
DOPC: 1,2-dioleoyl-*sn*-glycro-3-phosphocholine
DPhPC: 1,2-diphytanoyl-*sn*-glycero-3-phosphocholine
EC_{50}: half maximal effective concentration
EDTA: ethylenediaminetetraacetic acid
EDM: electrical discharge machining
F: farad, the unit of electrical conductivity
FDA: food and drug administration
FITC: fluorescein isothiocyanate
G: giga, 10^9
gA: gramicidin A
G-codes: computer code used to program CNC motion
HEK(293): human embryonic kidney (293 indicates type of cell line)
HEPES: 4-(2-hydroxyethyl)-1-piperazineethanesulfonic acid
hERG: human *ether-a-go-go* related gene (encoded ion channel)
HT: high throughput
Hz: hertz, the unit of frequency
I: ionic current
IC_{50}: half maximal inhibitory concentration
k: kilo, 10^3
KCL: potassium cholride
L: liter
m: meter
M: molar
MB: measurement buffer
mm: millimeter

mV: millivolt
μ: micro, 10^{-6}
n: nano, 10^{-9}
Ω: ohm, the unit of electrical resistance
PAMPA: parallel artificial membrane permeability assay
PDMS: polydimethylsiloxane
PEEK: Polyether ether ketone
PTFE: Polytetrafluoroethylene
QT: interval between Q wave and T wave in electrocardiogram trace
S: Siemens, the unit of electrical conductance
SBS: society for biomolecular sciences
Tris·HCl: tris (hydroxymethyl) aminomethane hydrochloride
TRPM8: transient receptor potential cation channel, subfamily M member 8
UV: ultraviolet
V: volt, the unit of electric potential
VDAC: voltage-dependent anion channel
W: watt, the unit of power

Acknowledgments

I am sincerely grateful to my advisor Jake Schmidt. He first impressed me with his willingness to go out of the way to deliver clarity in his class lectures. He was always confident and optimistic in my ability to solve problems. He also convinced me that while engineers ought to be accountable for knowing details pertaining to their field of study, physicists ought to be accountable for knowing the details of everything. Or, at least everything important. He has a brilliant way of thinking about things. He also has a wonderful sense of humor. I have thoroughly enjoyed my time in his lab.

I thank Jason Poulos for taking me under his wing after I first joined the Schmidt lab. He taught me how to make artificial lipid bilayers and measure ion channel activity, which formed the basis for my PhD work. Above all, he was an extremely patient teacher. I never once saw Jason lose his cool. He was always patient and in good spirits. Above all, he has a can-do spirit and a willingness to try new things that really opened my eyes.

Takashi Nisissako has been a great teacher and a great friend. We collaborated on our work with studying drug permeation in droplet membranes. He has such a refined knowledge of his field, and a great commitment to our work. Routinely he would be at the lab until the very early morning hours. He was always so kind and helpful. I always felt guilty about going to dinner with him at restaurants… because he would always insist on paying the complete bill. I hope that I will become so generous someday.

Tae-Joon Jeon was a post-doc in the lab when I first joined and he became a professor in South Korea shortly after. Needless to say, I learned a lot about how to think of and conduct research from him. He also gave me much insight into the world of academia itself.

Jeff Abramson, professor of physiology, UCLA, was very kind and helpful to me from helping me to learn how to do Western Blots to providing me with purified VDAC ion channels for use in experiments. A former PhD student in his lab, Gabriel Mercado, also was very helpful in teaching me how to do Western Blots.

Noah Malmstadt, professor of Chemical Engineering, USC, was extremely helpful in my early days of research when I frequently visited his lab to do experiments with a specialized fluorescence microscope. He was a former member of the Schmidt lab, and he has added much to the knowledge of our lab.

Dino DiCarlo, professor of Bioengineering, UCLA was very helpful in allowing us to use the fluorescence microscopes in his lab. Some of our experiments took many hours to do, and we are so grateful for the opportunity that he gave us. Additionally I thank him for being on my PhD committee and giving me additional insight through questions about my research.

I would like to additionally thank Professor Harold Monbouquette and Professor Giovanni Zocchi, who also served on my PhD committee. They patiently and thoughtfully listened to me describe my research and asked me important questions that made me think more carefully about my work.

Tanuj Thapliyal was a former undergraduate student in the Schmidt lab who was very helpful to me in doing automated pin tool bilayer experiments. He was always very eager to learn and very patient. He was also so professional, at such a young age. I was very impressed by him.

Ahmad El-Arabi, also a former undergraduate in the Schmidt lab, was also extremely helpful and always full of energy to do difficult tasks. I'm grateful to him for many things, especially for his help in creating figures for papers and presentations.

Carl Salazar co-authored a paper with me, and I am really happy that I got the chance to work with him. He was always a fun person to be with.

Rob Tan was a PhD student in the Schmidt lab who finished at the same time as me. He was always willing to help me when I needed him. He also brought a lot of joy to the lab by insisting that we do fun activities and visit interesting places.

Of course, I must thank the current student members of the Schmidt lab: Bin Lu, Leyla Esfandiari, Shiv Acharya, Alex Portman, Gayane Kocharyan. They have been very supportive and helpful. I can always rely on them to lift my spirits.

My friends outside of the lab have been very helpful to me just by giving me the ability to enjoy life and to understand how people live outside of our lab. That sounds funny, but it really is true. I especially want to thank Brent Kramer, a friend since elementary school, for being like a brother to me; we both live far from where we grew up, and it's always fun to reminisce about times from our childhoods.

Above all, I must thank my family for the limitless amount of love, support, and valuable advice that they have always given to me. My father is the person that I admire most in the world. He gives me everything that he can possibly give to ensure my success and happiness. My mother has always sought the very best for me and has been a source of enormous comfort. My sister, Sheela, has been like a second mother to me— she also helped raise me, and she always has very good and thoughtful advice for me. My brother-in-law Dan has been so nice and wonderful to me; I am so happy that he is a part of our family. Their beautiful baby boy, my nephew Ravi, is so cute and I can't wait to lift him up high in my arms when I visit them again.

Vita

2002	B.S.Eng., Electrical Engineering University of Pennyslvania
2002	B.S.Econ., Finance University of Pennsylvania
2005	M.S., Electrical Engineering University of California, Los Angeles
2005-2007	Staff Research Assistant Department of Neurology University of California, Los Angeles
2011	M.S., Biomedical Engineering University of California, Los Angeles

Publications and Presentations

Portonovo, S., Salazar, C., and Schmidt, J., "hERG Drug Response Measured in Droplet Bilayers", 2012. (Under Review)

Nisisako, T., **Portonovo, S.,** and Schmidt, J., "Microfluidic Device for Determining Drug Permeation Through Lipid Membranes", 2012. (Manuscript in Preparation)

Portonovo, S., Nisisako, T., and Schmidt, J., "Microfluidic Droplet Membrane Blood Brain Barrier Permeability Assay", 2012, (Manuscript in Preparation)

Nisisako, T., **Portonovo, S.,** and Schmidt, J., Microfluidic Passive Permeability Assay Using Arrayed Droplet Interface Membranes., Invited oral presentation at MicroTAS 2012 conference October 28 – November 1, 2012; Okinawa, Japan.

Portonovo, S., and Schmidt, J., "Masking Apertures Enabling Automation and Solution Exchange in Sessile Droplet Lipid Bilayers", *Biomed Microdevices*, 2012, 14, 187-191.

Poulos, J., **Portonovo, S.,** Bang, H., and Schmidt, J., "Automatable lipid bilayer formation and ion channelmeasurement using sessile droplets", *Journal of Physics: Condensed Matter*, 2010, 22, 454105 (6 pp).

Mostany, R., Chowdhury, T.G., Johnston, D., **Portonovo, S.,** Carmichael, S.T., and Portera-Cailliau, C., "Local hemodynamics dictate long-term dendritic plasticity in peri-infarct cortex", *J. Neurosci*., 2010, 30(42), 14116-26.

Nisisako, T., **Portonovo, S.,** and Schmidt, J., "Chemical Permeation Assay Using Droplet Membranes", Invention Disclosure filed, UCLA Case No. 2012-388, filed 12/19/2011

Portonovo, S., and Schmidt, J., "Masking Apertures Enabling Automation And Solution Exchange In Sessile Droplet Lipid Bilayers", U.S. Provisional Application Serial No. 61/543,771, filed 10/05/2011

Portonovo, S., Salazar, C., and Schmidt, J., "Solution Exchange in Sessile Droplet Lipid Bilayers for IC50 measurements of hERG", 2012, Biophysical Society, 56th Annual meeting, San Diego, CA. (Poster presentation).

Portonovo, S., and Yablonovitch, E., "High-speed Optical Code Division Multiple Access (OCDMA) Communication Network", 2004, UCLA Annual Research Review, Los Angeles, CA (Poster Presentation)

Portonovo, S., "Components of a CMOS Imager for a Polarization Difference Imaging Camera,",*NSF Summer Undergraduate Fellowship in Sensor Technologies*. http://www.seas.upenn.edu/sunfest/docs/papers/PortonovoShiva.pdf. (46 pp), 2000, Advisors: Jan Van der Spiegel and Nader Engheta

Introduction

Ion channels embedded in cell membranes play important roles in a wide range of physiological processes[1-7]. A better understanding of how ion channels work and how they may respond to various stimuli, including drugs, is key to the development of accurate models of cellular activity, as well as the diagnosing of disorders. Membrane proteins account for approximately 20-30% of deciphered functional code from the human genome, and genes encoding over 300 ion channel proteins have been identified[8,9]. Many diseases, such as cystic fibrosis and epilepsy, have been tied to ion channel disorders[10-12]. Of the top 100 selling drugs, 15 are modulators of ion channels having a market value of over $15 billion[13]. Adverse effects from drug interactions on ion channels have been implicated in numerous recalls of commercial drugs, and screening for such effects is greatly important in the processes of new drug discovery and drug safety testing. One particular example concerns FDA guidelines specifying the testing of all new systemic drugs for QT-elongation: a disorder which causes conditions such as cardiac arrhythmias, and has been linked with adverse drug interactions on the human ether-a-go-go related gene (hERG) encoded ion channel[14-16]. The cost of developing new drug compounds can often exceed $1 billion and can take more than 10 years[17]. Platforms enabling the high-throughput study of ion channel behavior in the presence of large numbers of compounds could give researchers powerful tools in creating a better understanding of how ion channels work and how they may respond when stimulated under various conditions. It is evident that a better understanding of how ion channels work carries great scientific, medical, and economic importance.

Technologies that currently allow for the high throughput study of soluble proteins are well established and are commonly used in academic studies as well as commercial pharmaceutical research. Ion channels are typically not compatible with such high throughput

assays due to their insolubility; ion channels are embedded in amphiphilic membranes and have hydrophobic surfaces that are exposed to membrane interiors. Additionally, it is the general functional behavior of ion channels and their responses to stimuli that is often the focus of research, and this is typically possible to study only when the channels are embedded within lipid membranes[18]. Few technologies designed for high-throughput study currently exist in which the activity of ion channels can be actively probed and measured.

In this report, I discuss the development of technologies that promote lipid bilayer studies for practical applications. Work from our group resulted in the demonstration of the automated formation of freestanding planar lipid bilayers using high-throughput fluid handling techniques; we successfully produced over 700 planar lipid bilayers per hour[19]. Additionally, we used standard fluid handling robotics commonly used in standard high throughput drug screens. We have also developed automated methods to measure the activity of ion channels in planar lipid bilayers, and have successfully measured the activity of bacterial ion channels such as alpha-hemolysin and gramicidin A[20]. Here, I discuss my work in combining the automated formation of lipid bilayers with automated measurement of ion channel activity from reconstituted ion channels using methods compatible with high throughput screening technologies. I also describe my efforts to expand upon my group's work by reconstituting physiologically relevant voltage-gated ion channels into the automatable platforms that I developed. Further, I discuss my efforts to increase throughput of studies on lipid bilayer membranes through the development of higher fluid exchange rate methods, which may be useful in ion channel drug studies. Finally I describe an automatable microfluidic assay that I have helped to develop which uses droplet lipid membranes between nanodroplets to achieve fast and accurate results for studying the lipid membrane permeability of drug compounds.

Main Current Methods of Functional Ion Channel Studies

Optical Assays

Optical assays are commonly used to detect cell membrane electric potentials and ion fluxes from ion channels in whole cells using optical indicators. These assays are generally amenable to high throughput data collection, and can sometimes share instrumentation with optical assays used in studies of soluble proteins[13]. Major drawbacks of current optical assay technologies include low temporal resolution and problems with loading dyes into cells. An additional drawback is the inability to optically maintain the cell membranes at voltage clamped conditions. Altering transmembrane potentials may often rely on chemically changing the bath solution, which requires additional time and complexity. Optical indicators that fluoresce due to changes in intracellular ion concentrations usually cannot distinguish between ion influxes through ion channels and ion release from intracellular storage sites, especially if the indicators localize in particular areas of the cell. Optical indicators may also be highly pH sensitive, susceptible to photobleaching, and may not be readily available for all ions of interest. Finally, differences among cell sizes and internal properties within a sample well may result in different background fluorescence among cells which can obscure signals produced from ion channel flux from any particular cell[13]. While recent developments have been promising, the accurate optical measurement of ion channels remains challenging and must overcome these serious obstacles before it can become a standard way to conduct high throughput studies of ion channel behavior.

Manual Patch Clamp

The patch clamp method is the most widely used method to study ion channel activity[21]. It can be employed to study both single channel ion behavior in detached cell patches and intact patches of live cells. It can also be used to study ensemble behavior of ion channels spanning the

outer membrane of an entire cell[22,23]. Various techniques have been employed in which researchers can access both the outer and inner leaflet of the cell membrane containing ion channels of interest. Ion currents below 1 picoamp can be measured at recording bandwidths greater than 10 gHz[24]. These are among the major reasons why the patch clamp method is unparalleled in its precision for the study of ion channel activity. The major tradeoff that researchers must make when using the traditional patch clamp method is that they must do so by patching on to a single cell at a time, which is a low throughput process. Additionally, the method itself is labor intensive. It requires glass pipettes to be heated, pulled, and fractured to yield pipette openings that can be as small as a few microns in diameter. The tips must be made smooth to avoid problems with sealing the glass pipette tip with a cell membrane. The pipette itself needs to be carefully positioned with a microscope and micromanipulators. A light vacuum must be applied to seal the pipette tip with the cell membrane, and resistances of at least 1gΩ between the inner pipette solution and the bath solution must first be obtained before accurate measurements of ion channel currents and precise voltage clamping of the cell membrane is possible. These requirements taken together make manual patch clamp impractical for carrying out large scale functional screens of ion channels against compounds such as potential drug candidates and drug combinations in an economic fashion.

Automated Patch Clamp

Efforts to increase the throughput of ion channel measurements using electrical recordings have led to the development of automated systems in which live cells in suspension are positioned over patch-size apertures, and suction is applied to form gigaseal patches similar to those produced in the manual patch clamp method. These systems are capable of parallel measurements taken from many cells simultaneously, typically in the whole cell patch

configuration[25]. While advances in these automated systems in the past few years have been impressive, the throughput of tests on functional ion channel activity still remains below what is needed to achieve high throughput screens. Tests of 10,000-30,000 compounds per day are not atypical in labs that conduct high throughput drug screens; a typical automated patch clamp system can successfully test 100s of compounds per day, while the latest systems can theoretically test several thousands of compounds per day. The success rates of forming gigaseals with patches of cells in the latest generation of such systems can be as low as 50%[26]. While the cost of obtaining data from a single cell using conventional manual patch clamp technology may be about $1 per cell, the cost of obtaining the same type of data in an automated patch clamp system may be about $5-$10 per cell[27]. The high cost of obtaining data from automated patch clamp systems and the need for even greater experimental throughput necessitates the consideration of alternative technologies for conducting high throughput studies on ion channels.

Ion Channel Studies in Artificial Lipid Bilayer Membranes

For the past 40 years, scientists have been investigating the functional behavior of ion channels by harvesting them from live cells and reconstituting them into artificial lipid bilayer membranes[28,29]. This enables ion channel studies in environments that are free of the potentially complicating cell machinery that is present in whole cells used in patch clamp studies. The environment surrounding the ion channels is controllable by the researcher, as the components and physical properties of the membrane into which the ion channels are reconstituted can be tailored as desired. Traditionally, forming freestanding artificial lipid bilayers has involved dissolving lipid molecules into an organic solvent, and spreading the mixture over a thin hydrophobic film containing a small aperture[30]. The film itself is set in a chamber surrounded

by aqueous electrolyte solutions which are electrically isolated from each other beyond the aperture of the film.

Soon after spreading the lipid containing organic solution over the aperture, self-assembly of a lipid bilayer having a thickness of a few nanometers will form. Ion channels can typically be reconstituted into such a membrane by first incorporating them into liposomes, and then inserting these ion-channel containing vesicles into the aqueous electrolytes on either side of the lipid bilayer[32]. Fusion of the vesicles with the bilayer results in the ion channels being incorporated into the lipid bilayer, after which functional tests on the ion channels can be carried out. Electrodes similar to those used in traditional patch clamp studies can be inserted on both sides of the bilayer. They allow for voltage clamping of the bilayer and recording of ion channel currents. Electrical measurements of ion channel activity are directly comparable to those obtained in patch clamp studies. Artificial lipid bilayers have been used to study ion channel activity in many physiologically relevant ion channels and have been used as tools in the process of drug discovery[33-36].

Traditional formation of artificial lipid bilayer membranes is a low-throughput process that requires the skills of a trained technician. Furthermore, like manual patch clamp, studies on ion channels embedded in a single membrane can only be carried out in one experiment at a time. Currently there are no widely commercially available systems that allow for automated formation of artificial lipid bilayers and testing of ion channels incorporated within, and research on parallel arrays of artificial lipid bilayers is still in its early stages[37,38].

Our lab investigates new methods of forming artificial lipid bilayer membranes and reconstituting ion channels in ways that can be scalable to high throughput experimental techniques[19,20]. The particular method that is the focus of my research involves contacting lipid

monolayers that form when lipids situated at the interfaces of two separate aqueous droplet solutions with the same organic solution are mechanically brought into contact. The lipids in each monolayer interact and self-assembly of lipid bilayers occurs.

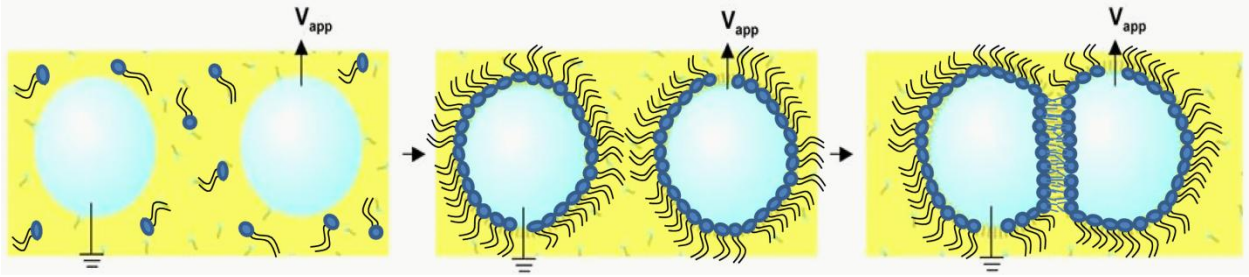

Figure 1-1: Monolayer contacting method for lipid bilayer membrane formation. Two aqueous droplets are submerged in a bath of organic solution containing dissolved lipid. A lipid monolayer forms around each droplet and a bilayer forms when these droplets are brought into contact[39].

The contacting monolayer technique for forming artificial lipid bilayers, first developed by Funakoshi et al.[39], has been shown to create stable bilayers that can exist for weeks[40]. Ion channel activity in such membranes have been measured by several groups including ours[38-41]. Major drawbacks in such measurements have been the lack of automation in forming the bilayers, and an inability to measure activity from ion channels in separate membranes simultaneously. Additionally, automatable lipid bilayer formation and measurement holds promise into advancing the study of passive drug permeation through lipid membranes. High-throughput experimentation in lipid bilayer research will require solutions to the current drawbacks. I discuss some feasible solutions to these problems in this work.

Automatable lipid bilayer formation and ion channel measurement using sessile droplets

Artificial lipid bilayers are widely used for scientific and sensing research involving ion channels because of their ease of use and ability to access and control the surrounding solution. However, practical applications of artificial lipid bilayers have been limited in part by their need to be formed individually and manually at the time and place of use. Recent work by our group and others has aimed to address these shortcomings through parallelizing and automating bilayer formation and measurement[42-49].

A high degree of automation and throughput in lipid bilayer formation was achieved by combining a contacting monolayer method of bilayer formation[50-52] with parallel fluid handling robotics[47]. Although the throughput of bilayer formation was high in that work (> 700 bilayers/hr), measurements were not high throughput because electrode positioning was manual and required a micromanipulator.

Here we report further development of this platform in which the measurement electrodes are fully integrated into the bilayer formation process. It operates similarly to other implementations of the contacting monolayer method, in which aqueous or hydrogel droplets directly contact AgCl electrodes[43,52-55], but unlike the manual production and placement of the droplets in that work, the production of the droplet in our work is achieved with automation compatible devices. For this we explored the use of pin tools, which are well established for automated, high throughput solution deposition in the preparation of microarray plates[56]. Here we describe the integrated production and measurement of artificial lipid bilayer membranes using pin tools, and the automation of the entire process using a motion control platform. We

first demonstrated the applicability of bilayer formation and measurement using pin tools in single measurement well experiments; position was done manually with micromanipulators. Next, a pin tool array was constructed, whereby 8 pin tool electrodes were employed in order to make parallel lipid bilayers in 8 separate measurement wells. Motion control in this multi-well measurement system was automated. By fully automating and integrating bilayer production and electrical measurement, we made progress toward practical applications utilizing artificial lipid membranes.

Experimentation

Microwell Plate for Bilayer Formation

Solutions for lipid bilayer formation and measurement were placed in standard hydrophobic 384-well plates (Fisher Scientific). These wells were modified by drilling a 500 μm hole in the bottom of each well and inserting a 200 μm silver wire (Ted Pella) through the hole and sealing it with Dow Corning 732 sealant. The silver wire was activated by placing 70 μL of Clorox bleach into the well for approximately 1 minute and thoroughly rinsing the well with DI water. While pin tools and pin tool arrays are compatible with plates of various sizes, the 384-well plate was chosen due to its frequent use in high throughput protein assays and compatibility with multichannel robotic pipettes. Aqueous solutions placed in the hydrophobic wells produced convex menisci; this allowed for easier control over positioning of the upper aqueous droplets and minimization of the size of the contact area and lipid bilayers formed using the pin tool system described below. Although bilayers could also be formed in hydrophilic wells, such wells produced concave menisci, and control of the sessile droplet position and bilayer area was experimentally found to be more difficult.

In preparation for artificial bilayer formation, 80 μL of an aqueous measurement buffer MB (1 M KCl, 10 mMTris-HCl, 1 mM EDTA at pH 8.0) was first deposited into a sample well and 30 μL of MB was added to a measurement well. Next, 40 μL of a solution of 5% (w/v) 1,2-diphytanoyl-*sn*-glycero-3-phosphatidylcholine (DPhPC) (Avanti Polar Lipids) in n-decane (MP Biomedicals), was pipetted directly on top of the MB solution, on which it floated, forming a lipid monolayer[43,47,54,55]

Lipid Bilayer Formation Using Pin Tools (Single Well)

Ag/AgCl pins were fabricated from 16 gauge silver wire (.999 purity, C.C. Silver & Gold). The pins were cut to approximately 1 inch and electrical discharge machining was used to create a blunt tip end and cut slots .05 inches long and .015 inches wide into the ends of the pins. Prior to use, all of the silver pins were immersed in bleach for approximately 1 minute to chloridize their surfaces, followed by a thorough rinse in DI water.

Bilayer formation with a silver pin was accomplished using the same measurement and sample well solutions described above, except that the aqueous solutions in the measurement and sample well contained liposomes made from DPhPC. The liposomes were made by dissolving 5mg of DPhPC in 1 mL of chloroform (Sigma) and subsequently evaporating the chloroform under vacuum for 3 hours. 2.5 mL of MB was added to this solution and vortexed for 10 seconds, followed by 5 freeze/thaw cycles. This resulting solution was then extruded through a 100nm hydrophilic syringe filter[57] to form ~100 nm diameter liposomes and stored at 4°C.

To acquire a droplet, the chloridized pin was lowered into the sample well to a depth of approximately 10mm for 1 second and removed. This resulted in a small ≈1.1 μL droplet hanging from the end of the pin. This procedure is similar to that used in systems that employ pin tools for fluid transfer[56]. To form a bilayer, the pin and droplet were lowered into the solution in

the measurement well. After waiting approximately 1 minute for lipid monolayer formation, the pin was lowered further using a micromanipulator until the droplet contacted the lower aqueous phase (Figure 2-1). Monomers of the gramicidin A dimer ion channel were dissolved into the aqueous solution to a final concentration of 1pg/mL for single channel measurements.

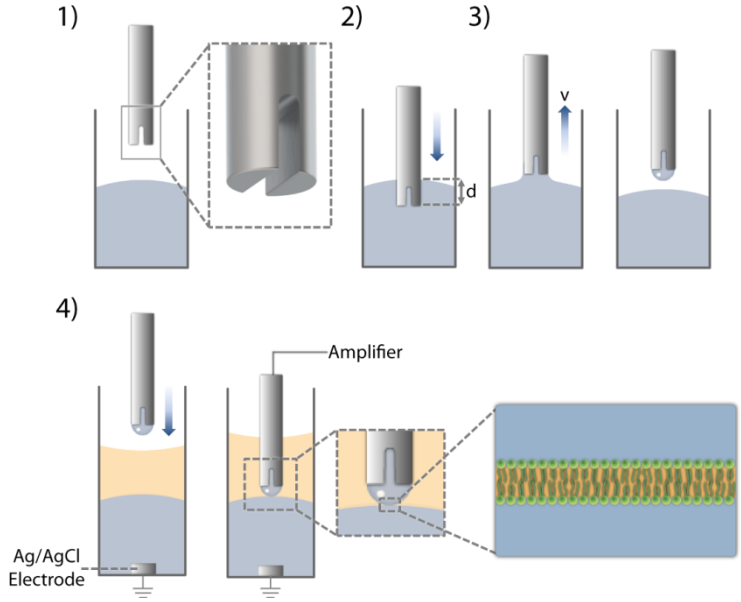

Figure 2-1 Schematic of bilayer formation using pin tools. Bilayer formation using the pin tool begins with the pin initially positioned above a sample well (1) and then is lowered into the sample well to a depth, d (2), and then retracted at a velocity, v (3). After removing the pin from the sample well a small droplet of aqueous solution hangs off the tip of the pin (3) and is moved to the measurement well (4) where the pin is then lowered through the organic phase and a monolayer is allowed to form for 5 minutes. The pin is further lowered after this time until it contacts the lower aqueous phase where a bilayer forms (4).

Automated Lipid Bilayer Formation using Pin Tools (Multi-well)

An array of eight pin tools, described above, was constructed by placing eight individual pins into a custom-machined aluminum mounting unit. Copper wires were soldered to the top of each pin to establish electrical connections. An additional array of eight 14-gauge silver wire electrodes was positioned across from the array of pins in such manner that each pin was paired with each electrode. The electrodes were electrically tied together and held at ground potential. The pin wire connections were each screwed into an individual channel of an 8-channel amplifier

head of a 48-channel electrical amplifier (Tecella).The pin-array mounting unit was attached to a vertical (Z) axis motion stage plate of a computer numeric controlled (CNC) machine (MAXNC). This allowed the array of eight pins to be lowered and raised in automated fashion. The lipid bilayer chambers employed in the automated pin tool experiments employed hydrophobic partitions, described in further detail in chapter 2. Briefly, each chamber consisted of bottom wells that were loaded with 300 μL ofaqueous electrolyte solution and dissolved DphPC liposomes, while the top wells were were loaded with an organic solvent such as n-decane (Sigma). The wells were patterned into 1/8" thick flat acrylic plates (McMaster Carr) by laser cutting (Universal Laser Systems) according to premade designs. A thin (0.003") hydrophobic Delrin film (McMaster Carr) was sandwiched by the top well and bottom well plates. Circular apertures roughly 200-250 μm in diameter were cut into the films with the laser cutter, and the films were positioned such that the bottom well aqueous fluid and the top well organic fluid came into contact only through the aperture in the hydrophobic film. As explained in chapter two, this bilayer chamber configuration led to the formation of stable lipid bilayers of well-defined size. Multi-well bilayer array plates consisting of as many as 48 separate, independent bilayer chambers were constructed for the automated pin tool array experiments. A single multi-well bilayer array plate was placed into a quadrant of a rectangular acrylic template which was fixed onto the lateral (XY) axis motion stage plate of the CNC. The other quadrants of the template included a multi-well plate filled with acidic wash solution for cleaning the pin tool array after successive experiments (multi-well cleaning plate), a blotting sheet (Bio-Rad) for drying the pintool array after successive washes, and a hydrophopic droplet mount. The hydrophobic droplet mount permitted the presentation of 1 μL -2 μL aqueous droplets with dissolved DphPC liposomes in such manner that the pin tool array could be lowered directly above the droplet

mount and subsequently raised, which would allow the automated transfer of the droplets onto the pins. While the droplets were pipetted onto the hydrophobic droplet mount by hand, by design it employs 96-well SBS standard spacing, which makes it compatible with dropletdispensation from a fluid handling robot. The automated pin tool array experiments were separated into steps as follows:

Step 1: Position pin tool array above hydrophobic droplet mount; transfer droplets to ends of pins by lowering and raising pin tool array to the surface of hydrophobic droplet mount

Step 2: Position pin tool array loaded with sessile droplets above multi-well bilayer array plate, which has been pre-loaded with lower compartment aqueous liposome solution and top well organic solution; lower pin tool array such that sessile droplets come into contact with the organic solution present in the top wells. Ground Ag/AgCl electrodes, which are attached to the pin tool array (but electrically isolated from the pin tools except through the amplifier circuit), enter the loading inlet of the lower compartment inlet wells of the multi-well bilayer array plate. Soon afterward (allowing at least 1 minute to establish lipid monolayer formation at the aqueous/organic interfaces) the pin tool array is further lowered such that the sessile droplets come into contact with the hydrophobic films separating the top and bottom fluid wells; bilayers are formed on contact of lipid monolayers surrounding the sessile droplets and the aqueous/organic interface present within the circular apertures cut into the hydrophobic films.

Step 3: Record electrical measurements of bilayers and any reconstituted ion channels. Voltage protocols preprogrammed into the 48-channel Tecella amplifier software was used for performing measurements.

Step 4: After measurements are made, raise pin tool array out of multi-well bilayer array plate, position above multi-well cleaning plate, lower pins and ground electrodes into cleaning

solution. Allow pins and ground electrodes to soak in acidic cleaning solution (V&P Scientific) for at least 1 minute, after which pin array is raised, and moved over adjacent wells in the same multi-well cleaning plate loaded with DI water. Pins were allowed to soak in water for at least 1 minute.

Step 5: Raise pin tool array out of multi-well cleaning plate, position pin tool array over blotting paper, gently lower pin tool array into contact with blotting paper; raise and lower pin tool array 3 times to gently "tap" pins and ground electrodes onto blotting paper allowing adequate drying of the tips. This concludes the cleaning step, after which pin tool array is ready for another experiment cycle.

Programming of the CNC to carry out each of the motions involved in performing the experiment steps were done in G-code. A graphical user interface written using MaxIII Controller Software (MAXNC) allowed for simple motion adjustments when needed, as well as easy execution. All of the motion steps were performed in automated succession using a single execution command. Amplifier recordings required the experimentalist to run the Tecella 48-channel amplifier user software while the pin tool array was submerged in the multi-well bilayer array plate, as discussed in Step 3 above.

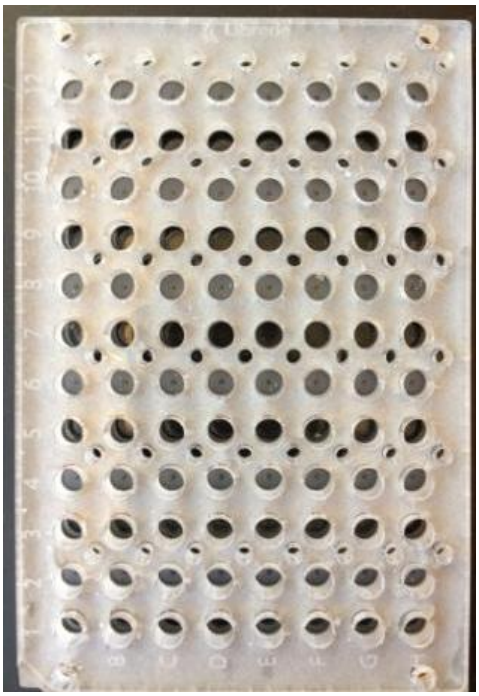

Figure 2-2 Top view of a multi-well bilayer array plate. The hydrophobic Delrin partitions can be seen in wells that will be loaded with organic solution; sessile droplets on pin tools are loaded into these wells; Aqueous wells contain a channel which flows directly underneath the organic solution wells; electrolyte solution is loaded into these wells through inlets located adjacent to the organic wells

1) 2)

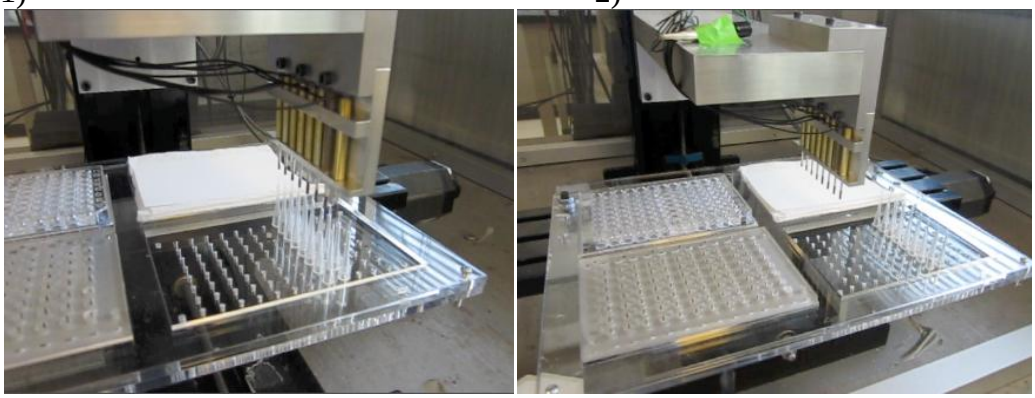

3) 4)

5) 6)

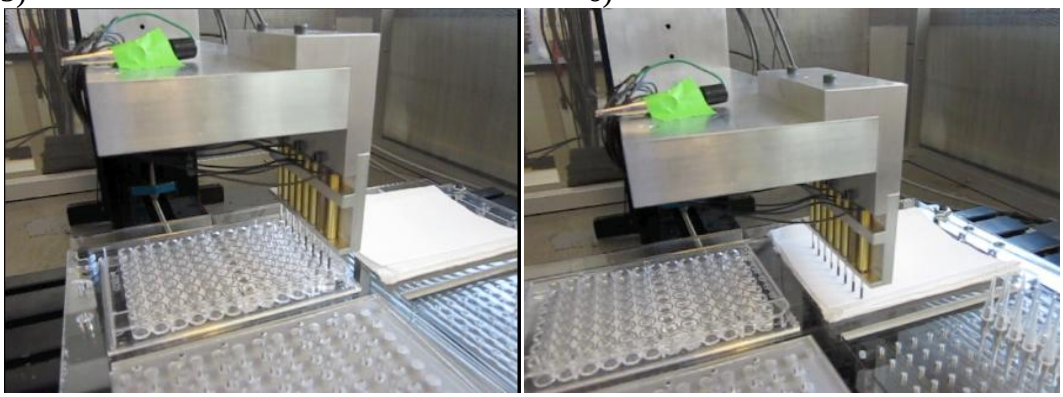

Figure 2-3 Automated pin tool array experiment steps. 1) Pin tool array is positioned over hydrophobic droplet mount, lowered and raised to deposit liposome-containing aqueous electrolyte droplets onto the ends of the pins. 2) Pin tool array is positioned over multi-well bilayer array plate. and initially lowered into the wells only about 2mm and held in place for at least 1 min to produce lipid monolayers around droplets. 3) Pins are lowered further into contact with hydrophobic partitions; amplifier recordings are made 4) Pins are raised out of bilayer chambers and moved to cleaning plate, where they are submerged in acid wash solutions, followed by DI water. 5) Pins are moved to blotting paper, where they are dried and made ready for next experiment cycle.

Electrical Recordings

Bilayers that were formed with pin tools were measured inside of a standard Faraday cage on a vibration isolation table. Single experiment well electrical measurements of bilayers and ion channels were made by connecting the Ag/AgCl electrode at the bottom of the measurement well (ground) and pin tool electrode to an Axopatch 200B amplifier (Axon Instruments), which was used to apply a transmembrane potential and measure the resultant ionic current. The signals were digitized with a Digidata 1332A (Axon Instruments) and analyzed with Clampfit software (Axon Instruments). Sampling was done at 5kHz.Multi-well experiments were conducted by connecting measurement well and pin tool electrodes to an 8-channel amplifier head of a Tecella 48-channel amplifier. Sampling with the Tecella amplifier was done at 20kHz.

Results

When an aqueous solution is placed in contact with an organic solution and either of these solutions contains lipids, the lipids will self-assemble at the aqueous/organic interface, forming a monolayer. Formation of a lipid bilayer is possible if two of these monolayers are mechanically brought into contact. In both of the systems presented here, 1-5 minutes was required for monolayer formation. Liposomes were present in the aqueous phase, and the monolayer stabilization time was only one minute[58]. If the droplets were made to contact the lower aqueous phase prior to the monolayer stabilization periods using either system, then the two aqueous phases would fuse shortly after being placed into contact. However, with properly formed monolayers, bilayers resulted with lifetimes of at least several hours.

In the single well experiments, bilayer formation was monitored by measuring the capacitive current resulting from an applied 8 Hz 20 mV (p-p) triangle wave. Bilayer formation

could also be monitored visually and verified electrically. In some cases a microscope was used to determine when the droplet interfaces touch (Figure 2-4a), after which the electrical behavior of the bilayer system could be monitored electrically. Initially, the capacitance started low and gradually grew and stabilized at a higher value, signifying bilayer formation. The final capacitance value could be controlled by changing the droplet contact area through adjustment of the pin heights (typically ranging from 150 pF to 600 pF). In general, bilayers containing no ion channels were observed to have resistances of at least 1gigaohm. Bilayers formed in both systems were able to support single channel measurements of gramicidin A (Figure 2-4b) and alpha-hemolysin (data not shown) with application of 100 mV holding potentials. After bilayer formation channel incorporation occurred spontaneously, it was observed that the time between the first insertion event and initial bilayer formation depended on protein concentration and bilayer area. In all cases when a bilayer formed in the presence of gramicidin A or alpha-hemolysin, protein activity was observed.

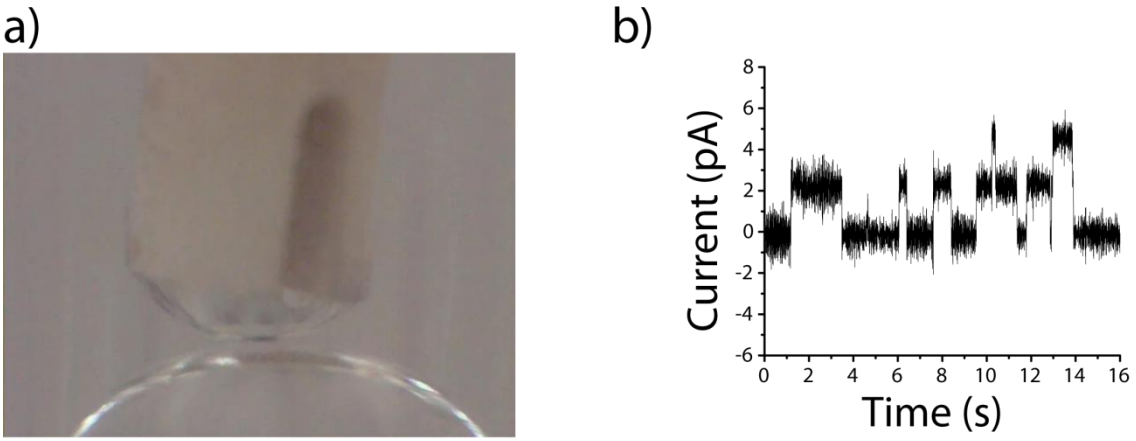

Figure 2-4 Formation and measurement of lipid bilayers formed with a pin tool. (a) microscope image of a sessile droplet formed with a silver slotted pin tool, contacting the lower aqueous phase, forming a bilayer. (b) Measurement of activity of gramicidin A ion channels

Bilayer area can be controlled in several ways. The first is to use a larger hanging droplet produced by increasing the droplet fluid volume that is either pipetted directly onto a pin tool in single well measurements or depositing larger droplets onto the hydrophobic droplet mounts used in multi-well experiments. Alternatively, the size of the droplets can be increased by increasing the depth to which the pin is immersed in a fluid sample well and/or by increasing the velocity of pin withdrawal from the sample well. Finally, bilayer area can also be controlled by modulating the vertical position of the hanging droplets in both systems relative to the lower aqueous/organic phase interface[53]. By lowering the hanging droplet into the lower aqueous phases without hydrophobic partitions to control bilayer areas, the droplets would deform and the areas of the bilayers would grow causing an increase in capacitance (Figure 2-5).

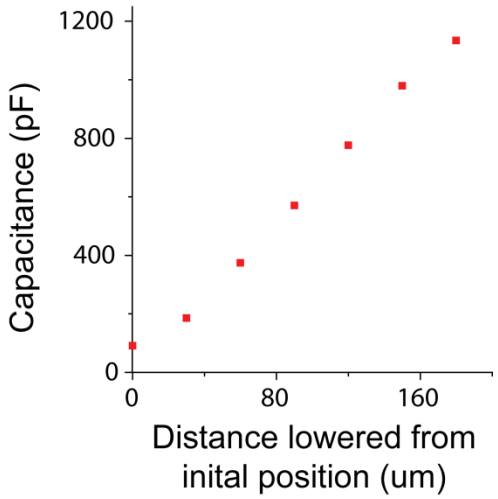

Figure 2-5 Changing the bilayer area by lowering the hanging droplet onto the lower aqueous phase. As the droplet comes into contact with the lower phase, both surfaces deform increasing the area of the bilayer. This increase in area can be measured by monitoring the capacitance of the system.

In the automated, multi-well experiments, bilayers were observed by monitoring capacitance traces after a 12.5 Hz, +/-10 mV (20 mV peak-to-peak) magnitude triangle wave was applied between each pin and ground electrode pair. Typically a 75% bilayer formation yield was observed, meaning bilayers were successfully formed in 6 out of 8 bilayer chambers. A

representative screen capture taken from the Tecella 48-channel amplifier control software is depicted in figure 6. It indicates signal (electrical current) traces from 8 bilayer chambers on a multiwell bilayer array plate. One of the traces is at background level, which occurred when no bilayer formed in that chamber. The other traces exhibited signal levels that are consistent with successful bilayer formation (confirmed previously by the presence of ion channels such as alpha-hemolysin). The background capacitance level is about 110-120 pF.The bilayer capacitances are calculated simply by dividing the current levels that are recorded at the zero-volt crossing of the applied triangle voltage wave by $\frac{dV}{dt}$, which was equal to 4.0 V/sec. The capacitances of the bilayers depicted in the figure, when background capacitance is subtracted, had values ranging from about 120-200 pF. The expected capacitance for a 250 μm diameter planar lipid bilayer, excited by the same triangle wave, is calculated to be 191.2 pF (using a dielectric constant of 2.2 to model the hydrophobic region within the bilayer and a circular area approximation). Calculation of this bilayer diameter size was calculated using the following formula, which applies to parallel plate capacitors:

$$\text{Bilayer diameter} = 2 * \sqrt{\frac{C*d}{\varepsilon_0*\varepsilon_r*\pi}}$$

Where C is the bilayer capacitance, ε_0 is the permittivity of free space, ε_r is the dielectric constant of the organic solution, and d is the thickness of the bilayer, taken to be 5nm. The bilayer traces indicate that the sizes of the lipid bilayers in the multi-well bilayer plate are roughly defined by the sizes of the circular apertures cut into the hydrophobic partitions that separate the upper and lower chamber wells. Data for bilayer size tended to be consistent across experiment cycles.

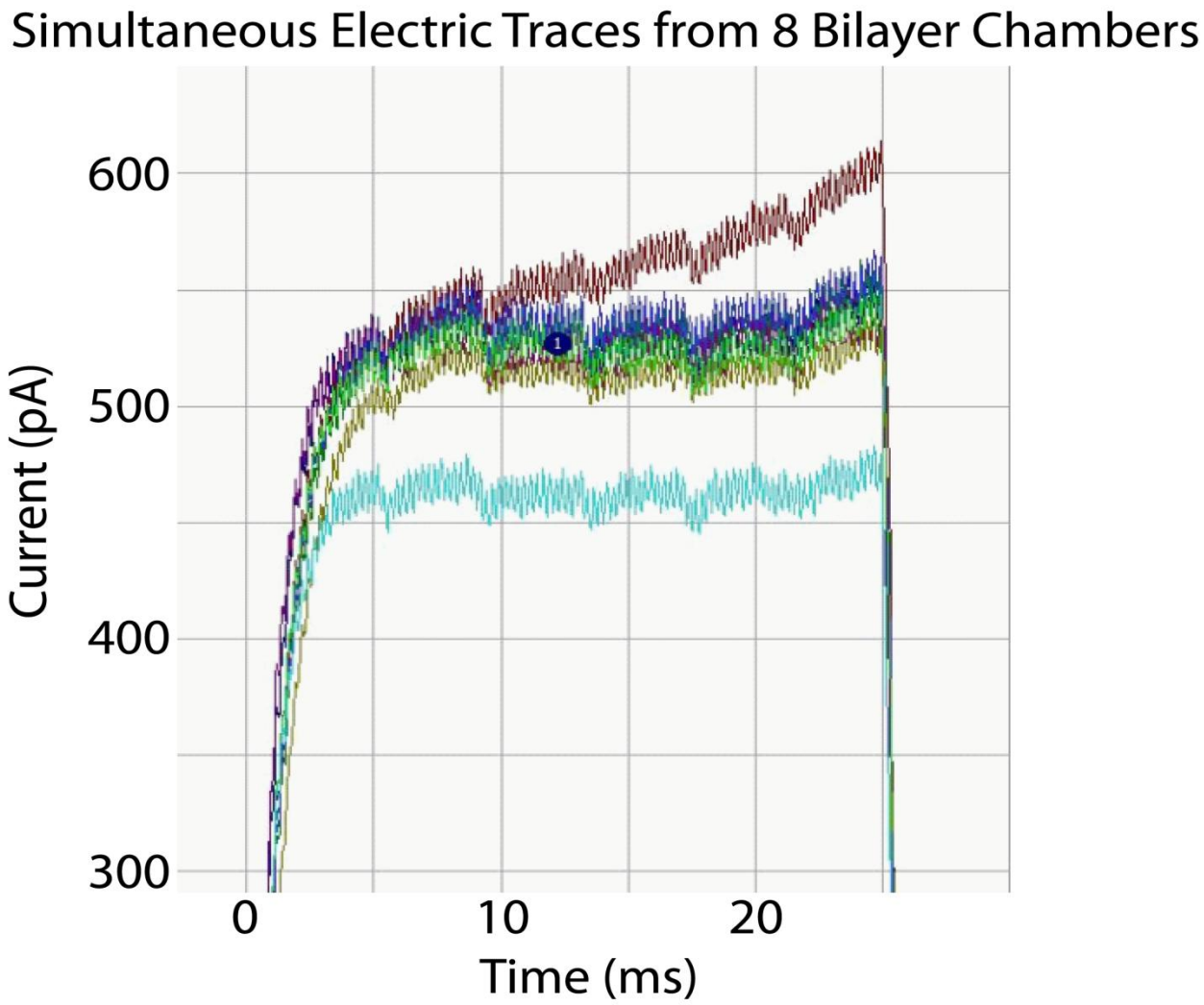

Figure 2-6 Capacitance traces of droplet lipid bilayers formed from automated pin tool array. Traces from 8 pins indicated that all but one (teal shaded trace) successfully formed a lipid bilayer, determined from previous measurements. The bilayers exhibited capacitances between 120-200pF, which was generally the case in these experiments. One of the bilayers (reddish brown trace) appeared less resistive than the others, as indicated by its sloped appearance. Variation in bilayer resistance levels was found to commonly occur across experiments.

Discussion

Previous work describing bilayer formation by contacting monolayers[43,51,52,54,57,59] utilized manual preparations for droplet formation and manipulation of the electrode and the droplet. Previously, work in our lab described an automated, gravity-ordered implementation of this method compatible with high throughput fluid handling systems, but without integrated measurement hardware[47].

Here we extend on that capability in our system, maintaining the automatable initial processes (dispensing of the lower aqueous and solvent phases), but integrating the production and manipulation of the upper aqueous phase with measurement electrodes also compatible with automatable robotic platforms. This is enabled by the use of pin tools to acquire and present a sessile droplet as the upper aqueous phase. In addition to automation, since protocols for washing and reusing pin tools are well established[56], these platforms are also compatible with high throughput systems. Both of these systems used the robust contacting monolayer method for bilayer formation, which formed bilayers in the majority of the cases after contacting the two monolayers. The most important step in assuring bilayer formation is waiting for a monolayer to form at the aqueous/organic interface. After this time the droplets are mechanically placed together. The mechanical movements do not need to be precise and bilayers will form over a wide range of heights. The different height positions will create bilayers with different areas which can be confirmed visually and electrically. In the pin tool system, the mechanical motion of the pin acquires and presents the sessile droplet. The size of the droplet hanging from the pin is dependent on the surface tension of the droplet with the pin material, as well as from mechanical motion of the pin through the solution. The rate of withdrawal from a sample (v), the depth of submersion (d), and pin diameter are also important factors for controlling droplet volume. The faster the pin is removed from the sample well, the larger the droplet hanging from the tip is. Furthermore, the deeper the pin is submerged into the sample well, the larger the droplet that forms at the end of the tip. Therefore to make the system reproducible, the speed and depth were kept constant during the experiment[56]. The end shape of the pin (e.g. flat, chamfered, slotted) also permits some measure of control over the droplet size. In addition, we employed

slotted pins to facilitate better adhesion of the acquired droplet to the pin and center the droplet on it.

In both systems, lipids can either be loaded in the aqueous or the organic phase. We found that the fluidic source of the lipids had an effect on measured bilayer resistance. When the lipids are present in the organic phase, the measured resistance was significantly lower than that measured in the aqueous phase (typically 5 GΩ with lipids in the organic phase and >30 GΩ when liposomes are used). Although the exact mechanism of this is not known, it is believed to be due to lipid participation in ionic transport across the organic phase[60,61]. When a large amount of lipid is present in the organic phase, reverse lipid micelles may be able to surround charged ions, reducing the ionic self energy in the organic phase, enabling transport across the organic phase under an applied voltage. When the lipids are present in the aqueous phase, there are fewer lipids in the organic phase available to transport ions across it, reducing any ionic current outside of the lipid bilayer. Regardless, the lower resistance did not affect the ability to measure single channel currents of ion channels such as gramicidin A. The amount of protein present in the bilayer was controlled by varying the concentration of the protein present in solution and the concentration used here allowed for single channel measurements.

The concentration of the liposomes in solution required optimization; if the liposome concentration was too high, droplet adhesion to the pin was generally poor, and droplets often detached from the pin when immersed in the organic phase. This poor adhesion is attributed to coating of the lipids/organic solution mixture onto the pin surface, decreasing the aqueous wetting to the pin. Conversely, if the liposome concentration was too low, there was an insufficient quantity of lipids (or insufficient time) to produce a lipid monolayer at the droplet surface and such droplets quickly fused with the lower aqueous phase upon being lowered into

contact. We found that a concentration of about 250 µg/ml of extruded lipid solution yielded satisfactory results

The bilayer area can be controlled by varying the height (Figure 3) and size of the upper aqueous droplet. Since the bilayer capacitance is proportional to its area, reduction in droplet size would serve to reduce the capacitance-related electrical noise which is important for low conductance measurements. Dispensation of small fluid volumes (~nL) may be problematic with pipette-based systems, but it is relatively straightforward with pin tools[56]. Thus, scaling this method may be best suited to the pin tool platform.

Automation of the pin tool platform yielded simultaneous formation and measurement of fluid droplet lipid bilayers, which, to our knowledge was the first demonstration of its kind. While the sizes of the bilayers that formed successfully were consistent, bilayers often varied in how resistive ("leaky") they were. Leaky bilayers exhibit lower resistances than non-leaky bilayers, and are easily seen with the application of triangle wave voltages. Such voltages produce square wave current traces in purely capacitive lipid bilayers, but produceohmic responses when conductance across the bilayers is significant. These ohmic responses produce sloped traces that occur in synchronization with the slopes of the applied triangle voltage waves. While bilayers formed consistently across experiments, the maximum bilayer yield did not commonly exceed 75%, or 6 of the 8 possible bilayers that could have been formed with the pin tool array. The most likely reason for this is droplet misalignment. We often noticed that even after droplets were deposited onto pins, the droplets did not always hang consistently off of the pins. Often times droplets would demonstrate preference for one side of a pin, or else droplets would not hang, but "climb" the surface of the pin. This was most likely caused by inconsistent surface cleaning of the pins, causing some parts of pins to be more hydrophobic than other parts

of the same pin as well as other pins. Thus, while all pins were submerged into organic solution containing bilayer chamber wells, some droplets may not have been present at the organic/aqueous solution interface cut into the hydrophobic partitions. Alternatively, some droplets may have fallen off of pins altogether at the stage of monolayer formation. The size of droplets generally determined the nature of droplet misalignment; smaller droplets (<1.5 µL) tended to cling to one side of the pins or climb the pins, while larger droplets (>2.5 µL) tended to fall off of pins more easily. The droplet size with the best bilayer formation yield (~75%) was found to be 2.5 µL. Cleaning of the pin tool array (step 4) was necessary for droplets to consistently cling or hang from the pins. Without the cleaning step, droplets often failed to deposit themselves onto the pins in step 1 of the experiment cycle; the tendency for droplets to fall off of pins also increased in the absence of the cleaning step. If such a system would be employed for the measurement of various types of reconstituted ion channels in lipid bilayers between experiment cycles, cleaning would also be necessary to avoid contamination. The speed of the experiment steps was largely limited by the speed of the CNC controller that we operated. A faster controller would lead to faster experiments, though a rate limiting step would be the necessary cleaning of the pins as well as the 1 minute monolayer formation time when the pins are initially submerged in the organic wells of the multiwell bilayer array plate. In general, cleaning steps are considered the bottleneck of pin tool liquid handling and there are continuing efforts to improve this technology[56].

Conclusions

Artificial lipid bilayer formation by mechanically contacting lipid monolayers offers some technological advantages over traditional methods. Here we have described two implementations of this process compatible with parallelization, automation, and cycling. We

have utilized pin tools, which are commonly used in high thoughput fluid handling applications and are compatible with automation robotics commonly used with microarrays. We have demonstrated the compatibility of our system with a 384 well plate and it may be possible to further scale this system to work with 1536 well plates. While we demonstrated automated pin tool arrays consisting of 8 pins for lipid bilayer formation and measurement, the design is scalable to fit the channel capacity of the amplifier. When scaling systems to work for high throughput measurements, reducing the cost per data point becomes a significant factor. As a result the pin tool method of bilayer formation may be more appropriate for high throughput cell-free electrophysiology since the pins can be cleaned and reused. Combining the automation with use of multichannel amplifiers allows for simultaneous measurement of many bilayers and increases measurement throughput. We are interested in exploring application of these systems to automated ion channel measurement for sensing and pharmaceutical discovery.

Masking Apertures Enabling Automation and Solution Exchange in Sessile Droplet Lipid Bilayers

In previous work, we and others have shown that bilayer areas are highly sensitive to variations in positioning of the two aqueous phases[62,63], which can in turn affect number of incorporated channels[64] and measurement noise[65,66]. It was thus determined that increased precision is needed from fluid handling and motion control hardware for to obtain repeatability and consistency across experiments.

To address this issue, we have designed an artificial lipid bilayer formation and measurement plate which constrains the contact area of the two aqueous phases, also constraining the bilayer area. The apparatus consists of a lower aqueous solution chamber plate, a hydrophobic film in which a small aperture is cut, and a top chamber plate that allows for top loading and electrical access of all solutions. Lipid bilayers are formed by contacting monolayers through the small aperture in the hydrophobic film, which constrains the bilayer size. We show measurements which demonstrate the reduced sensitivity of the bilayer area to the relative position of the aqueous phases, reducing the precision needed by fluid handling and motion control hardware in automation. The apparatus is also easily arrayed and compatible with SBS standard instrumentation. We also demonstrate fully automated fluid exchange of the lower aqueous solution with intact droplet bilayers allowing for stable solution perfusion. While masking of lipid bilayers formed by contacting monolayers has been studied previously[67], here were present a platform that is easily automatable and scalable, presenting a way forward toward high-throughput study of ion channels in planar lipid bilayers.

Experimentation

Bilayer formation apparatus

Chambers were made from 0.125” thick acrylic (McMaster-Carr) and 0.003” thick Delrin film (McMaster-Carr). Two acrylic pieces were milled to form fluidic wells and channels by stacking them vertically and sandwiching the Delrin. Apertures (50–200 μm in diameter) in the Delrin film were cut using a 25W CO_2 laser cutter (Universal Laser Systems) to connect the wells formed by the top and bottom acrylic pieces. Aperture sizes were measured microscopically. Two wells (an inlet and an outlet for aqueous solution) were connected through a channel in the bottom acrylic piece. A center measurement well was connected to the channel through the aperture in the Delrin film; lipid bilayers formed through this aperture. In initial experiments, a 0.0625” thick layer of PDMS elastomer (Sylgard, Dow Corning) cut with holes matching those in the acrylic pieces was placed on top of the Delrin film to form a sealing gasket. Once assembled, all pieces were clamped together. In later experiments, the acrylic plates and the hydrophobic Delrin partitions were bonded together by placing double-sided very high bond acrylic foam tape (McMaster-Carr) between the solid acrylic top and bottom plates, with the hydrophobic Delrin partition placed in the center.(Figure 3-1).

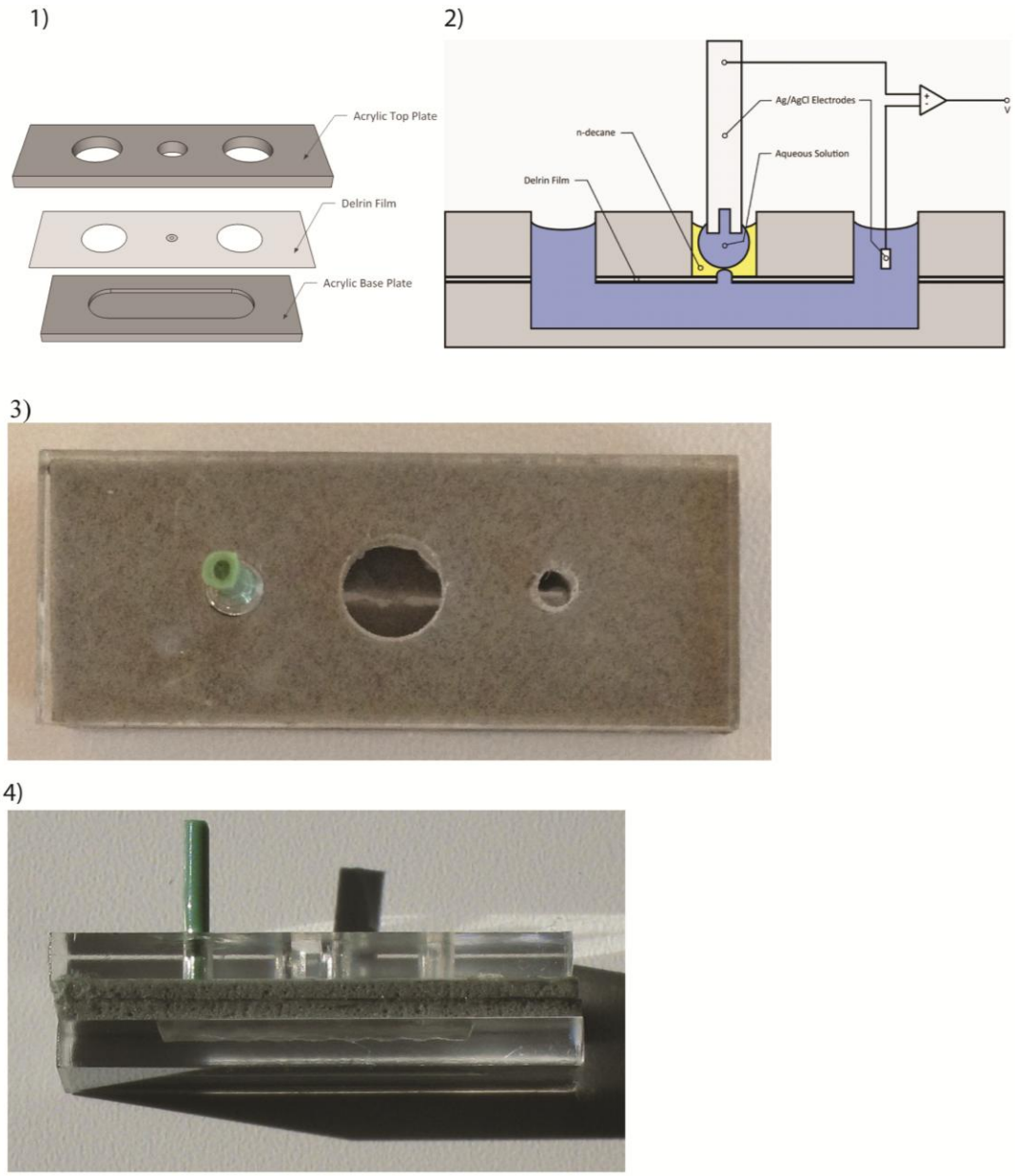

FIGURE 3-1: Single-Well Bilayer Measurement Chamber. 1) Acrylic top and bottom plates sandwich a thin hydrophobic film; plates were held together either with clamping or use of double sided acrylic tape. 2) Aqueous fluid is first loaded into one of the two side inlets, followed by loading of organic fluid (n-decane) into the central inlet. The center aperture size in the Delrin film masks the area available for contact between lower aqueous and organic fluids. Lipids initially present either in the organic solution or from liposomes in the aqueous solution form monolayers at the fluid interfaces. Inserting a pin electrode with sessile droplet into the central well and lowering it into contact with the film produces lipid bilayers having areas defined by the aperture in the Delrin film. After insertion of ground Ag/AgCl electrode into lower aqueous compartment, electrical measurements can be made. 3) Top view of fully assembled bilayer chamber-- green peek tubing inserted into aqueous inlet for use with syringe pump during fluid exchange experiments. 4) Side view of fully assembled bilayer chamber; lower aqueous compartment can be seen in bottom plate.

Lipid bilayer formation

Measurement buffer (MB) containing liposomes were made as previously described[62]. Briefly, a 1ml solution of 1 M KCL, 10 mM Tris-HCL (Sigma), pH 8.0, and additionally containing 33 mg of 1,2-Diphytanoyl-sn-Glycero-3-Phosphocholine (DPhPC) lipid (Avanti Polar Lipids), was extruded through a 200 nm filter (Avanti). 150 μl MB was first loaded into the aqueous inlet to completely fill the portion of the chamber below the Delrin film. Next, 40 μl of n-decane (MP Biomedicals) was loaded into the measurement well to fill the portion of the well directly above the pore in the Delrin film. This allows the liposome-containing aqueous solution below the film to come into contact with the n-decane present near the Delrin pore, where a lipid monolayer self-assembles.

Electrode fabrication

Silver pins were fabricated using 16-gauge silver wire (0.999 purity, C.C. Silver & Gold). The pins were cut to approximately 1 inch length and electrical discharge machining was used to create a blunt end and cut slots 0.05" deep and 0.015" wide into the ends of the pins. Counter ground electrodes were made from 200 μm diameter silver wire (Ted Pella). The silver wires were chloridized by immersing them in bleach for approximately 1 min, followed by a DI water rinse.

Bilayer formation and measurement

As described previously[62], the chloridized pin was lowered into liposome-containing MB to a depth of approximately 10 mm for 1s and removed, resulting in a small ≈1.1 μl droplet hanging from the end of the pin. This pin with hanging droplet was then lowered into the decane solution. After waiting approximately 1 min. for lipid monolayer formation, the pin was lowered further

using a micromanipulator (Newport) until the droplet contacted the lower aqueous phase within the Delrin pore, forming a lipid bilayer membrane.

For electrical measurement, the apparatus was placed inside a Faraday cage and the Ag/AgCl pin and counter-electrodes were connected to an Axopatch 200B amplifier (Axon Instruments). The signals were digitized with a Digidata 1332A (Axon Instruments) at 5 kHz, filtered in hardware with a 1 kHz Bessel filter and subsequently filtered further with a 30 Hz Bessel filter and analyzed with Clampfit software (Axon Instruments).

In fluid exchange experiments, PTFE or PEEK tubing (Zeus) was inserted into one of the inlet ports of the lower channel of the measurement chamber and connected to a syringe pump (KD Scientific) actuating a 10mL glass syringe (Hamilton) filled with MB. After the lower aqueous chamber was filled, the measurement well was loaded with n-decane and bilayers formed after pin insertion as described above.

Results

Best results for the laser cut apertures were obtained when the Delrin films were thinned by raster etching before cutting, which involves a laser burning away sections of material to reduce film thickness. Bilayer formation was never successfully observed without thinning of the Delrin. For apertures 50 μm-200 μm in diameter, bilayer formation, measured capacitively, was observed to occur upon contact of the sessile droplet to the Delrin film, enduring stably at least several hours, as previously described[62,68]. Measurements of ion channels in lipid bilayers formed using the masking apertures were indistinguishable from those made without the apertures. Bilayer formation was highly repeatable, and droplets could easily be removed and replaced to subsequently form bilayers—in a repeatability experiment, 51 bilayers were formed in 51 attempts.

Bilayer areas without these masking apertures are highly sensitive to the relative positions of the droplets[62,63]. We explored the influence of the apertures on this result. In one set of experiments, we lowered the pin to contact the droplet to the Delrin apertures until an increase in capacitance was measured, signifying bilayer formation. The pin was then further lowered in steps of 50 µm and the capacitance measured again. From these values the 30 pF background capacitance, measured with the pin approximately 1 mm away from the aperture, was subtracted and the resulting bilayer capacitance was plotted, shown in figure 3-2. The variation of measured capacitance with vertical pin position was markedly reduced with the hydrophobic Delrin partition films as compared to our previous measurements.

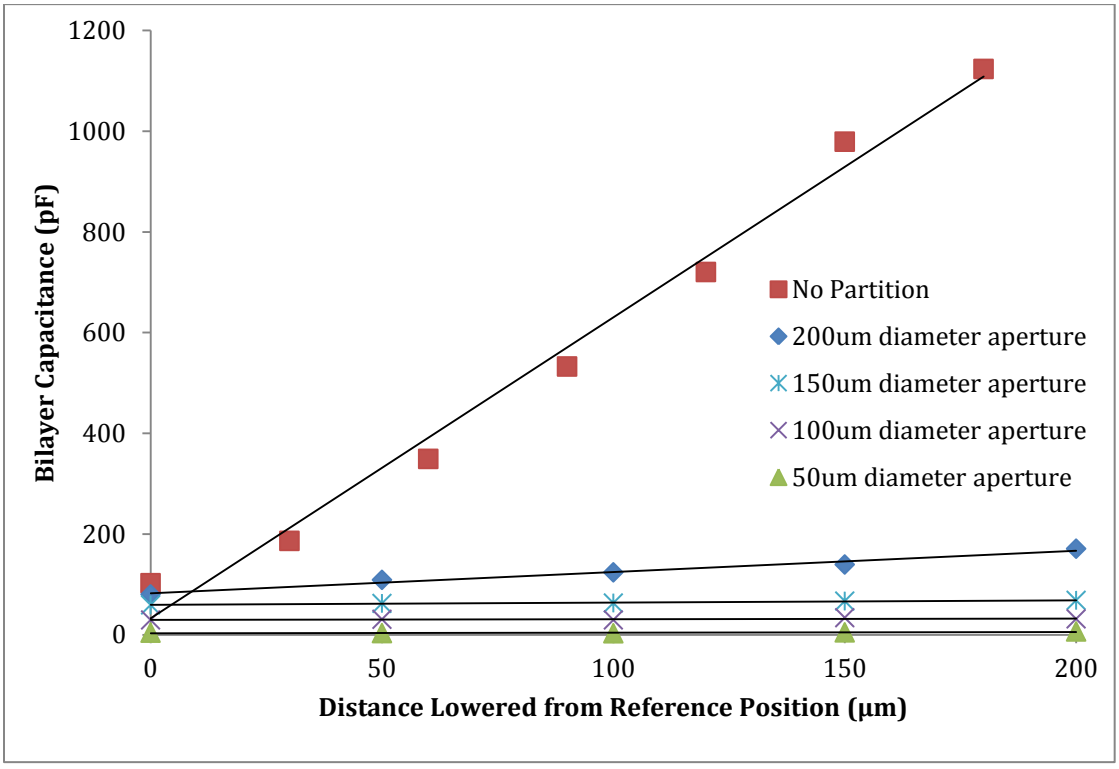

FIGURE 3-2: Bilayer capacitances changes with respect to pin position from a common origin position. As the pin with sessile droplet and lipid monolayer is lowered into contact with the lower compartment lipid monolayer, the capacitance of the bilayer is observed to increase[62]. Adding a Delrin film with an aperture of defined diameter, and forming the lipid bilayer through this aperture allows for control over the size of the bilayer; results shown with aperture sizes of 200 µm, 150 µm, 100 µm, and 50 µm.

We also investigated the sensitivity of bilayer area to the lateral position of the pin. A pin with 2µl sessile droplet was axially aligned with the center of a 150 µm aperture and lowered to form a bilayer. After each capacitance measurement, the pin was raised and moved in 200 µm steps laterally before being lowered again, after which the capacitance was measured. These experiments were compared to measurements taken with no separating Delrin film. With the Delrin film, the bilayer capacitance was still within 90% of its original value when the droplet was positioned over 500µm from the aperture center. In contrast, without the masking aperture, the bilayer capacitance decreased to approximately 15% of its original value (Figure 3-3).

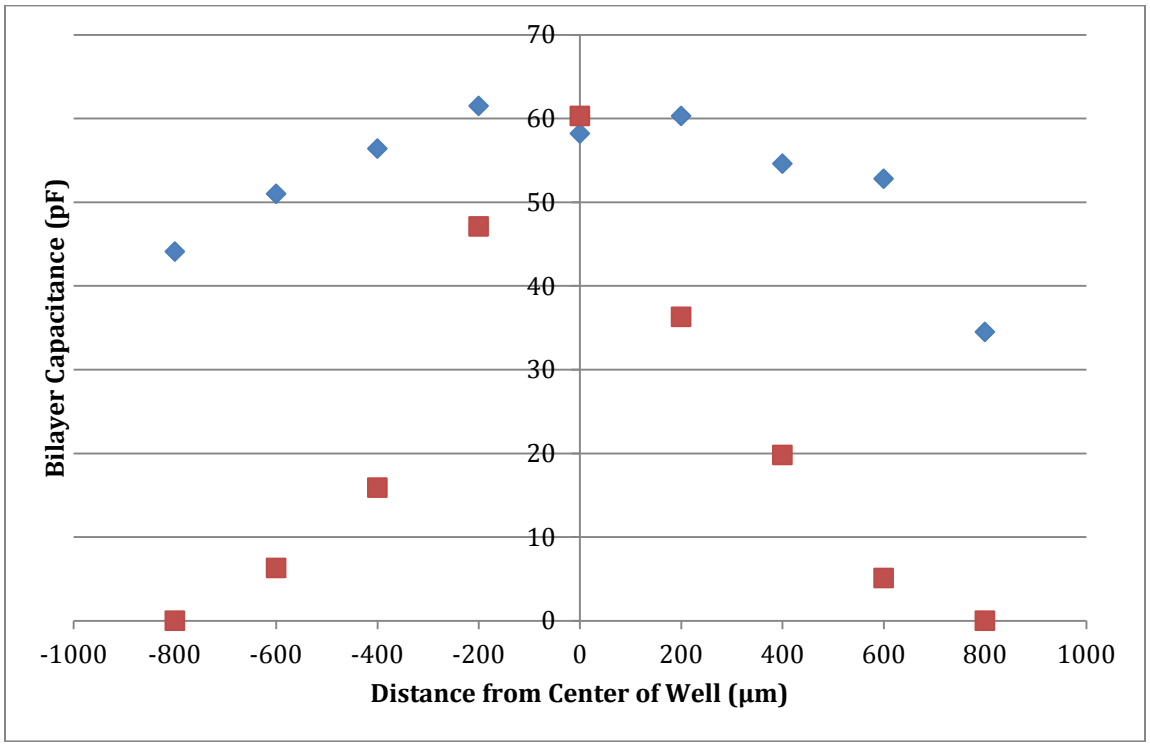

FIGURE 3-3: Changes in bilayer capacitance as droplet-laden pin is moved across either a partitioned measurement well containing a 150 µm diameter hole at the center (red squares) or a non-partitioned measurement well (blue diamonds). Well diameter is 3.7mm. Pin is moved laterally from left-of-center to right-of-center before being lowered to allow for bilayer formation. Between measurements, pin is raised vertically 500 µm

In addition to improved bilayer stability, the hydrophobic partitions allowed for improved noise performance, which was readily apparent when measuring ion channel activity. This is primarily due to the reduction of bilayer area—noise performance is known to correlate inversely with bilayer area[69]. The capability to form small lipid bilayers (diameters <100 μm) with arbitrary droplet volumes allows for convenient fluid handling; for example, as discussed in the previous chapter, 2.5 nL droplets were found to be optimal for producing sessile droplets on 16-guage Ag/AgCl pins, but we found that droplets of such do not easily form stable bilayers smaller than 100 μm unless formed through a partition. Improved noise performance was observed in the measurement of the gramicidin A ion channel activity in lipid bilayers produced using the hydrophobic partitions. Partitions with smaller apertures performed better than those with larger apertures, as measured by peak-to-peak noise level (figure 3-4).

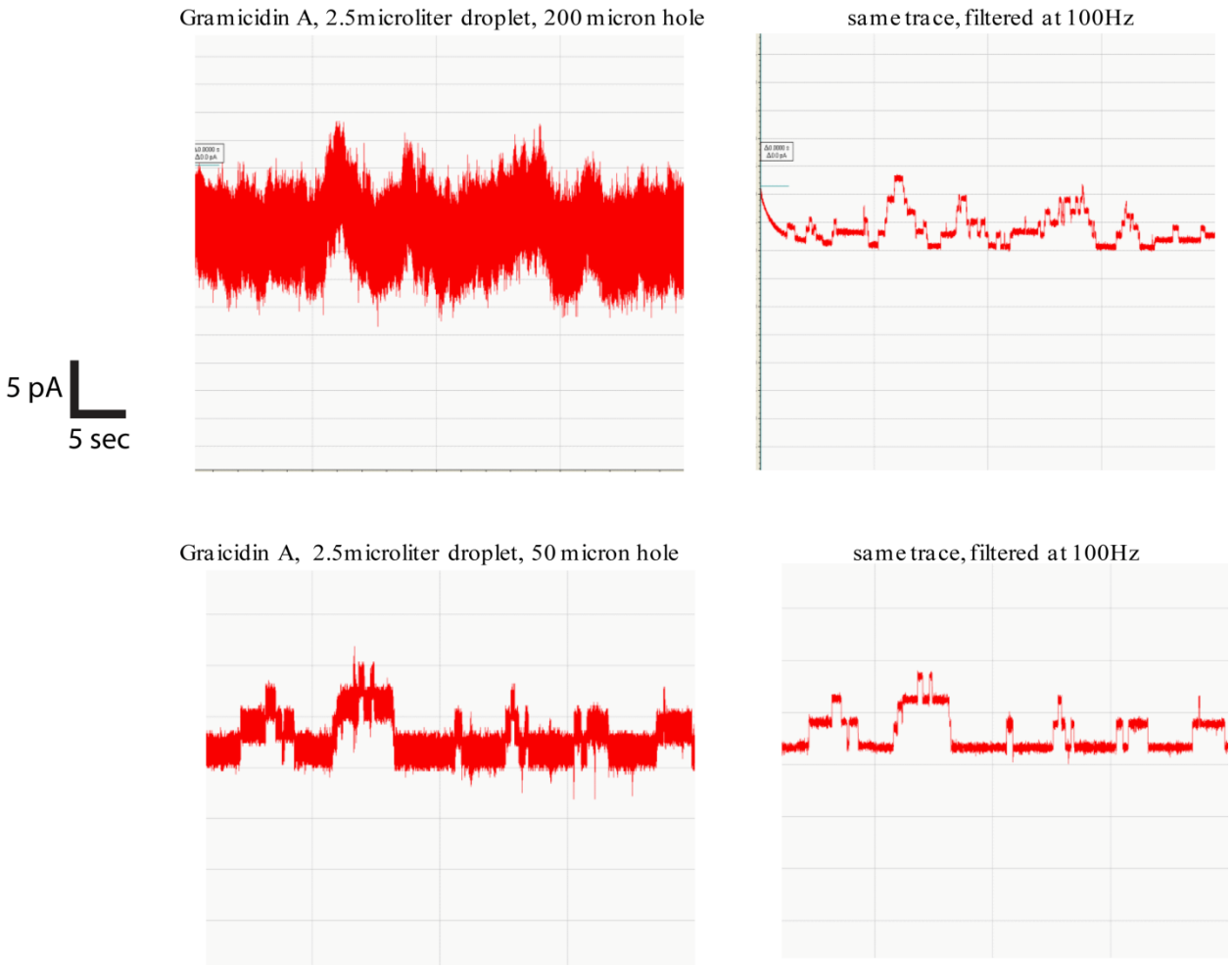

FIGURE 3-4: Illustration of noise improvements when smaller partitions are used, given same size of droplets (note that this type of data was collected for hours, negating issues of bilayer size changes with time), lowered to same the level in measurement wells

The effect of active solution exchange through the lower chamber was determined by measuring bilayer capacitance while fluid was pumped through the lower aqueous channel of the bilayer chamber at different flow rates using a syringe pump. Lipid bilayers were formed using a 200 µm diameter aperture and measured at flow rates of 0-20 mL/hr. Data are shown in Figure 3-5 from two experiments. Similar experiments without the masking aperture resulted in

immediate bilayer failure as the lower aqueous solution would rise up through the measurement well, even at very low flow rates.

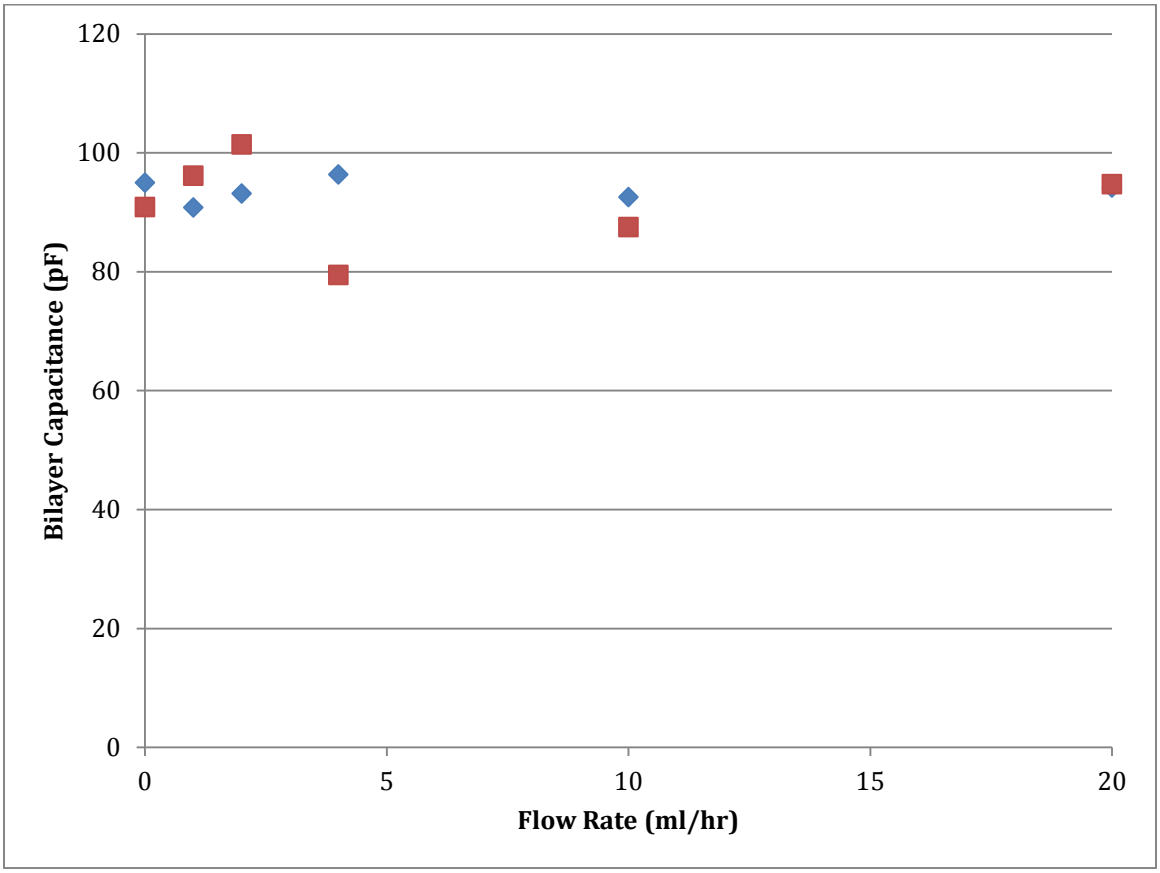

FIGURE 3-5: Simultaneous fluid exchange and bilayer measurement. Lipid bilayer capacitances are measured while measurement buffer in the lower aqueous chamber is exchanged at given flow rates. Capacitances were stable over the time required to allow for complete fluid exchange. Diameter of aperture in Delrin film was 200 µm

Discussion

In our previous work, we demonstrated apparatus for lipid bilayer formation and measurement using sessile droplets suspended from silver pins compatible with automated motion control and fluid handling technologies[62]. We and others[62,63] have shown that the bilayer capacitance (proportional to area) is strongly dependent on the contact area of the aqueous

phases, which can be affected by their positioning and size. Specifically, we showed that the bilayer capacitance (proportional to area) varied approximately linearly with the upper droplet's vertical position (Figure 2). As shown, the measured capacitance increases from 102 pF to 186 pF as the droplet is lowered 30 μm.

From this we may estimate that, to obtain 10% repeatability in bilayer capacitance and area, the relative position of the aqueous fluid interfaces must be precise within 3.6 μm. This relative position is determined by the position of the pin holding the sessile droplet, the volume of sessile droplet, and the position of the lower aqueous interface, which itself depends on the volume of the lower fluids and the dimensions of the channels and wells. Estimating the shape of the 2.5 μL sessile droplet on the pin as a spherical cap, 3.6 μm precision in height of this droplet corresponds to 15 nL required precision in droplet volume. Further, for development of parallel arrays, this vertical precision also requires a high degree of machining tolerance, uniformity, and alignment of the component parts.

It was with these concerns that we investigated the possibility of masking the aqueous phases aiming to provide an upper bound to their contact area and thus reduce the sensitivity of bilayer area to variations in fluidic volumes and mechanical positioning. With masking apertures in Delrin films between 50 and 200 μm in diameter, formation and measurement of stable bilayers were highly repeatable, with the bilayer area controlled by the pore size (Figure 2). The dependence of bilayer capacitance on vertical and lateral relative positions of the aqueous interfaces was significantly diminished when using the aperture mask (Figure 3). A change in the capacitance of a masked bilayer of 10% only resulted after vertical displacements of >100 μm for the 50 μm, 100 μm, 150 μm apertures and 30 μm for the 200 μm masks. Similarly, the dependence of measured capacitance on lateral droplet alignment was markedly reduced with

150 μm aperture as compared to no aperture. With the aperture, consistent bilayer sizes resulted even with the pin positioned over 400 μm from the well center. The bilayer chambers are designed to produce lipid bilayer areas that are roughly equal to the areas of the apertures cut into the hydrophobic Delrin partitions. An estimate of the size of the surface that forms between the bottom aqueous well of the chamber and the top organic solution filled well through the aperture can be found from relating the fact that the pressure in the lower aqueous wells can be estimated from the height of the water columns that form at the chamber inlet and outlet using Pascal's theorem. The contact angle the forms between the organic solution and the aqueous solution can be found using the Young-Laplace equation:

$$\rho g h = \frac{2\gamma cos\theta}{a}$$

Where ρ = density of 1M KCL (1040 kg/m^3), g = acceleration due to gravity (9.8 m/s^2), h = height of chamber from bottom of bottom plate to top of top plate (about 0.01 m when using double-sided acrylic tape to fix chamber together), γ = surface tension between aqueous and organic interface (0.048 N/m, which is the surface tension between n-decane and water[70], a = radius of aperture in 100μm Delrin partition. The angle produced between the curvature of the aqueous fluid and the n-decane at the aperture is thus calculated as about 84º, resulting in an incline angle of the aqueous solution at the Delrin boundary of about 6º. This implies a relatively flat interface, with size defined by the size of the aperture, which was about 200 μm in diameter. While the surface tension in the calculation did not account for the lipid present at the interface due to the formation of lipid monolayers, experimentally it was determined that the size of the apertures yielded a good rough estimate for the size of the bilayers produced (figure 2). Care had to be taken that the thickness of the hydrophobic film was small enough to permit lipid bilayer formation from monolayer contact of the sessile droplet/organic interface monolayer with the

organic/lower aqueous interface monolayer. Generally it was found that apertures in hydrophobic Delrin partitions had to have diameters at least equal to the thickness of the film (about 76 μm) to form bilayers easily; bilayer formation with smaller apertures was possible only with the application of tension between the pin electrode attached to the sessile droplet and the surface of the partition film.

Easy control and repeatability of bilayer size allows for the number of incorporated ion channels to be specified, as well as for a level of control over measurement noise associated with the bilayer capacitance[65]. Noise was observed to decrease as aperture size and bilayer capacitance decreased and was accomplished solely through reduction in the aperture size, holding constant the apparatus and volumes and positions of the fluids.

Fabrication of the hydrophobic Delrin partition films required repeatable production of apertures ranging in diameter size from 50 μm -250 μm. A 25W CO_2 laser cutter loaded with a design file (made in Adobe Illustrator) was employed and yielded satisfactory results for aperture diameters larger than 100 μm. For aperture diameters less than 100 nm, a 50W CO_2 laser was employed. In all cases, before the apertures were cut into the film, the films were thinned by raster etching to a thickness of about 0.001". Optimal laser settings were determined empirically (figure 3-6).

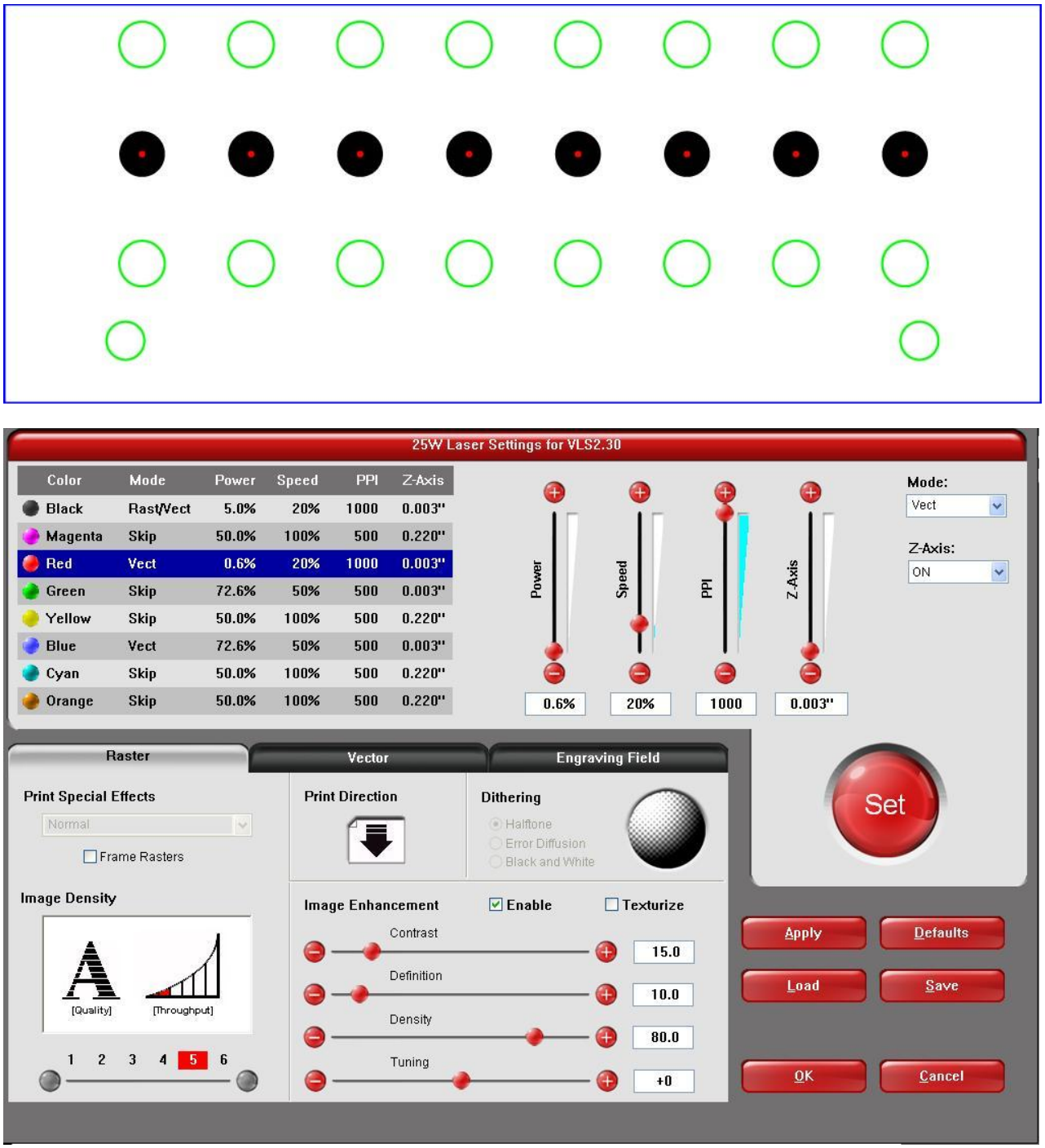

Figure 3-6. Design file and settings for manufacture of hydrophobic Delrin partitions in a multi-well lipid bilayer chamber. Top: Holes are vector cut where the color green is indicated: top and bottom rows of 8 circles serve as fluid inlets and outlets to lower aqueous compartment of chamber, bottom 2 holes are used for chamber alignment during assembly. Middle row of 8 circles indicates area wheredroplet bilayers are formed. Black area is raster thinned, middle red circle is vector cut, resulting in hole diameters from 100µm-250µm, depending on the laser power setting. Bottom: laser cutter settings indicate the necessary power and speed settings for the indicated colors in the top design.

The construction of the lipid bilayer chamber in initial experiments required gaskets to be placed between the acrylic top and bottom plates and the hydrophobic Delrin film. The gaskets, made from PDMS, prevented leakage of organic fluid out of the top measurement well. While lipid bilayers with reconstituted ion channels such as alpha-hemolysin and gramicidin A were consistently measured using this configuration, it was found that organic solution from the top well would be slowly absorbed into the gaskets; after about 1 hour, a significant reduction in organic fluid volume was typically observed. This prompted a search for alternative gasket material for use in chamber construction. The use of double-sided acrylic foam tape was found to yield satisfactory results; chambers built using the double-sided tape also supported lipid bilayer formation with measurable reconstituted ion channel activity with little to no reduction of organic well fluid observed over the course of experiments. Additionally, the tape was easily cut using the CO_2 laser cutter machine, which allowed for the well patterns to be cut according to the same computer aided design files used in producing the top and bottom acrylic plates. The chamber did require extensive cleaning before use in bilayer and ion channel measurement; failure to do so resulted in excessive noise in measurements. Cleaning typically consisted of rinsing the top and bottom wells of the fully constructed chambers with methanol, followed by 2-propanol, followed by deionized water. Additionally, the top well was allowed to soak in organic solution (such as n-decane) for at least 30 min, while the bottom well was filled with water. It is believed that this organic solution soak dissolves hydrophobic debris produced from laser cutting the double-sided tape more thoroughly than the alcohol and water rinses. After the organic solution soak, an additional round of alcohol and water rinses was conducted, followed by drying of the chambers in a vacuum chamber for several hours.

Hydrophobic partitions of the type described here employ a scalable design. While initial experiments were conducted were on single well, detached bilayer chambers, multi-well arrays were used as well. The discussion in the previous chapter of the automated formation and measurement of an array of 8 bilayers employed a 48-well chamber plate which employed an 8x6 array of bilayer chambers, each incorporating a hydrophobic partition. We have frequently used 8x1 bilayer arrays (figure 3-7) to conduct fluid exchange experiments. Changing the design of the bilayer chambers to accommodate various applications is made easy by the fact that we employed a laser cutter to rapidly cut all parts from pre-made computer aided design files.

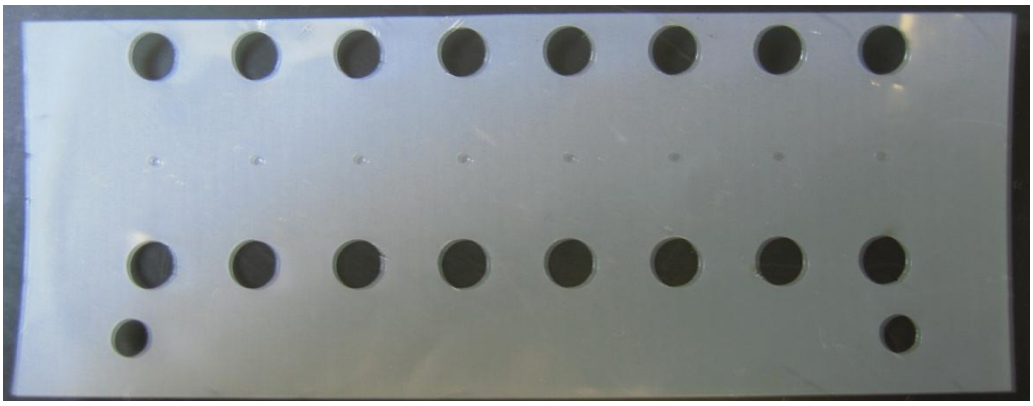

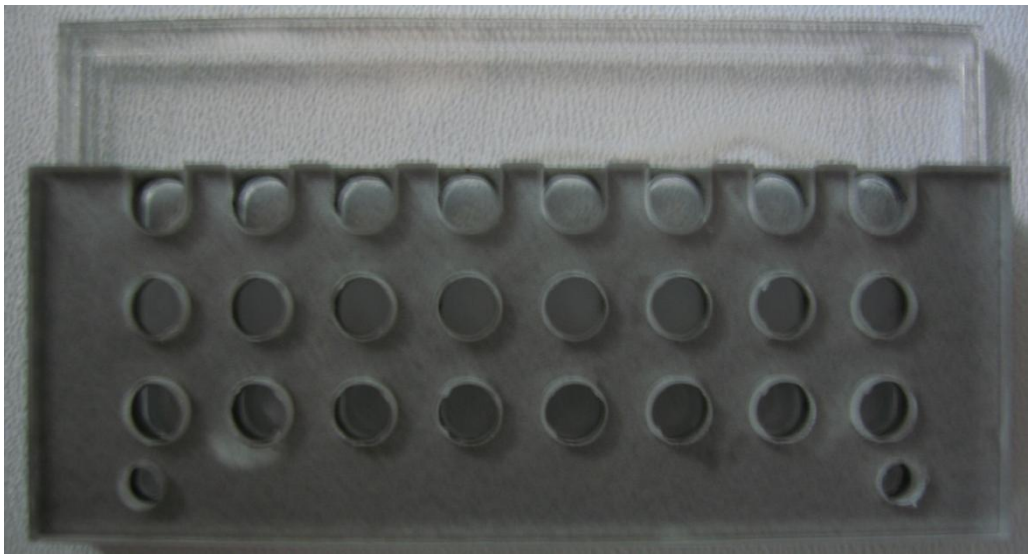

Figure 3-7. Laser cut hydrophobic Delrin partition used in forming a parallel array of 8 droplet lipid bilayers (top), bird's-eye view of fully assembled 8-well droplet lipid bilayer array chamber equipped for fluid exchange (bottom); a trough for collecting fluid spill over upon fluid exchange is included.

In addition, of key technological importance is the ability to support solution exchange. Without the masking aperture, pumping of the lower solution significantly displaced the fluidic interfacial boundary, rupturing the bilayer even at low flow rates (< 1 mL/hr). However, with the mask, we were able to flow solution through the lower chamber, stop the flow, and resume measurement, simulating an experiment in which analyte concentration in the lower solution is changed. We were also able to measure bilayers during exchange at flow rates at rates of up to 20 mL/hr (Figure 5). Data from two bilayers are shown, demonstrating that the measured bilayer capacitance remains within 10% of its original value. While the ability for the chamber to support faster flow rates was not thoroughly examined, it is possible that rates in excess of 20mL/hr may be achievable with a redesign of the bilayer chamber architecture and fluid inlets/outlets. In chapter 4 of this work, we explore bilayer perfusion in an 8 channel bilayer array system (modified from the bilayer chamber design discussed in this chapter) that supported fluid exchange by hand pipetting at rates of about 20 mL/min and that employed a vacuum to remove excess perfusion fluid. Measurement of bilayers and ion channel activity during and after the fluid exchange in those experiments was successful, which indicates that much faster fluid exchange rates than 20 mL/hr are indeed possible with the basic elements of the bilayer chamber design discussed here.

Based on subsequent preliminary work, we believe that 20 mL/hr is far from the maximum rate achievable and is primarily dependent on the channel design. Solution exchange enables increased experimental throughput by allowing for a variety of different experimental conditions to be tested in a short time, as well as measuring the activity of a large but fixed number of ion

channels in the presence of varying concentrations of pharmaceutically active compounds for IC_{50}/EC_{50} determination.

Conclusions

We are developing apparatus and materials to enable automated, repeatable high yield formation and measurement of artificial lipid bilayers and ion channels reconstituted into them. Here we have presented progress toward this goal, which we achieved by constraining the bilayer area using a masking aperture. The devices that use these apertures are easily arrayable, and can be made in the form of multi-well plates for parallel bilayer and ion channel measurements. This parallelization, in combination with improved compatibility of bilayer formation with automation and the ability to support solution exchange without disturbing the bilayer, may result in significantly increased throughput ion channel studies using artificial bilayers, a subject of our ongoing work.

hERG Drug Response Measured in Droplet Bilayers

The voltage-gated ion channel encoded by the human ether-à-go-go-related gene (hERG) found in cardiac tissue plays a major role in the repolarization of cardiac action potentials through its inwardly rectifying potassium ion currents[71]. Both the blockage and mutation of hERG channels have been shown to suppress rectifying currents, leading to elongated action potentials; this has in turn been linked to QT elongation in electrocardiogram traces[72]. The hERG channel has been shown to be particularly 'promiscuous' in the sense that is blocked relatively easily by a variety of different chemical agents[73]. No other cardiac ion channel has been shown to be as strongly linked to QT elongation as has the hERG channel[74]. QT elongation has been shown to increase a person's risk for acquiring cardiac arrhythmia caused by a condition called torsades de pointes[75] (figure 4-1) which in turn has been shown to cause ventricular fibrillation and sudden death. While the occurrence of torsades de pointes is rare even for people the exhibit QT elongation, its consequences are severe enough that its proximate causes, including blockage of cardiac hERG channels, is of acute interest by researchers and those in the pharmaceutical industry[74].

In recent years, many compounds have been linked to the occurrence of torsades de pointes in humans. Table 4-1 includes a list of drugs (some no longer commercially available) that have all been shown to put patients at risk for developing torsades de pointes, and all have also been shown to affect on hERG channel function[74]. Most are hERG channel inhibitors. Due to the wide variety of drugs that affect hERG channel activity and the potentially life threatening consequences that can arise from their use, the Food and Drug Administration has issued guidelines recommending that all new drug candidates be screened for potential effects on hERG channel activity[76]. For this reason, safety screening for potential effects on hERG channel activity is of critical importance for drugs being developed by pharmaceutical companies.

Currently, the most widely employed techniques for hERG channel safety screening are traditional and automated patch clamp techniques on whole cells[77]. In this chapter, we show measurements of the hERG activity in droplet lipid bilayers incorporated directly from commercial membrane preparations of HEK293 cells. Specifically, we employed the method of droplet lipid bilayer formation using sessile droplets on pin tool electrodes, described in chapter 1.Measurement of ensemble hERG currents in the presence of astemizole, a once commercially available antihistamine drug[78], and E-4031, a specific inhibitor of the hERG channel, showed dose dependent inhibition with IC_{50} values in good agreement with published literature. The availability of engineered HEK cells expressing a variety of ion channels, combined with the compatibility of the platform with parallelization and automation, suggests that it has considerable potential for ion channel drug discovery and safety screening.

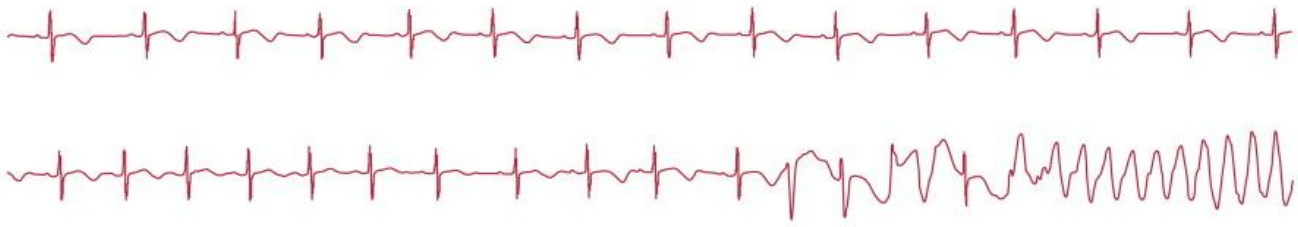

Figure 4-1: Develoment of torsades de pointes in an ECG signal from a patient with long QT syndrome. Inhibition of hERG channel activity has been associated with the development of torsades de pointes.

Drug Name	Therapeutic Action
Amiodarone	Antiarrhythmic
Astemizole	Antihistamine
Bepridil	Antianginal
Cholorquine	Antimalarial
Cisapride	Antipsychotic
Clarithromycin	Antibiotic
Dofetilide	Antiarrhythmic
Domperidone	Anti-nausea
Erythromycin	Antibiotic
Halofantrine	Antimalarial
Haloperidol	Antipsychotic
Ibutilide	Antiarrhythmic
Levomethadyl	Opiate agonist
Mesoridazine	Antipsychotic
Methadone	Opiate agonist
Pentamidine	Anti-infective
Pimozide	Antipsychotic
Probucol	Anti-hyperlipidemic
Procainamide	Antiarrhythmic
Quinidine	Antiarrhythmic
Sotalol	Antiarrhythmic
Sparfloxacin	Antibiotic
Terfenadine	Antihistamine
Thioridazine	Antipsychotic

Table 4-1: A list of drugs that have been associated with the development of torsades de pointes in patients. Nearly all have been shown to inhibit hERG activity.[74]

Conductance measurements of ion channel ensembles are used to determine drug potency as well as to detect off-target drug interactions, such as with the hERG channel[74]. In these measurements, the inhibition (or enhancement) of the ensemble channel conductance is measured as a function of drug concentration, from which the IC50 (or EC50) is determined, defined as the concentration for which the measured channel conductance is 50% of the maximum.

These conductance measurements are predominantly made from ion channel ensembles in

whole cells using patch clamp; however, ion channel ensembles have also been measured in lipid bilayers[79-84]. Lipid bilayer platforms offer simplified apparatus and the ability to easily control membrane and solution composition. Droplet bilayers have been shown to be especially promising technologically, supporting automation and parallelism[43,85], which may indicate significant potential for this platform in drug discovery and safety screening of human and mammalian ion channels.

Measurement of ion channels directly from animal cells and native tissue preparations simplifies protein expression and eliminates most purification steps and is well established at the single channel[86-88] and ensemble levels[79]. Schindler and Quast prepared vesicles from Torpedo marmorata containing acetylcholine receptor (AChR) and used them to form lipid monolayers at the air-water interface for Montal-Mueller bilayer formation[79]. They observed ion channel currents, at the ensemble to single channel levels depending on dilution, which were activatable and inhibitable by AChR-active compounds. Recently Leptihn et al. showed a similar process using droplet bilayers, in which ion channel-containing membranes were used to form lipid monolayers at oil-water interfaces before bilayer formation, measuring a variety of ion channels, including hERG[82].

We developed an automation-compatible apparatus enabling solution perfusion of droplet bilayers[89] and used it to measure the dose-dependence drug activation and inhibition of ensembles of the cold and menthol sensitive ion channel TRPM8 expressed in E.coli[83]. Here we describe measurement of hERG ensembles in droplet bilayers from commercially available HEK cell membrane preparations and dose-dependent attenuation of hERG conductance resulting from perfusion of astemizole and E-4031. Analysis of the conductance as a function of drug concentration enabled determination of IC50 values for these drugs comparable to published

values[78,90]. These results, combined with the large variety of ion channels expressed in engineered HEK cells and the technological potential of droplet bilayers, indicate considerable promise for this platform in ion channel drug discovery and safety screening.

Experimentation

Membrane preparations of hERG-expressing HEK293 cells (Millipore) were used without further purification. Western blotting was used in verifying the presence of hERG channel protein in the sample (figure 4-2). Membrane preparations were diluted from 1:100,000 to 1:1,000,000 in measurement buffer (MB: 350 mMKCl, 10mM HEPES, pH7.5). Diphytanoyl Phosphatidylcholine (DPhPC, Avanti Polar Lipids) was dissolved at 1% (wt/vol) in hexadecane (Sigma).

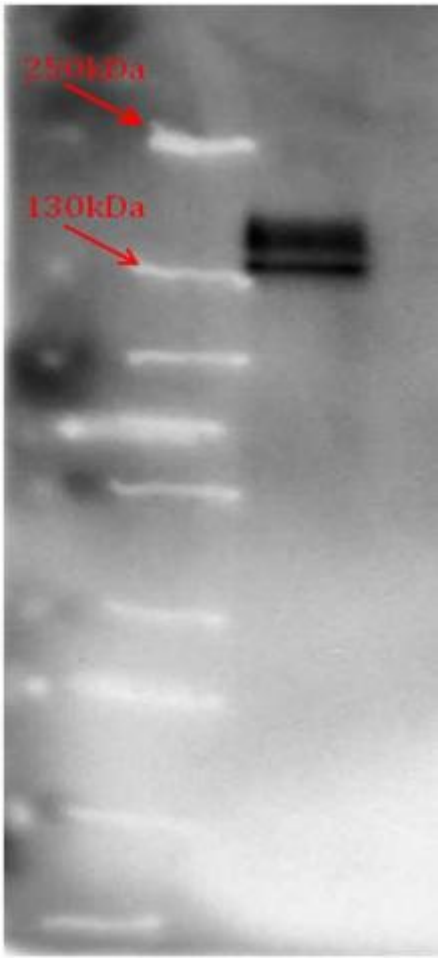

Figure 4-2. Western blot results indicating the positive confirmation of the presence of fully assembled hERG channel protein in membrane preparations used. Line at approximately 135kDa indicates unglycosylated hERG protein; line at approximately 150kDa indicates glycosylated hERG protein.

Bilayer measurement chambers and droplet bilayer formation were identical to previous work[83, 89]. Each chamber consisted of a lower compartment and an upper compartment, connected by a 200 µm circular aperture in a 0.003" thick Delrin sheet. 200 µL of the diluted hERG preparation was added to the lower compartment, followed by the addition of 50 µL of DPhPC/hexadecane to the upper compartment (Figure 4-3a). A 2 µL sessile droplet of hERG solution was deposited on an Ag/AgCl pin electrode made from 16 gauge silver wire (C.C. Silver and Gold). The droplet was lowered into the DPhPC/hexadecane solution for 15 minutes to allow for lipid

monolayer formation[85] at the aqueous/organic interface (Figure 4-3b). The droplet was then lowered into contact with the monolayer formed at the lower aqueous/organic interface, bounded by the Delrin masking aperture. An Ag/AgCl counter electrode made from 22 gauge silver wire (Ted Pella) was inserted into a side well accessing the lower aqueous solution, which served as the ground electrode. Both electrodes were chloridized for at least 20 min in Clorox bleach. Transmembrane voltages and electronic measurement of ion channel currents were measured using an Axopatch 200B amplifier (Molecular Devices) and digitized with a Digidata 1332A (Molecular Devices) at a sampling rate of 20 kHz. Bilayer formation was observed capacitively after lowering the pin electrode with the sessile droplet into contact with the lower

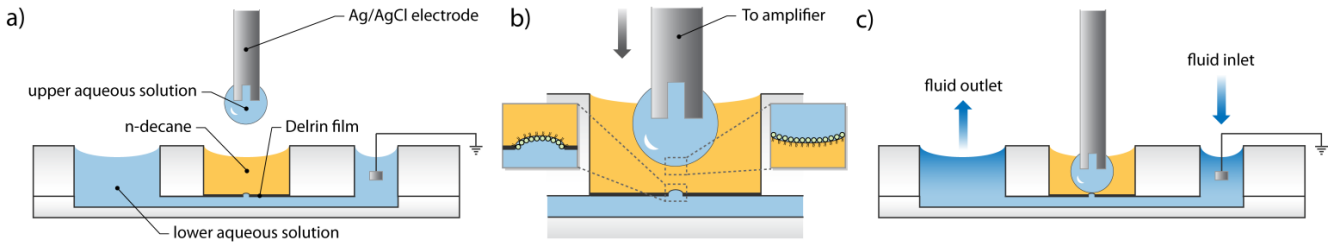

Figure 4-3 Measurement chamber and its use: (a) Side wells are loaded with lower aqueous solution containing hERG membrane preparation. The central well is loaded with 1% DPhPC-hexadecane solution. The lower aqueous solution and center well are separated by a Delrin film containing a 200 µm aperture. (b) An Ag/AgCl electrode with sessile aqueous droplet containing hERG membrane preparation is lowered into the center well from above. Lipid monolayers spontaneously form at the aqueous/hexadecane interfaces (insets). (c) A lipid bilayer is formed by lowering the sessile droplet into contact with the lower aqueous solution, bounded by the Delrin aperture. The lower solution may be perfused through the side wells.

aqueous interface. For channel measurement, the transmembrane potential was held at 0 V for 2 seconds followed by steps ranging from -12 mV to -60 mV for at least 10 seconds. Resultant currents from tens to hundreds of pA were observed (Figure 4-4).Since the same buffer was used on both sides of the bilayers formed in all experiments, any non-zero offset currents that were observed with 0 V applied were eliminated using hardware adjustment. Using a 1:1,000,000 dilution of the membrane preparations, measured single channel currents showed spikes of magnitude 13.4 pS ± 2.5 pS (Figure 4-4c), comparable to values that have been previously

reported at high ionic strength[91].We did not attempt to estimate the amount of hERG protein available in the stock membrane preparation solutions or the diluted samples.

After 5-10 minutes, solutions of MB containing either astemizole or E-4031 were added to the lower compartment of the measurement chambers in step-wise increasing concentrations. Astemizole is an anti-histamine drug no longer commercially available in many countries due to its role in producing cardiac arrhythmic side effects including Long QT syndrome. It is a known antagonist to voltage-gated potassium ion channels, including hERG[92]. Astemizole (Sigma) was first dissolved in DMSO to yield a 10 mM stock solution, which was diluted to 5.0 µM in MB. 2 µL of this diluted astemizole solution was pipetted into one of the side wells of the bilayer chamber, followed by gentle agitation, resulting in a 50 nM solution of astemizole in the 200 µL lower chamber. Sequential additions of 1 µL of the diluted astemizole solution into the lower chamber increased the astemizole concentration to 75 nM, 100 nM, 150 nM, 200 nM, and 500 nM. Finally, 1 µL of the undiluted stock solution was added to achieve a 50 µM final concentration.

Results and Discussion

We had earlier noted the ability to block large currents present in bilayers that were prepared in the presence of hERG membranes, and also to activate them in the presence of hERG activator by flowing drug solutions past the bilayers in the chambers (figure 4-4). In this work, our goal was to establish the dose-dependent relationship of observed ensemble currents. The effect of adding astemizole to bilayers made with hERG membrane preparations had an inhibitory effect. After each dose of astemizole was added, ion currents were observed to decrease and eventually stabilize (Figure 4-5a). Additional solutions were not added until stable currents were recorded for 5-10 minutes. To confirm that the measured change in current did not result from changes in

bilayer area or number of channels,

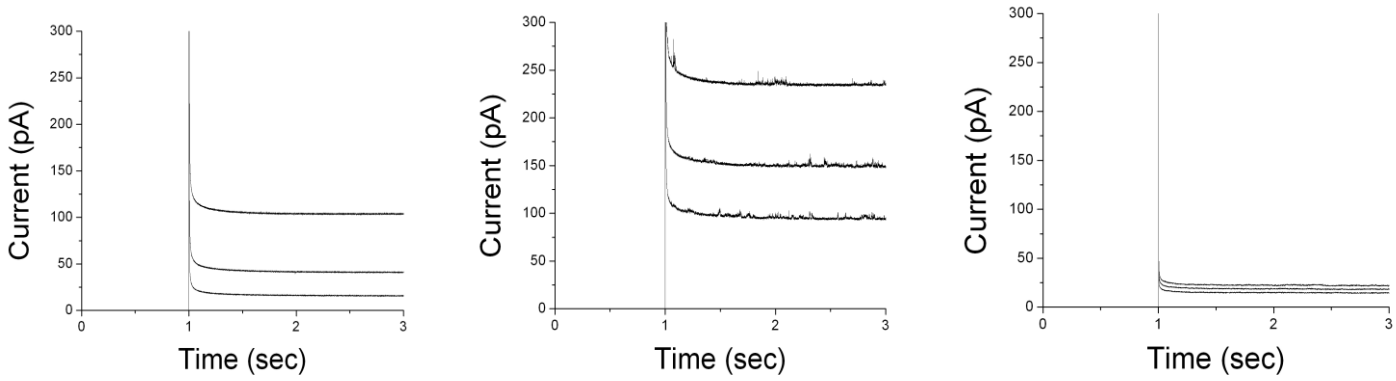

Figure 4-4: Measurements of hERG ensemble currents in the droplet lipid bilayer platform. For all plots, at t=1 sec, the applied voltage is changed from -80 mV to +60 mV, +80 mV, or +100 mV, resulting in respectively increasing currents. Left: Ensemble currents in bilayers prepared with hERG expressing membrane preparations. Center: Same as Left, but with 20 µM Mallotoxin, a hERG activator, added. Right: Same as Left, but with 20 µM Astemizole, a hERG blocker added.

the bilayer capacitance was measured throughout the experiment. In some experiments, small residual currents remained following administration of the final 50 µM solution concentration. The total fraction of DMSO in the measurement solution did not exceed 0.5%. In control experiments, identical amounts of astemizole and DMSO were added to DPhPC droplet bilayers made without hERG membrane preparations, with no change in membrane conductance observed.

Experiments using the hERG-specific drug E-4031 (Sigma) were conducted similarly to those conducted with astemizole. E-4031 doses were sequentially added to the lower aqueous compartments of active bilayer chambers to produce resultant concentrations of 10 nM, 20 nM, 30 nM, 40 nM, 50 nM, 80 nM, and 10 µM. Currents were observed to decrease with each added dose of drug (Figure 4-5b). As with astemizole, a small residual current was measured for the 10 µM concentration of E-4031. Control experiments applying E-4031 to DPhPC lipid bilayers

without hERG did not produce ion currents. Each set of experiments was repeated at least three times for astemizole and E-4031.

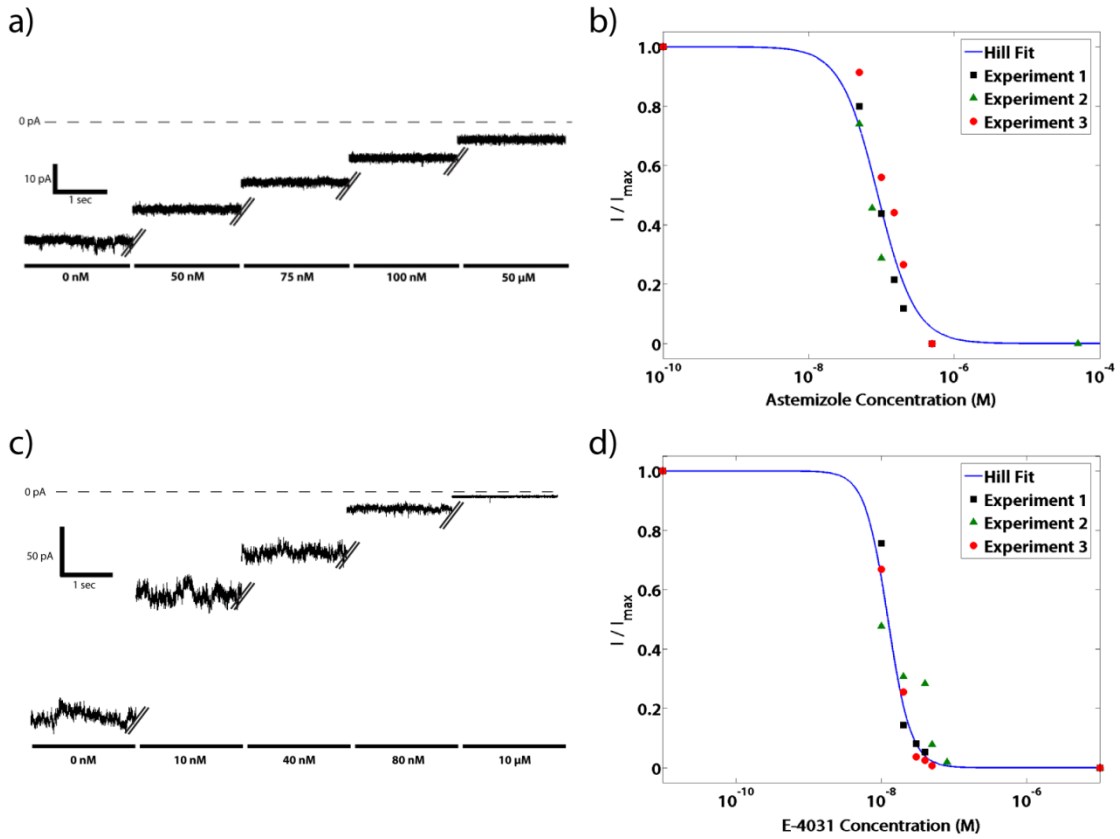

Figure 4-5. (a) Dose-dependence effect of astemizole on hERG currents. hERG currents measured following sequential application of solutions with increasing astemizole concentration shows dose-dependent inhibition, with a small amount of measured unblockable current remaining at high (50 µM) astemizole concentration (-100 mV applied). (b) This unblockable current was subtracted from each measured current and the difference was normalized to the current measured before application of astemizole to result in the ratio I/I_{max}. This ratio was plotted versus astemizole concentration and fit to the Hill equation (see text) to find the concentration at 50% conductance, IC_{50}. (c) hERG currents measured in increasing E-4031 concentration, with a small unblockable current at high (10 µM) E-4031 concentration (-100 mV applied). (d) As with astemizole, the normalized blockable current ratio, I/I_{max}, was plotted versus E-4031 concentration and fit to the Hill equation to the IC_{50} for E-4031.

To analyze the measured currents from each experiment, any unblockable current measured at the maximum concentration was subtracted from the current recorded for each concentration to obtain the magnitude of drug-responsive current. The ratio of this drug-responsive current to the maximum blockable current (obtained before administration of any drug) was plotted as a function of concentration to obtain dose-response plots for astemizole and E-4031 (Figures 6a and 6b). Curves were fit to these plots following the Hill equation:

$$\frac{I}{I_{max}} = \frac{1}{1 + 10^{(\log_{10} IC50 - \log_{10} X) * Hillslope}}$$

to obtain IC50 values of 90.1 nM for astemizole and 13.3 for E-4031. The Hill coefficients calculated for astemizole and E-4031 were 1.53 and 2.65, respectively. These values are similar to those reported in literature from whole-cell patch clamp experiments, which have been reported in ranges from 1 nM-70 nM for astemizole and 8 nM - 48 nM for E-4031[78,90,93].

As reported by Schindler and Quast, we also did not observe rectification[79].

One consideration regarding functionality of hERG in planar lipid bilayers is that ensemble kinetic activity and voltage rectification reported in whole-cell patch clamp experiments[94] did not appear with similar buffer conditions and voltage protocols. Currents were ohmic in nature. I-V curves taken after subsequent drug dose administrations revealed that conductance was lowered progressively with each dose, but that conductance itself remained ohmic throughout the experiments (figure 4-6). In bilayers made from monolayers formed at air-water interfaces, Schindler and Quast observed that reconstituted AChR was oriented, but did not display characteristic rectification.

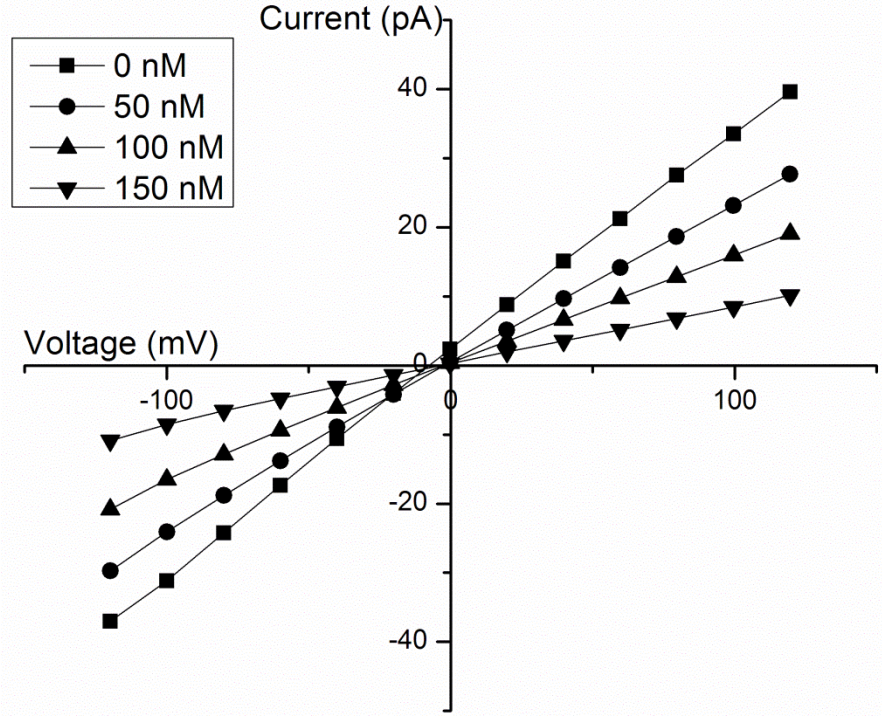

Figure 4-6: I-V curves obtained on a planar lipid bilayer produced with membrane preparations of cells having over-expressed hERG channels. Conductance is ohmic in nature.

Although we did not measure the orientation of hERG in the droplet bilayers, the lack of rectification observation is similar and may suggest that the hERG and AChR channels are affected similarly by their exposure to hexadecane and air, respectively, potentially limiting the applications of droplet bilayers for measurement of ion channel ensembles. Additionally, the conditions in which the membrane preparations were produced may have damaged the proteins in a way that precluded normal voltage gating function in the ion channels. We continue to work to investigate the potential causes of this, including effects of processing, buffers, and membrane co-factors; however, hERG pharmacological studies often do not specifically elicit kinetic activity and rectification[95].

Conclusions

In conclusion, we have shown measurements of the dose-dependent modulation of hERG ion channels reconstituted in droplet bilayers. This is the first time, to our knowledge, that dose-

dependent drug curves for the hERG ion channel have been produced using artificial lipid bilayer technology. Although we did not observe kinetic activity and rectification characteristic of hERG, the droplet bilayer technology is easily implementable and produces reliable pharmacological data. We are currently conducting experiments with other mammalian ion channels and testing their drug response in our bilayer measurement system. Since this platform is scalable and automatable, large-scale screens of ion channel drugs on mammalian and human ion channels can be envisioned.

Fast Fluid Exchange in Partitioned Chambers Supporting Lipid Bilayers Formed By Contacting Monolayers

In chapter two and in a published report[89], we demonstrated that we could fully exchange aqueous solution adjacent to one side of a partitioned droplet lipid bilayer, which was the first time, to our knowledge, that this had been achieved. The rate of fluid exchange was measured to be 20mL/hr. It is desirable to achieve faster fluid exchange rates, since one of the goals of a high throughput platform for the measurement of ion channels in lipid bilayers includes the rapid collection of drug response data. Previous work in our group demonstrated dosage response curves from drug inhibitors on reconstituted TRPM8[83] and hERG channel proteins in lipid bilayers. The method of drug delivery in those earlier works relied upon the diffusion of small volumes (typically 1 – 2 µL) of concentrated drug solutions into aqueous compartment volumes of 200 – 300 µL. The production of dose-dependent curves using this method typically required 40-60min. We initially set out to increase the rate of fluid exchange so that we could increase the throughput of dose dependent data collection in droplet lipid bilayer chambers. In doing so, a new method of forming lipid bilayers in partitioned chambers was devised: one that could support higher rates of fluid exchange. To test this new method, we sought to form lipid bilayers with reconstituted voltage-dependent anion channel (VDAC), which is a mammalian ion channel that is expressed in mitochondria in single chamber experiments and parallel chamber experiments.

Experimentation

Bilayer formation apparatus

Droplet bilayer array plates incorporating 8 individual measurement chambers of the same basic construction as described in chapter 2 was employed in this work. Briefly, array plates were made from 0.125" thick acrylic plates (McMaster-Carr) and 0.003" thick Delrin film (McMaster-Carr). Two acrylic pieces were laser cut to form fluidic wells and channels by stacking them vertically and sandwiching the Delrin. Apertures (200 - 300μm in diameter) in the Delrin film were cut using a 25 W CO_2 laser cutter (Universal Laser Systems) to connect the wells formed by the top and bottom acrylic pieces. Aperture sizes were measured microscopically. Each measurement chamber consisted of two outer wells (an inlet and an outlet for aqueous solution) that were connected through a channel in the bottom acrylic piece to create a single channel. A center measurement well was connected to the channel through the aperture in the Delrin film; lipid bilayers formed through this aperture. The acrylic plates and the hydrophobic Delrin partitions were bonded together by placing double-sided very high bond acrylic foam tape (McMaster-Carr) between the solid acrylic top and bottom plates and the hydrophobic Delrin partition was placed in the center.

Bilayer formation method

Aqueous buffer contained 250 μg/ml of 1,2-diphytanoyl-*sn*-glycero-3-phosphatidylcholine (DPhPC) (Avanti Polar Lipids) in solution (1M KCL, 5 mM $CaCl_2$, 10 mM HEPES, pH 7.2, all chemicals from Sigma) and was prepared to make liposomes using an extruder and a 200 nm pore-size filter (Avanti Polar Lipids). 500 μL of this solution was loaded into the lower aqueous compartment of the bilayer chamber, while 50 μL of n-decane (Sigma) was loaded into the center measurement well of each bilayer chamber in use. The method of bilayer formation differed from the method described in the previous three chapters; it did not involve sessile droplets on pin tool electrodes being brought into contact with the lower aqueous/organic

interface inside a measurement well after being coated with a surface monolayer. Instead, 25 - 50 µL of the liposome containing solution was pipetted directly into the measurement well after the n-decane was deposited. Self-assembly of lipid monolayers preceded the formation of lipid bilayers upon contact. A 16 gauge Ag/AgCl pin was then lowered through the organic phase and into the deposited aqueous phase in the measurement well, after which bilayer and ion channel measurements could be made electrically. Single well measurements were made by placing a ground Ag/AgCl electrode into the lower compartment of the bilayer chamber, and by using an Axopatch 200B amplifier and digitized using a Digidata 1332A (both from Molecular Devices) to apply and record signals. Data was sampled at 5 kHz. For parallel bilayer measurements, an array of Ag/AgCl electrodes was made; 8 measurement electrodes were placed in each of the 8 measurement wells, while 8 ground electrodes were placed in each of the 8 lower aqueous compartments. A 48-channel amplifier (Tecella) was used in taking measurements. Data was sampled at 20 kHz.

Fluid exchange method

Fluid exchange of the lower aqueous compartment was carried out. In single bilayer experiments, we sought to use a conventional 1 mL hand pipette (Corning) to exchange fluid in lipid bilayer chambers. In parallel bilayer experiments, we sought to use an 8-channel 1 mL pipette. By dispensing the full volume of a 1 mL at a typical rate, we sought to conduct fluid exchange at a rate of about 30 mL/min, which greatly exceeded the rate that we achieved previously, which was 20 mL/hr. A total volume replacement time of less than two seconds was sought using this fluid exchange rate. Since standard pipetting was employed, the technique should be scalable and easily adaptable for use with pipetting robots. We used a set of pipette tips connected to a vacuum to collect waste fluid in parallel bilayer experiments. In single bilayer experiments,

waste fluid was collected using a paper wipe (Kimberley Clarke) with care taken so that fluid did not leak into the measurement well.

VDAC measurement

Purified VDAC protein was given to us by Professor Jeff Abramson, Dept. of Physiology, UCLA. We obtained a 100 µM stock solution in the same buffer solution described above, which we diluted to 0.5 µM using the liposome solution described above. This VDAC/liposome solution was then added to the measurement well of each bilayer measurement chamber following the addition of n-decane to the wells. VDAC is a 32 kDa mitochondrial channel that has a predominantly open channel conductance of about 4 nS at low magnitude voltage holding potentials (<-30 mV, >+30 mV), while it has a partially open channel conductance of about 2 nS at higher magnitude voltage holding potentials in the buffer conditions that we used[96]. The simple addition of the VDAC/liposome solution into one side of the bilayer chambers was all that was required to produce measurements (buffer reagents were the same on both sides of the bilayer). To test the system operation, fluid exchange with an inhibitor of VDAC was flowed into the lower aqueous compartment of the chambers after stable VDAC current was observed. The inhibitor was a phosphorothioate randomer, G3139 (Trilink Industries) that has been shown to reversibly block ion currents from VDAC[97]. In initial experiments, 30 µM of G3139 solution was used. Blocker solution was diluted with the 1M KCL buffer described above.

Results and Discussion

Fluid exchange rates in lipid bilayer chambers that employed sessile droplets from pin tool electrodes were found to be limited to tens of mL/hour before causing instability and eventual fusion in the chambers that we constructed. While it is certainly possible that a modification of the chamber design could lead to higher fluid exchange rates in such a system, researchers in our

lab devised a new bilayer formation technique using the same chamber design that could support much faster fluid exchange rates. The method involved bilayer formation by contacting monolayers, just as in the earlier method. However, instead of utilizing a (1-2 µL) droplet hanging from an Ag/AgCl pin electrode to first form a lipid monolayer and then bring into contact with another lipid monolayer through an aperture inside of an organic solution containing measurement well, the new method simply involves pipetting a volume (20-50 µL) of liposome solution directly into the organic solution containing measurement well. An Ag/AgCl electrode is then inserted directly into the liposome solution to make electrical measurements (along with the ground electrode already inserted into the lower aqueous compartment). This method offered an advantage of being more robust to misalignment over the bilayer aperture in the hydrophobic partition, since the aqueous solution volume covered the entire upper surface of the hydrophobic partition. It is not currently known why this bilayer formation method is more robust to fast fluid exchange of the lower aqueous compartment than the method employing sessile droplets. Nevertheless, lipid bilayers could typically be formed and measured after 5 or more instances of 1 mL dispensation using a hand pipette at a normal rate (typically about 0.5 mL/sec).

VDAC was successfully measured in single chamber lipid bilayer experiments (figure 5-1). Exchange of the fluid in the lower aqueous compartment with 30 µM G3139 solution led to a cease in step currents equal to the conductances of single VDAC channels. A gradual decrease of measured ion current over the course of about 10min was also observed, while bilayers size remained stable. In parallel lipid bilayer experiments, large currents which were partially blocked by G3139 were also observed. Experiments with parallel lipid bilayer arrays are ongoing.

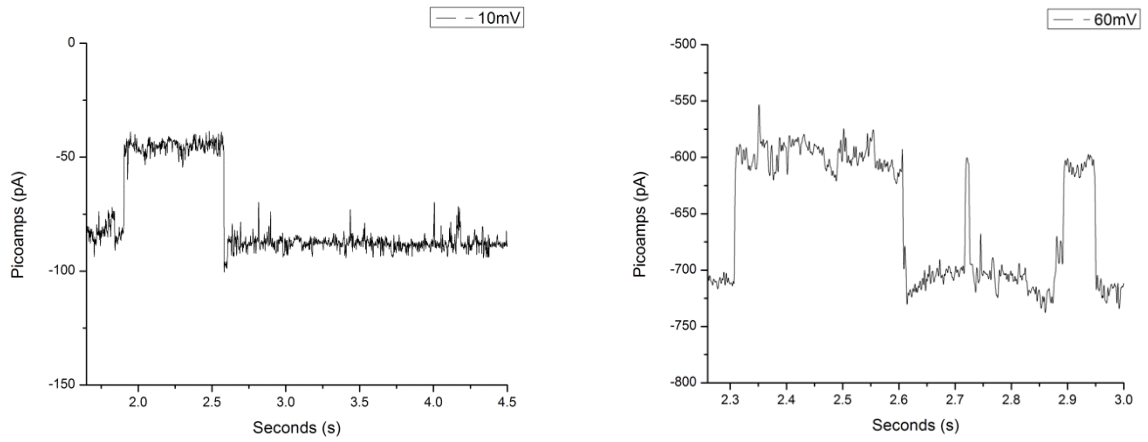

Figure 5-1. VDAC signal in lipid bilayer chambers before fluid exchange with blocker solution by standard hand-pipetting. Left: at low applied voltage, step changes indicating conductances of about 4 nS were observed. Right: At higher magnitude voltage holding potentials, step changes of about 2 nS were observed. Immediately after fluid exchange with blocker, no more step changes were observed, and flat currents were observed to decrease over 10min.

Conclusion

We noted that fluid exchange in droplet lipid bilayer systems discussed in previous chapters was limited to rates of about 20 mL/hr. We were able to perform fluid exchange at rates of at least several mL/min using a new method of forming bilayers through partitioned chambers that is also amenable to high throughput fluid handling systems. Measured bilayers were stable over the span of at least 5 compartment replacement cycles. Ion channel activity, such as those from VDAC, could be measured and inhibited with blocker solution that fully replaced initial perfusion buffer in seconds. Faster rates of fluid exchange may aid in increased throughput drug testing on ion channels.

Microfluidic Droplet Lipid Membrane Permeation Assay

Membrane permeation assays play an important role in drug discovery to assess passive transport of pharmaceutical compounds across biological membranes. Passive permeation through cell membranes is the most common method of transport for drugs to enter cells[98]. Currently, the most commonly used high-throughput permeation assays are the Caco-2 assay and the parallel artificial membrane permeation assay (PAMPA)[99]. The Caco-2 assay employs a chamber (figure 6-1) divided by a membrane on which a monolayer of Caco-2 cells grows to confluence. When this occurs, neighboring cells form tight junctions which can force compounds from one compartment (donor) to travel through the Caco-2 cell membranes into the neighboring compartment (acceptor) in order from transport to occur. This method is commonly used by drug companies, but relies upon the culturing of Caco-2 cells, which can often take weeks and requires regular feedings[99]. Futhermore, the tightness of junctions formed by cells in the monolayer can vary within and across test chambers, which can result in leaks of compounds across compartments. Also, depending on the drug, certain transporter proteins on the cell membranes of Caco-2 cells may provide an active transport component which is typically not desirable. Finally, Caco-2 cell membranes are not easily modified, and can make for poor modeling of permeation through various tissue having cell membranes that not similar to those of Caco-2 cells[99]. While other cell lines that can produce monolayers with relatively tight junctions on filter surfaces, Caco-2 cells are used overwhelmingly[99].

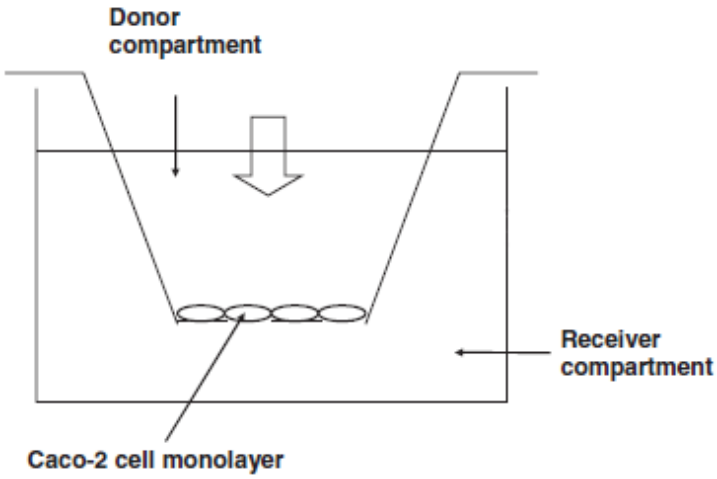

Figure 6-1. A diagram of a Caco-2 test chamber. Compounds must permeate through a monolayer of cells; drug permeability is calculated from the change in receiver compartment concentration over time.[99].

PAMPA assays employ artificial membranes made of a mixture of lipid and inert organic solvents supported by hydrophobic filter[100]. Each membrane separates two compartments: a drug donor compartment and a drug acceptor compartment, in a well of a multi-well plate. Chambers are often assembled by sandwiching together separate donor and acceptor plates. Assembled chambers are incubated before being disassembled at pre-specified time intervals to measure the concentrations of compound in each of the compartments, after which permeation is calculated[101]. PAMPA offers some advantages over the Caco-2 assay, such as not needing to culture cells, being able to modify the types of lipid in the hydrophobic membranes, and the absence of active transport mechanisms[101]. Major difficulties with the PAMPA assay include the thickness of the lipid/organic membranes, the amount of incubation time needed (typically hours), and non-specific binding of compounds to the hydrophobic support filters in the membranes[99]. In particular, PAMPA membranes are far thicker than the cell membranes which they are intended to simulate; often they at least 100 μm thick[98], while cell membranes are typically about 4 nm-5 nm thick[102].

Here, we describe a microfluidic method for a diffusion-based permeation assay using droplet lipid membranes. Nanoliter-sized donor and acceptor aqueous droplets are alternately formed at a cross-junction in cross-flowing hexadecane containing lipids. Subsequently, at the downstream channel, selective removal of oil through hydrophobic porous sidewalls induces the contact of two monolayers, creating arrayed planar lipid bilayers between donor and acceptor compartments. As a model compound we chose fluorescein (molecular weight Mw = 332.32 g/ mol) and measured the variation of fluorescein concentrations in the droplets over time by fluorescent microscopy using donors at three different pHs: 5.4, 6.4, and 7.5. We built a simple model of the passive diffusion between the arrayed droplets, and from the measured data we calculated a permeability coefficient of ~6.0×10^{-6} cm/s, which is found to be close to the values reported in literature[103]. We could also measure the permeation of a pharmaceutical compound, caffeine (Mw = 194.19 g/mol) by using UV-VIS microspectrophotometry and obtained a permeability of ~ 2.1×10^{-6} cm/s.

In chapters 1-3, we described the use of droplet-based artificial lipid bilayer formation and measurement, which we demonstrated through electrophysiological measurements of bilayer membranes and reconstituted membrane proteins. In this chapter, we have extended the use of droplet lipid membranes. Aqueous droplets are immersed in hydrocarbon oil, and lipids mixed with the organic phase and/or aqueous solution with dissolved liposomes have been employed to allow for the self-assembly of lipid monolayers at the aqueous/organic interfaces. Droplets are then brought into contact with each other, creating lipid membranes or possibly a lipid bilayer. Despite the enormous potential of droplet bilayer systems described earlier, they all involved the application of electric potentials to move charged ions to the lipid membranes and through ion channels. Passive permeation of compounds through lipid membranes, however, does not use

electric potentials for transport. As a result, the designs of the systems described in previous chapters are not optimal. The droplet sizes in those systems are typically 0.5 µL-2.5 µL, which, if modeled as spherical droplets, means that they have radius sizes about 490 µm-840 µm. It has been shown that transport across planar lipid membranes is diffusion rate limited, and that even in systems that employ mechanical stirring, and unstirred layer with thickness (>200 µm) exists; this unstirred layer presents resistance to transport that can effect permeation calculations[104]. Since mechanical stirring of the droplets in a droplet membrane system is impractical, it is necessary to use droplet sizes that are no larger than the unstirred layers that occur even in stirred systems. We therefore needed to make a microfluidic system and could make droplet lipid membranes with droplets on the order of 5 nL or less. We sought to have precise control over fluid volumes and flow speeds, which required the used of syringe pumps. The system that we build is, to our knowledge, the first that uses droplet lipid membranes in a quantitative assay to determine the membrane permeability of compounds.

Here, we report a passive membrane permeability assay using high-throughput formation of droplet lipid membranes in a microfluidic channel on a chip. The microfluidic network has two droplet generators that can generate smaller droplets at higher throughput than in the conventional pipetting technology. We first generated nanoliter-sized donor and acceptor aqueous droplets alternately in an oil/lipid solution mixture at a cross-shaped channel. Next, excess oil was selectively aspirated through pseudo-porous side walls to induce the contact of neighboring aqueous droplets covered by lipid monolayers, producing parallel droplet lipid membranes between donor and acceptor compartments. We fluorometrically measured permeation of fluorescein molecules using donor drops at three different pHs, and calculated permeability values at the droplet membranes using a model based on diffusion transport

between arrayed 2-5 compartments. We also measured the permeation of caffeine between two aqueous compartments at physiological pH by using UV-VIS photomicrospectroscopy.

Experimentation

Figure 6-2a schematically shows the layout of the microfluidic channels. This geometry consists of a sequence of two key elements: a cross-junction with two droplet generators at the upstream, where aqueous donor and acceptor droplets are generated into cross-flowing organic lipid solution (Fig. 6-3c); a pseudo-porous main channel at the downstream, where excess oil between arrayed droplets is selectively withdrawn to form droplet lipid membranes (Fig. 6-2d). The cross-junction and main channel are 200 μm in width, while subchannels in the side walls of the main channel are 20 μm in width and are placed at 50 μm pitch over 3 mm, with a uniform depth of 100 μm. This geometry was microfabricated on a synthetic quartz chip by deep reactive ion etching (Fig. 6-2b), and the surface with microfabricated grooves was fusion bonded with another chip to prepare the confined channel network. Prior to use, the entire channel was modified to be hydrophobic by octadecyltrichlorosilane to enable both formation of aqueous droplets and selective removal of oil through sub channels.

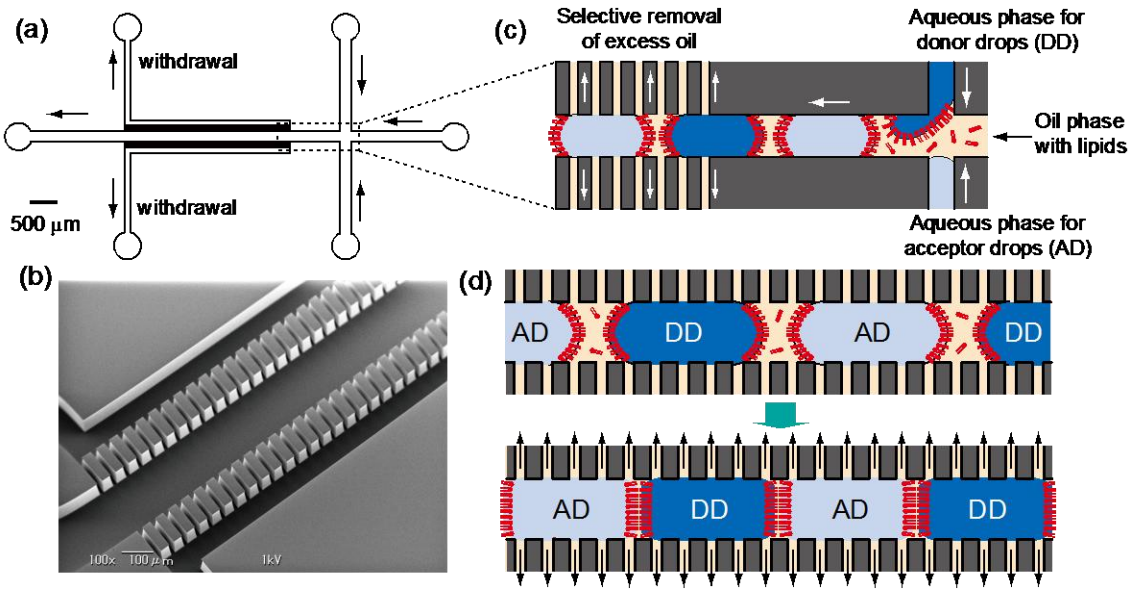

Figure 6-2.(a) Schematic of the channel layout comprised of two T-shaped droplet generators and pseudo-porous channel for selective removal of oil phase.(b) A scanning electron microscopy (SEM) image of the main channel (width 200 µm) with side channels (width 20 µm) for the removal of oil. (c,d) Schematic illustrations of the formation and accumulation of aqueous droplets in carrier oil phase for making bilayers between arrayed between donor and acceptor droplets, not to scale.

For the organic phase, DOPC (1,2-dioleoyl-*sn*-glycro-3-phosphocholine, Avanti Polar Lipids) phospholipids were dissolved in hexadecane (Sigma-Aldrich) to make a 5 mg/mL solution. The lipids, which were originally dissolved in chloroform, were dried to a thin film under a continuous stream of argon gas, before being resuspended in the hexadecane solution. Unless otherwise stated, all chemicals used in experiments were purchased from Sigma-Aldrich. For the measurement of fluorescein permeation, we prepared three donor aqueous phases (250 uM fluorescein, 350 mM KCl, 10 mM HEPES) at three different pHs (pH 5.4, 6.4, and 7.5). An aqueous buffer at pH 7.5 (350 mM KCl, 10 mM HEPES) was used for the acceptor phase. In the measurement of caffeine permeation, 10 mM caffeine aqueous solution (10 mM caffeine, 350 mM KCl, 10 mM HEPES, pH 7.4) was used as a donor phase. The acceptor phase was the same buffer without caffeine at pH 7.4. Gastight glass syringes (Hamilton) were filled with those solutions. For infusion and withdrawal of those solutions, we employed three syringe pumps that

can operate two syringes simultaneously (KDS 220 and Legato 200, KD Scientific). Fluorescence and bright field images were observed and recorded with a Nikon Eclipse Ti inverted microscope; excitation light at was produced from a mercury lamp while emission through a FITC filter was captured with a cooled digital CCD camera (CoolSNAP HQ2, Photometrics). Objective lenses of 4x and 10x were used. The software used for image acquisition was NIC-Elements AR (Nikon). The captured fluorescent images were processed using ImageJ (NIH).

Nanoliter-sized acceptor and donor droplets of similar sizes were alternately formed from the two inlets when two aqueous streams were supplied at the same flow rate into the cross-flowing organic stream under low Reynolds and Capillary number conditions. Although the generation frequency can be increased as high as 10^3-10^4 Hz at higher flow rates, we typically set low flow rates so as to produce plug-shaped aqueous droplets of ~5 nL in the dripping regime at moderate frequency below 10 Hz (Fig. 6-3a). This slow generation at low flow rates functions to minimize the movement of droplets by residual pressure-driven stream when the infusions by the syringe pumps were stopped. Also, we set the aqueous flow rate Q_w and the oil flow rate Q_o to satisfy $Q_w/Q_o = 0.1–0.2$ so that the prepared droplets can be kept separated from neighboring droplets in the main channel. Arrays of alternating droplets from the two aqueous streams could be formed; in addition to an alternating ABAB sequence, other sequences like AABAAB could also be made when two streams were driven at different flow rates, although the sizes of acceptor and donor droplets are varied.

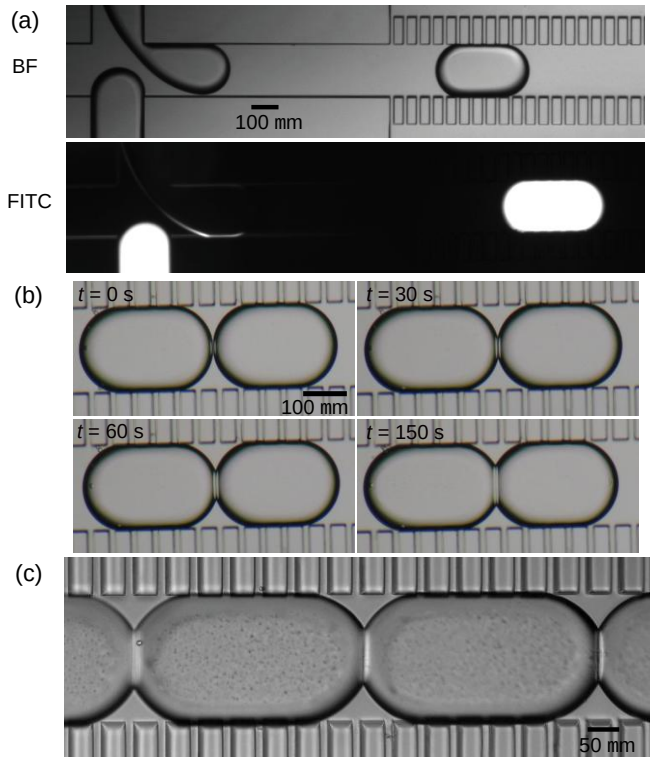

Figure 6-3. Formation of aqueous droplets and droplet lipid membranes in a microfluidic channel. (a) Formation of fluorescent donor droplets and non-fluorescent acceptor droplets at a cross junction observed in bright-field (BF) mode (top) and FITC mode (bottom). (b) Growth of a planar lipid membrane at the interface between two stationary aqueous droplets. (c) Arrayed droplet lipid membranes between stationary donor and acceptor droplets.

After the infusion of fluids was stopped, the droplets were kept separated from neighboring droplets in the main channel for 20–30 seconds so as to stabilize the formation of lipid monolayers at the surfaces of the droplets. Without this waiting time, the droplets frequently fused upon contact. Then, the withdrawal pump was turned on and driven for a short amount of time (typically < 10 seconds) to selectively aspirate the organic phase in the main channel and to carry the droplets slowly to induce the contact of neighboring droplets. We could selectively remove the organic phase without aspirating the aqueous droplet phase because the Laplace pressure in the hydrophobic pseudo-porous sidewalls prevented the intrusion of aqueous phase into the narrower channels. Upon contact, the droplets did not coalesce, and lipid membranes were formed at the interfaces. We observed the gradual increase of membrane area over a few

minutes (Fig. 6-4b). Thus, we could produce 1-4 parallel lipid membranes between 2-5 droplet interfaces in the microfluidic channel (Fig. 6-4c).

We confirmed that the membranes formed in the microfluidic channel were in fact lipid bilayers by observing the permeation of calcein through droplet membranes in the presence of the transmembrane nanopore magainin 2. As reported in (Tamba, 2010), vesicles containing lipid bilayers made with DOPC and with low concentrations (<10 μM) of magainin 2 are highly permeable to calcein in buffers at neutral pH. Also reported was that in the absence of magainin 2, calcein did not permeate through the vesicle membranes. In our experiments, we loaded fluorescent and non-fluorescent aqueous solutions with magainin 2 to a final concentration of 32.4 μM. Fluorescent solutions contained calcein at a concentration of 250 μM. Both fluorescent and non-fluorescent solutions were made with the same 350 mM KCL buffer solutions described earlier, at pH 7.4. Aqueous droplets loaded into the microfluidic chamber were surrounded in hexadecane solution with dissolved DOPC at concentration of 25 mg/ml. As shown in figure 6-4, we did indeed image the permeation of calcein across the lipid membrane separating the fluorescent donor droplet and the non-fluorescent acceptor droplet. In similar experiments conducted using the same conditions but in the absence of magainin 2, we did not observe any evidence of calcein permeation. We also performed off-chip electrophysiological measurement and confirmed that the set of aqueous and organic solutions that we used could indeed support low-resistance (leaky) bilayers, most probably due to the presence of reconstituted magainin 2 pores. We employed calcein in experiments specifically designed to verify if lipid membranes separating aqueous droplets in the microfluidic chamber were indeed lipid bilayers, due to calcein's low permeability across lipid bilayers in neutral pH. All other fluorescence experiments described in this work were conducted using fluorescein.

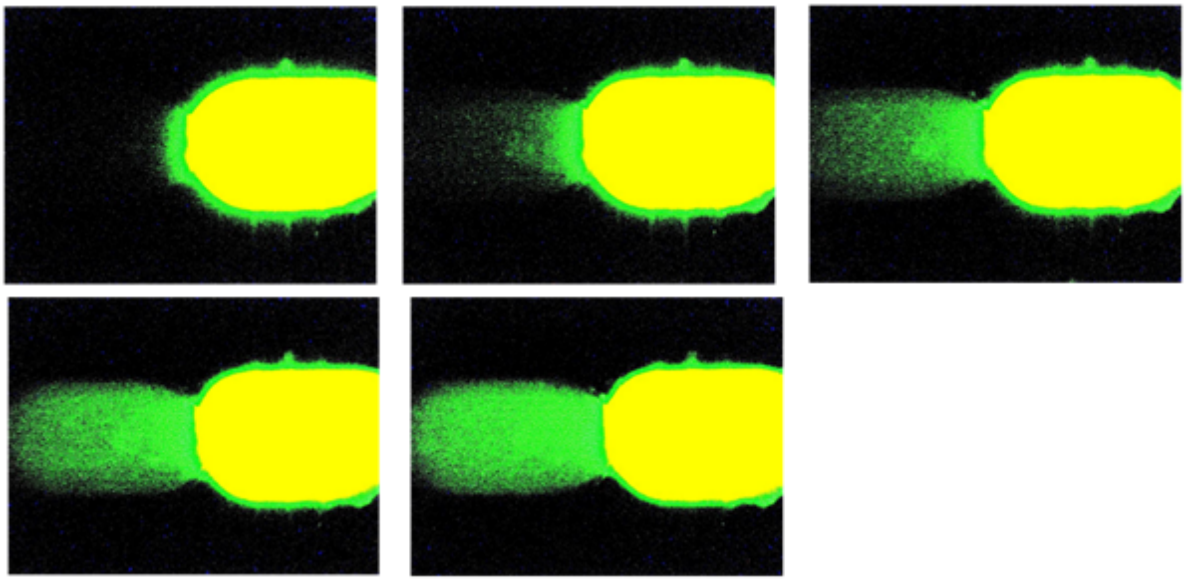

Figure 6-4. Observation of calcein permeation from a donor droplet to an acceptor droplet across a lipid membrane in the presence of magainin 2 nanopore protein. Images were taken in time progression. Top-left: t = 0min; top-middle: t = 20hr 47min; top-right: t = 48hr 24min; bottom-left: t = 72hr 50min; bottom-middle: t = 96hr 49min

To calculate the concentration of fluorescein in the microfluidic droplets from fluorescence images, we conducted a series of calibration experiments designed to report the fluorescence intensity of fluorescein at various known concentrations in aqueous solutions having various pH values. In particular, we examined the intensity of fluorescein solutions with measured concentrations of 25 µM, 50 µM, 100 µM, 200 µM, and 250 µM in buffer solutions with measured pH values of 5.4, 6.4, and 7.5. Care was taken so that spatial intensity differences arising from varying excitation or emission sensing properties of the fluorescence microscope was minimized. This was done by taking a series of fluorescence calibration data at different positions of the microfluidic channel corresponding to the positions of droplets in permeation experiments. Additionally, images were captured using a shutter speed 20 ms-50 ms to minimize photobleaching. With a set of discrete data points mapping fluorescein concentration to fluorescence intensity, we were able to fit the data to lines of best-fit, which were linear. An example of a calibration curve is given in figure 6-5.

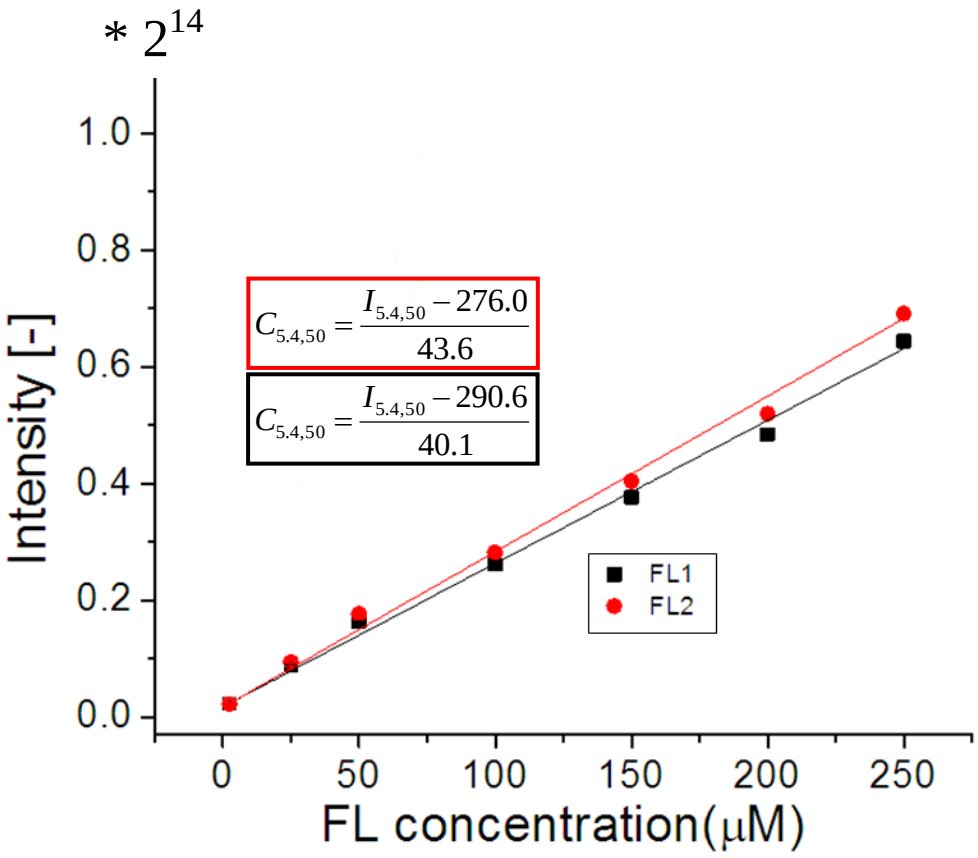

Figure 6-5: Calibration curves mapping mean intensity of fluorescein-containing droplets at pH 7.4 to concentration of fluorescein. The two different linear fits represent data taken from two different locations in the microfluidic chamber, and results from the fact that fluorescence intensity varied with position.

To calculate the permeability of fluorescein across droplet membranes formed in the microfluidic channel, we fluorometrically measured the time-lapse variation of fluorescein concentration in arrayed donor and acceptor compartments. For example, Figure 6-6a is an array of five droplets, in which four parallel droplet membranes are formed with two fluorescent donor droplets (DD1 and DD2) at pH 5.4 and three non-fluorescent acceptor droplets (AD1, AD2 and AD3) at pH 7.5. After waiting for the formation and growth of the droplet membranes for around 1-2 min, we started (at t = 0 in Fig. 6-6c) time-lapse capturing of fluorescent images at a time interval of 30s. The fluorescent intensity in donor droplets gradually decreased over time, suggesting that the donor droplets were losing fluorescein molecules. On the other hand, the

fluorescence intensity in acceptor droplets increased over time, suggesting the acceptors were gaining fluorescein molecules. Finally, after about 20 min, the acceptor droplets became much brighter than the donor droplets (Fig. 6-6b) for reasons explained below. We also observed that the acceptor droplet adjacent to two droplet membranes (AD2) became brighter more rapidly than the other two acceptors adjacent to only a single droplet membrane (AD1 and AD3). All of these phenomena clearly prove that fluorescein molecules were transported from donor to acceptor droplets. From the variation of fluorescence intensities and the concentration calibration curves prepared earlier, we obtained time-concentration curves for each of five droplets. Thus, we could see clear evidence permeation of fluorescein in 10–20 min.

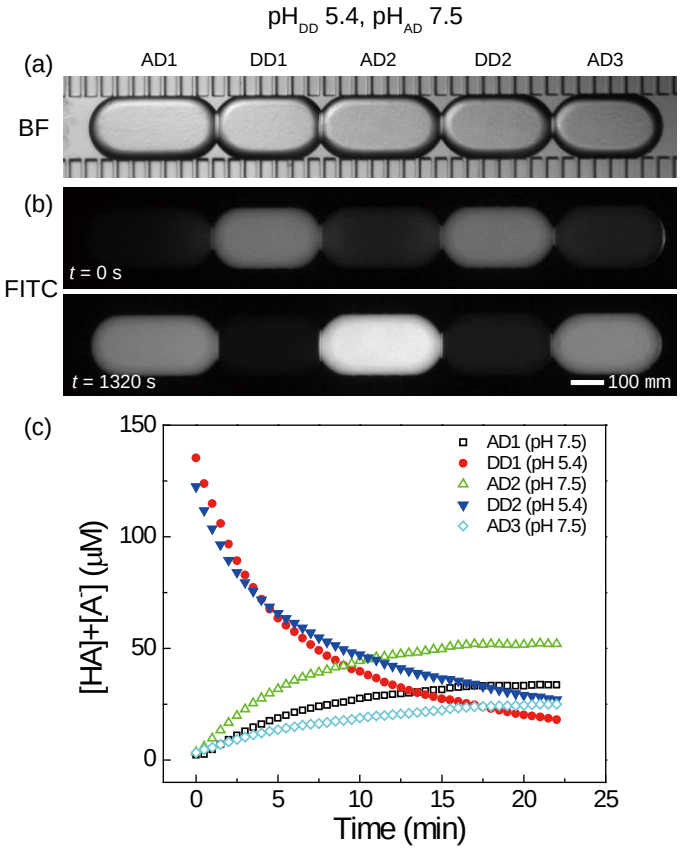

Figure 6-6. Measurement of fluorescein permeation in an array of five droplets comprised of two donor droplets (DD)at pH 5.4 and three acceptor droplets (AD) at pH 7.5. (a) A bright field microscopy image of the five droplet array. (b) Time-lapse fluorescent microscopy images at start and end of the measurements (c) Measured variation of fluorescein concentrations in droplets over time.

In contrast, we observed significantly slower permeation when we used donor droplets at higher pH. Figure 8a is an array of four droplets, with two acceptor and two donor droplets, both at pH 7.5. In this experiment, variation of fluorescent intensity in the droplets was very slow. Although a slight variation of intensity was observed over time, there was a significant difference in the intensity between the donor and acceptor droplets even after 2 hours after the formation of the droplet membranes (Fig. 6-7b). This suggests that the permeation of fluorescein is slow when pH levels are high in both donor and acceptor droplets, as supported by the time vs. concentration graph in Fig. 8c. In this experiment we also found that the concentration in the acceptor droplet adjacent to two droplet membranes increased faster than the one with adjacent to only a single droplet membrane (Fig. 6-7c, inset).

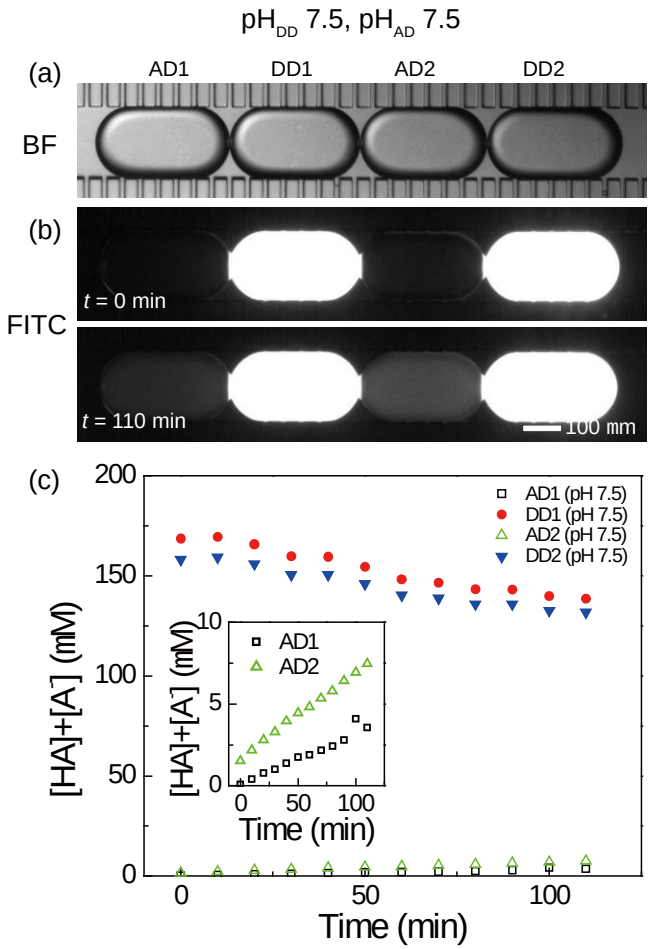

Figure 6-7. Measurement of fluorescein permeation in an array of four droplets comprised of two donor droplets (DD) at pH 7.5and two acceptor droplets (AD) at pH 7.5. (a) A bright field microscopy image of the four droplet array. (b) Time-lapse fluorescent microscopy images at the start and end of the measurements (c) Measured variation of fluorescein concentrations in droplets over time. The inset shows a zoomed-in window of the fluorescein concentrations in two acceptor droplets.

Discussion

The rate of fluorescence change between acceptor and donor droplets clearly differed in the two experiments described above. This difference can be explained by considering the ionization state of fluorescein molecules in the droplets. The fluorescein that we used has one acid dissociation constant (pK_a) value of 6.4 in water. From this pK_a value and the Henderson-Hasselbalch equation, which is in the form of pH = pK_a + log[A^-]/[HA], we can expect that fluorescein molecules are predominantly (~ 90.9%) in a more charge neurtral form at pH 5.4 and

is less fluorescent. In the aqueous solution at pH 7.5, they are predominantly (~92.6%) dissociated and fluoresces strongly. On the other hand, it is known that lipid bilayer membranes are less permeable to charged particles due to the low interior dielectric constant. Therefore, the donor phase at pH 5.4 works as a good source of permeable, non-charged particles. In addition, the acceptor phase at pH 7.5 works as a good sink because most of the incoming non-charged fluorescein molecules become dissociated and do not return to the donor phase. This explains the faster concentration variation in the first experiment. Additionally, after about 20 min, when the concentration of fluorescein in acceptor droplets and donor droplets reached equilibrium, the fluorescence intensity of the pH 7.5 acceptor droplet exceeded that of the pH 5.4 donor droplet since the fluorescein that we used is predominantly fluorescent in its dissociated form. On the other hand, in the second experiment, the fluorescein molecules in the donor phase at pH 7.5 were predominantly dissociated, causing slower permeation across the droplet membranes.

Considering Fick's first law and the fact that the membrane is less permeable to charged species, passive diffusion across droplet bilayers can be expressed as a system of ordinary differential equations. When two droplets have a bilayer at the interface, for example, the passive diffusion among two aqueous droplets and surrounding organic phase is expressed by the following equations:

$$V_{w1}\frac{dC_{w1}}{dt} = k_1\left(C_{w2}'-C_{w1}'\right)+k_2\left(C_o'-C_{w1}'\right)$$
$$V_{w2}\frac{dC_{w2}}{dt} = k_1\left(C_{w1}'-C_{w2}'\right)+k_3\left(C_o'-C_{w2}'\right)$$
$$V_o\frac{dC_o}{dt} = k_2\left(C_{d1}'-C_o'\right)+k_3\left(C_{d2}'-C_o'\right)$$
$$V_{w1}C_{w1}+V_{w1}C_{w2}+V_oC_o = \text{Const.}$$

Where V_{w1},V_{w2}, and V_o are volumes of droplet-1, droplet-2 and the surrounding organic phase, and C_{w1}, C_{w2}, and C_o are the concentrations in each phase, C'_{w1}, C'_{w2}, and C'_o are the concentrations of non-dissociated particles in each phase. Considering these equations together with the Henderson-Hasselbalch equation, we can numerically calculate from the experimental data the k_1, k_2, and k_3, which are the coefficients for the permeation across the droplet membrane, the water-oil interface of the droplet 1, and the water-oil interface of the droplet 2, respectively, as expressed by the following equation.

$$k_i = \frac{D_i S_i}{L_i}$$

Where D is the diffusion coefficient [L^2/s], S is the membrane area [L^2], L is the thickness of the membrane [L]. Permeability P_e is defined as $P_e = k_i / S_i$ [L/s]. This model can be easily enhanced for an array of more than two droplets.

Based on the described permeation model and experimental data, we calculated permeability coefficients for all the interfaces, which are water-oil interfaces and lipid bilayer membranes between donor and acceptor droplets. We prepared a computer program in MATLAB (code attached at the end of this report) that numerically calculates permeability coefficients of all the involved interfaces from a dataset of time-lapse variation of fluorescein concentration in droplets, which was converted by the obtained fluorescence calibration curves described above. The volumes and surface areas of the droplets were measured by image analysis and used in the calculation. The areas of droplet membranes were obtained from the image assuming that the membranes were oval in shape, and were used in calculation as well. Numerically solving for the permeation constants involved solving both sides of the system of differential equations listed above. The differential term $\frac{dC}{dt}$ was calculated using the central

difference formula, with concentration values from 2 time points as such:

$\frac{\Delta(Concentration_{time_{x+1}} - Concentration_{time_{x-1}})}{2*\Delta(\mathrm{time_{x+1}} - \mathrm{time_x})}$. The other parts of the equation could be calculated arithmetically. A cost function evaluated the equality condition of the right and left sides of the equations for various values of rate constants *k* and assigned incrementally favorable outcomes for incremental changes in *k* that brought the system closer to equality. Increment sizes on each *k* value were specified to be 0.0001. An optimization algorithm based on golden-section search supplied incremental changes to *k* values that successively brought right and left sides of the system of differential equations closer to equality. After settling on optimized *k* values from the program results, we could then obtain permeability values.

Figure 6-8 shows the distribution of the permeation coefficients of 11 droplet membranes, which were calculated from 4 experimental datasets each having 1-4 droplet membranes. The average permeability coefficient of the droplet membranes was 4.7×10^{-6} cm/s, which was close to previously reported values measured in *in-vivo* ($(3.0 \pm 0.50) \times 10^{-6}$ cm/s)[103] and *in-vitro* (~5.8×10^{-6} cm/s)[105] experiments using living cells. Our calculated membrane permeability values formed a distribution with the standard deviation of 2.13×10^{-6} cm/s. In further experiments, we found that with donor drops at higher pH, smaller permeability values would be obtained. This result is reasonable since, at higher pH, the percentage of fluorescein molecules in uncharged free-acid form is significantly low, resulting in reduced overall permeation flux as shown. In contrast, permeability coefficients at water-oil interfaces were on the order of 10^{-8}–10^{-9} cm/s, as small as 0.1–1% of the permeability through droplet membranes.

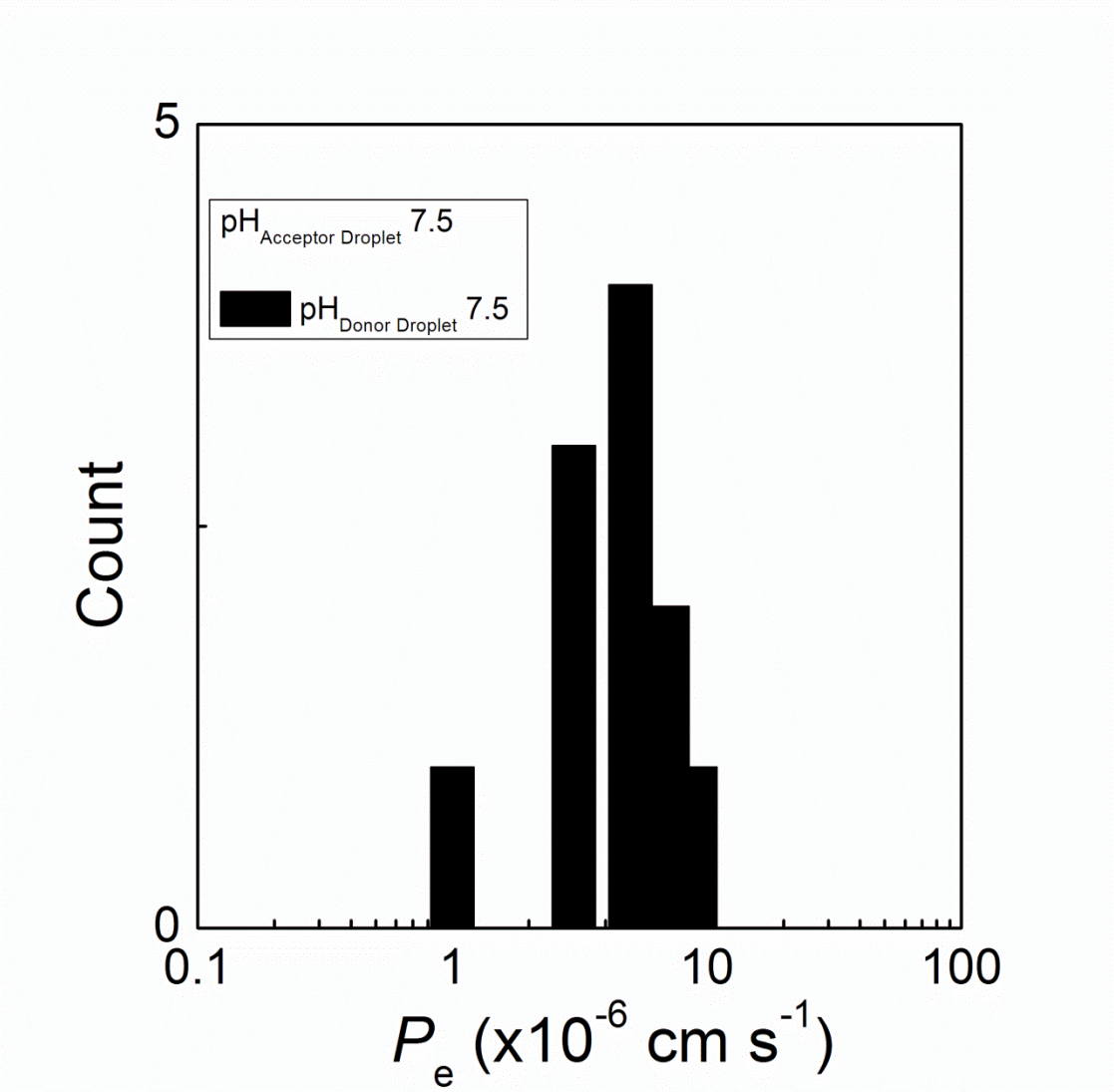

Figure 6-8. Distribution of permeability constants obtained from droplet bilayers. Acceptor droplet and donor droplets had pH 7.5. Mean permeability was 4.7 × 10^{-6} cm/s, with a standard deviation of 2.13 x 10^{-6} cm/s. The number of samples = 11 droplet bilayers.

To illustrate the further potential of our technique, we also measured the permeability of a non-fluorescent compound by using UV-VIS microspectrophotometry in the microfluidic channel. We chose caffeine (M_w = 194.19), a well-known drug commonly used as a popular central nervous system (CNS) stimulant. Caffeine has a pK_a value of 14.0 at room temperature[106] in water, indicating that most of the molecules are in the non-charged form at physiological pH7.4. We prepared a donor droplet of caffeine solution (10 mM caffeine, 350 mM KCl, 10 mM

HEPES, pH 7.4) and an acceptor droplet of an aqueous solution without caffeine (350 mM KCl, 10 mM HEPES, pH 7.4) and made a single droplet membrane at the interface between the two droplets. Right after the formation of the droplet membrane, we found that the absorbance spectrum in the acceptor droplet started to increase, and the absorbance in the donor droplet started to decrease, which indicated the transport of caffeine molecules from the donor to acceptor compartment. Figure 6-9 shows the variation of caffeine concentration in the donor and acceptor compartments. The concentration became nearly the same after about 5–10 minutes. By using the permeation model and the computer program described above, we could calculate a permeability of caffeine of about ~2.1 x 10^{-6} cm/s.

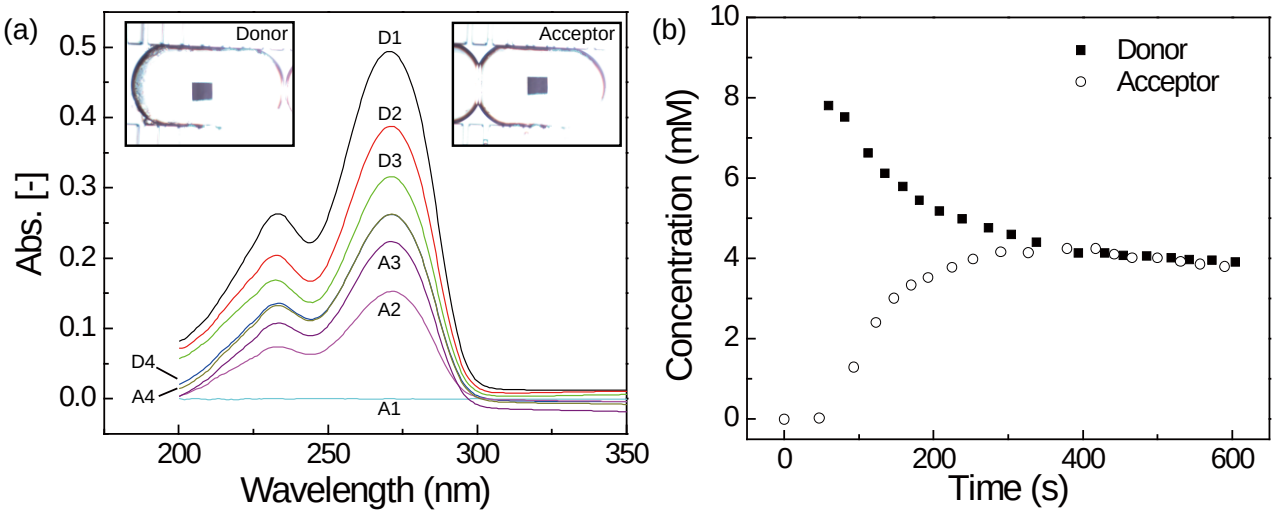

Figure 6-9. Measurement of a permeability of caffeine through a droplet membrane by UV microspectroscopy. (a) Results of time-lapse measurement of the absorbance spectrum in acceptor (A1–A4) and donor (D1–D4) droplets. A1: t = 0 s, A2: t = 123 s, A3: t = 193 s, A4: t = 327 s. D1: 59s, D2: 135 s, D3: 238 s, D4: 394 s. Inset images are donor and acceptor droplets. Solid squares in the middle of each droplet are the measurement area. (b) Time vs. concentration of caffeine in donor and acceptor droplets.

As was the case with the fluorescence experiments, we also mapped absorption to caffeine concentration by creating a set of calibration curves. In all cases, droplets containing no caffeine were taken as reference and set to zero absorbance. Absorption peaks at 271 nm of droplets with measured caffeine concentrations of 0.5 mM, 1 mM, 2.5 mM, 5 mM, 7.5 mM, and 10 mM were

used for calibration points. A best-fit linear curve was fit to the calibration data, and used to determine the concentrations of caffeine in the droplet membrane permeation experiments. Calculation of caffeine permeation then proceeded as described earlier for the case of fluorescein permeation. The apparatus employed to measure the UV absorption of caffeine was a microspectrophotometer (CRAIC, 20/20 PV). With this device, we were able to take absorption spectra measurements covering 200 nm - 400 nm in 10 seconds or less, which we estimated as time point measurements. The device had the additional advantage of being able to produce bright field images and UV spectra of the droplets in the microfluidic channel without modification. Drug concentrations used in UV absorption experiments, from 1 mM to 10 mM, were high relative to traditional permeability assays which typically extend to a few hundred micromolar[99]. This was caused by absorption of UV light through the quartz layers the surrounding the microfluidic chamber; more sensitive measurements would require thinner layers or the use of a material that is more transparent to UV light. To our knowledge and the knowledge of the technical employees at CRAIC Technologies, Inc. that we spoke to, our experiment was the first of any kind to use such a device to track the movement of a drug compound across a lipid or cell membrane of any sort.

To additionally demonstrate the versatility of this technique, we altered the lipid content in the organic solution so that membranes that more closely mimic those of a particular tissue could be used to develop tissue specific permeability calculations. Permeability assays that are tissue specific are commercially available. For example, PAMPA assays that model gastrointestinal epithelium, blood brain barrier, and skin tissue have been developed[101]. We sought to produce permeability calculations of drugs in tissue that closely resembles the blood brain barrier. To do this, we repeated the conditions described earlier for the 2 compartment (donor and acceptor)

model, but instead of dissolving DOPC phospholipid into the hexadecane organic solution that was infused into the microfluidic chamber, we dissolved porcine brain lipid extract (Avanti Polar Lipids). Brain lipid extract has been used in adapting the traditional PAMPA assay to a blood brain barrier model[107]. Using brain lipid extract in our microfluidic assay with microspectrophotometry, we observed the permeation of various drug compounds: caffeine, naproxen, metoprolol, imiprimine, clonidine, and piroxicam (Sigma). The absorption spectra for several drug compounds are shown in figure 6-10. In each case, the magnitude of donor droplet absorption was observed to decrease while the magnitude of acceptor droplet absorption was observed in increase in less than 10 minutes, though the rates of concentration changes clearly differed for different drugs—each donor droplet had a measured concentration of 10 mM at the start of each experiment. It is clear that the microfluidic droplet membrane permeability assay described in this report is versatile to membranes that can model different tissue types.

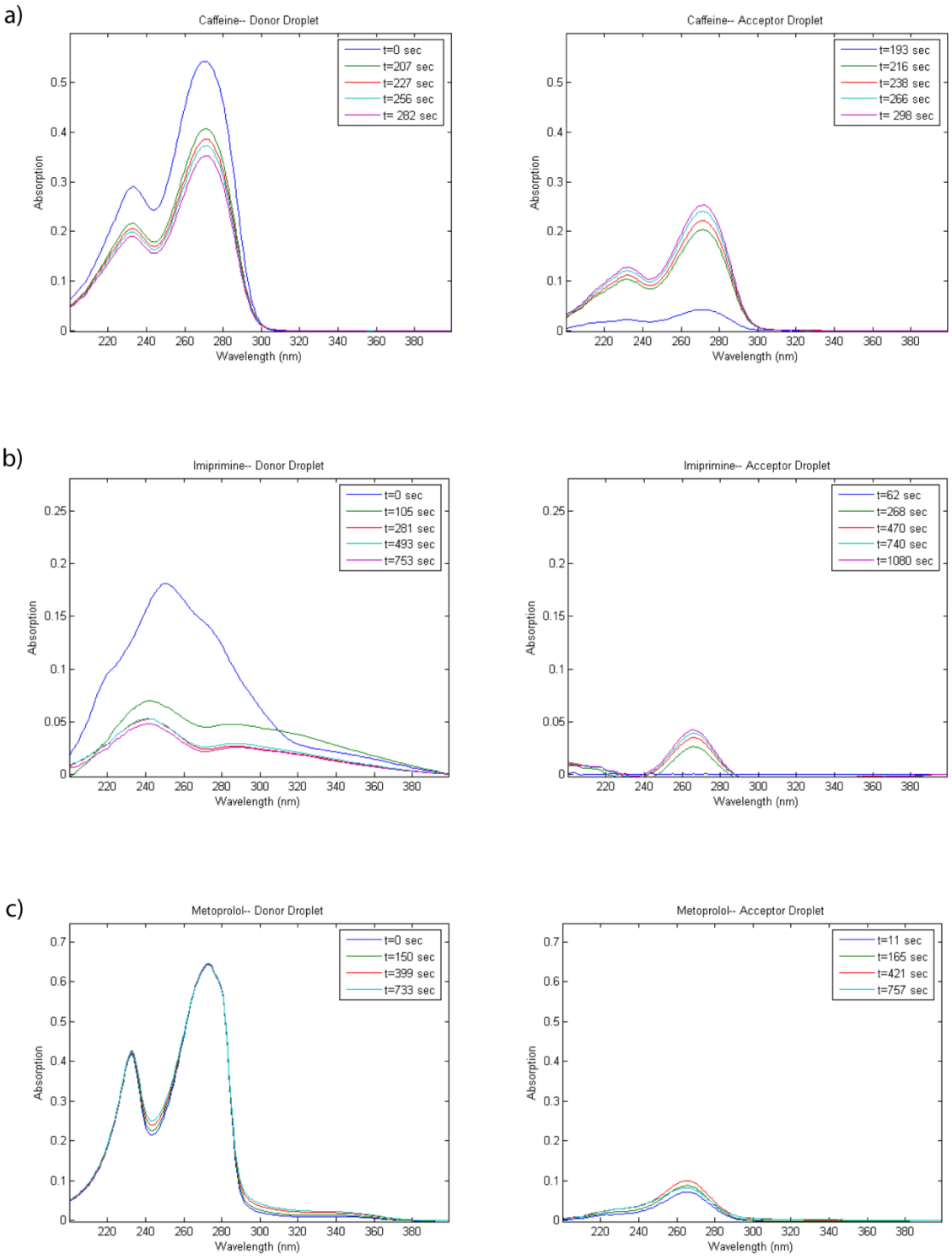

Figure 6-10. Absorption spectra observed in a 2 compartment microfluidic droplet membrane permeability experiment performed using porcine brain lipid extract dissolved in hexadecane to form the organic solution. Data is given for the donor droplets (left side) and acceptor droplets (right side) for 3 drugs: a) caffeine, b) imiprimine, and c) metoprolol.

Conclusions

In conclusion, we have presented a microfluidic platform for a permeation assay using droplet lipid membranes. We have demonstrated the formation of arrays of alternating nanoliter-sized donor and acceptor aqueous droplets, which are subsequently brought into contact by selective removal of excess oil, forming parallel planar droplet lipid membranes between donor and acceptor compartments. We demonstrated that at least part of the membrane has a bilayer structure due to the observed permeation of calcein across membranes incorporating magainin 2 nanopores. We employed a simple multi-box diffusion model was to calculate permeability from experimental data, and the calculated permeability values were reasonably close to the values reported in literature. In addition to the permeation of fluorophores, we calculated the permeation of caffeine (a non-fluorescent drug compound) using a UV-VIS microspectrophotometer, which suggests our platform can analyze the permeability of numerous pharmaceutical compounds. Finally, we demonstrated the versatility of the assay by using it with different lipid membrane types that can be used in modeling different types of tissue. We believe the method presented here could become a basis for a high-throughput permeability assay in drug screening.

PERMEABILITY CALCULATION SOURCE CODE EXAMPLE

```
function [display_matrix, optimized_s, gradient_vector, cost_holder, S, optimized_rate_constants] =
droplet_membrane_permeation_2drops(delta,D,fluorescent_drop_concentrations_vector,
non_fluorescent_drop_concentrations_vector, organic_concentrations_vector)

for z = 1:1:100

    D1 = D + delta;
    D2 = D - delta;

    for i = 1:1:size(D,1)
        masked_D1 = D;
        masked_D1(i) = D1(i); % Increment a single permeation rate constant in the  rate constant vector by
delta
        masked_D2 = D;
        masked_D2(i) = D2(i); % Decrement a single permeation rate constant in the  rate constant vector
by delta
        gradient_vector(i,1) = ( droplet_permeation_cost_ph5_4_2drops(masked_D1) -
droplet_permeation_cost_ph5_4_2drops(masked_D2) ) / (2 * delta); % calculate the gradient value of a
particular incremental change
    end

    S = (0:(0.6e-18):(0.6e-15))';
    cost_holder = zeros(size(S,1),1);

    for i = 1:1:size(S,1)
        cost_holder(i) = droplet_permeation_cost_ph5_4_2drops(D - (S(i) * gradient_vector));
    end

    iterations = 100;

    display_matrix = permeation_search(iterations, cost_holder, S, D, gradient_vector);
    optimized_s = display_matrix(size(display_matrix,1),3);

    %%% calculate new rate constant vector here %%%

    D = D - (optimized_s * gradient_vector);

end

optimized_rate_constants = D

function [iterations_holder] = permeation_search(iterations, cost_holder, S, D, gradient_vector)

a = S(1);
c = S(end);
[min_cost,min_index] = min(cost_holder);
b = S(min_index);

iterations_holder = zeros(iterations + 1,5);  % Initialize display matrix
```

```
iterations_holder(1,:) = [0 a b c golden_section_search(b, D, gradient_vector)];  % Enter initial values into
display matrix

for i = 2:1:(iterations+1)
   if ( (b - a) > (c - b) )   % Checks to see if interval (b - a) is larger than interval (c - b)
      d = d_calculation_b_minus_a([a b c]);  % calculates the value of d accordingly
      if ( golden_section_search(d, D, gradient_vector) < golden_section_search(b, D, gradient_vector) ) %
if f(d) < f(b), reclassify a, b, and c accordingly
         a = a;
         b = d;
         c = b;
      elseif ( golden_section_search(d, D, gradient_vector) > golden_section_search(b, D,
gradient_vector) )  % if f(d) > f(b), reclassify a, b, and c accordingly
         a = d;
         b = b;
         c = c;
      elseif ( golden_section_search(d, D, gradient_vector) == golden_section_search(b, D,
gradient_vector) ) % if f(d) = f(b), reclassify a, b, and c accordingly
         if ( golden_section_search(a, D, gradient_vector) < golden_section_search(c, D, gradient_vector) )
            a = a;
            b = d;
            c = b;
         elseif( golden_section_search(a, D, gradient_vector) > golden_section_search(c, D,
gradient_vector) )
            a = d;
            b = b;
            c = c;
         end
      end
   elseif ( (b - a) < (c - b) )  % Checks to see if interval (b - a) is smaller than interval (c - b)
      d = d_calculation_c_minus_b([a b c]);
      if ( golden_section_search(d, D, gradient_vector) < golden_section_search(b, D, gradient_vector) )  %
if f(d) < f(b), reclassify a, b, and c accordingly
         a = b;
         b = d;
         c = c;
      elseif ( golden_section_search(d, D, gradient_vector) > golden_section_search(b, D,
gradient_vector) )  % if f(d) > f(b), reclassify a, b, and c accordingly
         a = a;
         b = b;
         c = d;
      elseif ( golden_section_search(d, D, gradient_vector) == golden_section_search(b, D,
gradient_vector) )  % if f(d) = f(b), reclassify a, b, and c accordingly
         if ( golden_section_search(a, D, gradient_vector) < golden_section_search(c, D, gradient_vector) )
            a = a;
            b = b;
            c = d;
         elseif( golden_section_search(a, D, gradient_vector) > golden_section_search(c, D,
gradient_vector) )
            a = b;
            b = d;
            c = c;
         end
      end
```

```
    end
    iterations_holder(i,:) = [i-1 a b c golden_section_search(b, D, gradient_vector)];  % Update display
matrix to record new values for a, b, c, and f(b)
end

function [f_result] = golden_section_search(b, D, gradient_vector)
    f_result = droplet_permeation_cost_ph5_4_2drops(D - (b * gradient_vector));  % Calculate function on
which the search is being performed

function [d_result] = d_calculation_c_minus_b(interval_vector)  % Calculate the new d value when (b - a)
> (c - b)
    c = interval_vector(3);
    b = interval_vector(2);
    d_result = (((3 - sqrt(5))/2) * (c - b)) + b;

function [d_result] = d_calculation_b_minus_a(interval_vector)  % Calculate the new d value when (b - a)
< (c - b)
    b = interval_vector(2);
    a = interval_vector(1);
    d_result = b - (((3 - sqrt(5))/2) * (b - a));


function [total_cost] = droplet_permeation_cost_ph5_4_2drops(D)

% Rate constants are multiplied by
% compartment volumes in meters cubed
% D(1) is rate constant from fluorescent drop to non-fluorescent drop
% D(2) is rate constant from non-fluorescent drop to organic solution
% D(3) is rate constant from fluorescent drop to organic solution

fluorescent_drop_concentration = (1e-6) * fluorescent_drop_concentrations_vector;
non_fluorescent_drop_concentration = (1e-6) * non_fluorescent_drop_concentrations_vector;
organic_solution_concentration = (1e-6) * organic_concentrations_vector;

time = time_points_vector;
delta_time = time(2) - time(1);

for i = 2:1:size(time,2)

dC_nfl_dt(i-1) =(1/(5.06e-12))*( D(1)*((.909*fluorescent_drop_concentration(i)) -
(.074*non_fluorescent_drop_concentration(i))) - D(2)*((.074*non_fluorescent_drop_concentration(i)) -
organic_solution_concentration(i)));
dC_fl_dt(i-1) = (1/(5.6e-12))*(-D(1)*((.909*fluorescent_drop_concentration(i)) -
(.074*non_fluorescent_drop_concentration(i))) - D(3)*((.909*fluorescent_drop_concentration(i)) -
organic_solution_concentration(i)));
dC_org_dt(i-1) =(1/(33.84e-12))*( D(2)*((.074*non_fluorescent_drop_concentration(i)) -
organic_solution_concentration(i)) +  D(3)*((.909*fluorescent_drop_concentration(i)) -
organic_solution_concentration(i)));

end

 for i = 2:1:size(time,2)-1
```

```
dC_nfl_dt_star(i-1) = .074*( non_fluorescent_drop_concentration(i+1) -
non_fluorescent_drop_concentration(i-1) ) / (2*delta_time);
dC_fl_dt_star(i-1) = .909*( fluorescent_drop_concentration(i+1) - fluorescent_drop_concentration(i-1) ) /
(2*delta_time);
dC_org_dt_star(i-1) = ( organic_solution_concentration(i+1) - organic_solution_concentration(i-1) ) /
(2*delta_time);

end

% Cost Function
% At each time point, there is a cost associated with each dCn/dt - dCn/dt*. We will define a cost for
each %time point using the magnitude of the vector that contains all the differences. The total cost will
then be %the magnitude of all the time point costs
C_nfl_time_costs = dC_nfl_dt - dC_nfl_dt_star;
C_fl_time_costs = dC_fl_dt - dC_fl_dt_star;
C_org_time_costs = dC_org_dt - dC_org_dt_star;

for i = 1:1:size(C_nfl_time_costs,2)
    time_costs(i) = norm([C_nfl_time_costs(i) C_fl_time_costs(i) C_org_time_costs(i)]);
end

total_cost = norm(time_costs);
```

REFERENCES

1. Schatz, G., *Protein Transport - The Doors to Organelles.* Nature 1998(395): p. 439-440

2. Taylor, J.P., Hardy, J. and Fischbeck, K.H., *Biomedicine - Toxic Proteins in Neurodegenerative Disease.* Science, 2002(296): p. 1991-1995

3. Knust, E., Bossinger, O., *Composition and Formation of Intercellular Junctions in Epithelial Cells.* . Science 2002(298): p. 1955-1959

4. Torres, G.E., Gainetdinov, R.R. and Caron, M.G., *Plasma Membrane Monoamine Transporters: Structure, Regulation and Function.* . Nature Reviews Neuroscience 2003(4): p. 13-25

5. Gouaux, E. MacKinnon., R., *Principles of Selective Ion Transport in Channels and Pumps.* . Science, 2005(310): p. 1461-1465

6. Okuse, K., *Signaling Pathways: From Cytokines to Ion Channels.* . International Journal of Biochemistry & Cell Biology 2007. **39**: p. 490-496

7. Clapham, D.E., *Calcium Signaling.* . Cell, 2007. **131**: p. 1047-1058

8. Venter, J.C. et.al., *The Sequence of the Human Genome.* Science, 2001. **291**: p. 1304-1351.

9. Casadio R., *How Many Membrane Proteins in the Human Genome?*, in *BITS Annual Meeting 2005*. 2005: Milan, IT.

10. Gribkoff, V.K. et.al., *Targeting Acute Ischemic Stroke with a Calcium-Sensitive Opener of Maxi-K Potassium Channels.* Nature Medicine 2001. **7**: p. 471-477

11. Kemp, J.A. McKernan., R.M, *NMDA Receptor Pathways as Drug targets.* Nature Neuroscience 2002. **5**: p. 1039-1042

12. Nilius, B., *TRP Channels in Disease.* Biochimica Et Biophysica Acta-Molecular Basis of Disease 2007. **1772**: p. 805-812.

13. Molokanova, M., Savchenko., A. , *Bright Future of Optical Assays for Ion Channel Drug Discovery.* Drug Discovery Today 2008. **13**: p. 14-22

14. Armijo, J.A. et.al., *Ion Channels and Epilepsy.* Current Pharmaceutical Design 2005. **11**: p. 1975-2003

15. Keating, M.T., Sanguinetti, M.C., *Molecular and Cellular Mechanisms of Cardiac Arrhythmias.* Cell, 2001. **104**: p. 569-580

16. Kunzelmann, K., Mall, M., *Pharmacotherapy of the Ion Transport Defect in Cystic Fibrosis.* Clinical and Experimental Pharmacology and Physiology 2001. **28**: p. 857-867

17. Smith, A., *Screening for Drug Discovery: The Leading Question.* Nature, 2002. **418**: p. 453-459

18. Numann, R., Negulescu, P., *High-Throughput Screening Strategies for Cardiac Ion Channels.* Trends in Cardiovascular Medicine, 2001. **11**(2): p. 54-59.

19. Poulos, J.L., Jeon TJ, Damoiseaux R, Gillespie EJ, Bradley KA, and Schmidt JJ., *Ion Channel and Toxin Measurement using a High-Throughput Lipid Membrane Platform.* Biosensors & Bioelectronics 2009. **24**: p. 1806-1810

20. Poulos, J.L., Portonovo, S., Schmidt, J., *Automatable Lipid Bilayer Formation and Ion Channel Measurement Using Sessile Droplets.* Journal of Physics: Condensed Matter, 2010. **22** 454105.

21. Wood, C., Williams, C. and Waldron, G.J., *Patch Clamping by Numbers.* Drug Discovery Today, 2004. **9**: p. 434-441

22. Cordero-Morales, J.F., Cuello, L.G., Perozo, E., *Voltage-Dependent Gating at the KcsA Selectivity Filter.* Nature Structural & Molecular Biology, 2006. **13**: p. 319-322.

23. Kirichok, Y., Navarro, B., Clapham, D.E., *Whole-Cell Patch Clamp Measurements of Spermatozoa Reveal an Alkaline-Activated Ca2+ Channel.* Nature, 2006. **439**: p. 737-740.

24. Dunlop, J., Bowlby, M., Peri, R., Vasilyev, D., and Arias, R., *High-Throughput Electrophysiology: an Emerging Paradigm for Ion Channel Screening and Physiology.* Nature Reviews Drug Discovery, 2008. **7**: p. 358-368.

25. Rast, G., Fejtl, M., *Patch Clamping hERG: Validation of an Automated Assay for Safety Studies.* Screening Trends in Drug Discovery, 2007(3/2007): p. 30-33.

26. Mathes, C., Friis, S., Finley, M., and Liu, Y., *QPatch: The Missing Link Between HTS and Ion Channel Drug Discovery.* Combinatorial Chemistry & High Throughput Screening, 2009. **12**(18): p. 78-95.

27. LoBuono, C., *New Paper Suggests QPatch Data May Benefit Automated Patch-Clamp Research*, in *Cell-Based Assay News*. 2009.

28. Mueller, P., Rudin, D.O., Tien, H.T. and Wescott, W.C., *Reconstitution of Cell Membrane Structure in Vitro and Its Transformation into an Excitable System.*

Nature, 1962. **194**: p. 979-980.

29. Montal, M., Mueller, P., *Formation of Bimolecular Membranes from Lipid Monolayers and a Study of their Electrical Properties.* Proceedings of the National Academy of Sciences of the United States of America 1972. **69**: p. 3561-3566

30. Mayer, M., Kriebel, J.K., Tosteson, M.T. and Whitesides, G.M., *Microfabricated Teflon Membranes for Low-Noise Recordings of Ion Channels in Planar Lipid Bilayers.* Biophysical Journal 2003. **85**: p. 2684-2695.

31. Miller, C., *Ion Channel Reconstitution*. 1986, New York: Plenium Press. 577.

32. Blake, S., Mayer, T., Mayer, M. and Yang, J. , *Monitoring chemical reactions by using ion-channel-forming peptides.* Chembiochem, 2006. **7**: p. 433-435.

33. Arispe, N., Rojas, E., and Pollard, H.B., *Alzhemier-Disease Amyloid Beta-Protein Forms Calcium Channels in Bilayer Membranes- Blockade by Tromethamine and Aluminum.* Proceedings of the National Academy of Sciences of the United States of America, 1993. **90**: p. 567-571.

34. Jiang, Y.X., Ruta, V., Chen, J.Y., Lee, A., and MacKinnon, R., *The Priniciple of Gating Charge Movement in a Voltage-Dependent K+ Channel.* Nature, 2003. **423**: p. 42-48.

35. Tester, D.J. et.al., *A Mechanism for Sudden Infant Death Syndrome (SIDS): Stress-Induced Leak via Ryanodine Receptors.* Heart Rhythym, 2007. **4**: p. 733-739.

36. Karginov, V.A., Nestorovich, E.M., Moayeri, M., Leppla, S.H. and Bezrukov, S.M., *Blocking Anthrax Lethal Toxin at the Protective Antigen Channel by using Structure-Inspired Drug Design.* Proceedings of the National Academy of Sciences of the United States of America 2005. **102**: p. 15075-15080.

37. Le Pioufle, B., Suzuki, H., Tabata, K.V., Noji, H. and Takeuchi, S., *Lipid Bilayer Microarray for Parallel Recording of Transmembrane Ion Currents.* Analytical Chemistry 2008. **80**: p. 328-332

38. Ide, T., Kobayashi, T., Hirano, M., *Lipid Bilayers at the Gel Interface for Single Ion Channel Recordings.* Journal of Analytical Chemistry, 2008. **80**(20): p. 7792-7795.

39. Funakoshi, K., Suzuki, H. & Takeuchi, S., *Lipid Bilayer Formation by Contacting Monolayers in a Microfluidic Device for Membrane Protein Analysis.* Analytical Chemistry, 2006. **78**: p. 8169-8174

40. Holden, M.A., Needham, D. & Bayley, H., *Functional Bionetworks from Nanoliter Water Droplets.* Journal of the American Chemical Society 2007. **129**: p. 8650-8655

41. Heron, A.J., Thompson, J.R., Mason, A.E. & Wallace, M.I., *Direct Detection of Membrane Channels from Gels using Water-in-Oil Droplet Bilayers.* Journal of the American Chemical Society 2007. **129**: p. 16042-16047

42. Baaken, G., et al., *Planar microelectrode-cavity array for high-resolution and parallel electrical recording of membrane ionic currents.* Lab on a Chip, 2008. **8**(6): p. 938-944.

43. Ide, T., T. Kobayashi, and Hirano, M., *Lipid bilayers at the gel interface for single ion channel recordings.* Analytical Chemistry, 2008. **80**(20): p. 7792-7795.

44. Le Pioufle, B., et al., *Lipid bilayer microarray for parallel recording of transmembrane ion currents.* Analytical Chemistry, 2008. **80**(1): p. 328-332.

45. Malmstadt, N., Nash, M.A., Purnell, R.F., and Schmidt, J.J., *Automated formation of lipid-bilayer membranes in a microfluidic device.* Nano Lett, 2006. **6**(9): p. 1961-5.

46. Osaki, T., et al., *Multichannel Simultaneous Measurements of Single-Molecule Translocation in alpha-Hemolysin Nanopore Array.* Analytical Chemistry, 2009. **81**(24): p. 9866-9870.

47. Poulos, J.L., Jeon TJ, Damoiseaux R, Gillespie EJ, Bradley KA, and Schmidt JJ.,, *Ion channel and toxin measurement using a high throughput lipid membrane platform.* Biosensors & Bioelectronics, 2009. **24**(6): p. 1806-1810.

48. Syeda, R., et al., *Screening Blockers Against a Potassium Channel with a Droplet Interface Bilayer Array.* Journal of the American Chemical Society, 2008. **130**(46): p. 15543-15548.

49. Thapliyal, T., J.L. Poulos, and Schmidt, J.J. *Automated lipid bilayer and ion channel measurement platform.* Biosensors and Bioelectronics. 2011 Jan 15;26(5):2651-4.

50. Tsofina, L.M., Liberman, E.A., and Babakov, A.V., *Production of Bimolecular Protein-Lipid Membranes in Aqueous Solution.* Nature, 1966. **212**(5063): p. 681-683.

51. Funakoshi, K., Suzuki, H., and Takeuchi, S., *Lipid bilayer formation by contacting monolayers in a microfluidic device for membrane protein analysis.* Anal Chem, 2006. **78**(24): p. 8169-74.

52. Holden, M.A., Needham, D., and Bayley, H. *Functional bionetworks from nanoliter water droplets.* J Am Chem Soc, 2007. **129**(27): p. 8650-5.

53. Heron, A.J., Thompson, J.R., Mason, A.E. and Wallace, M.I., *Direct detection of membrane channels from gels using water-in-oil droplet bilayers.* Journal of the American Chemical Society, 2007. **129**(51): p. 16042-16047.

54. Thompson, J.R., Heron, A.J., Santoso, Y., and Wallace, M.I., *Enhanced stability and fluidity in droplet on hydrogel bilayers for measuring membrane protein diffusion.* Nano Letters, 2007. **7**(12): p. 3875-3878.

55. Zagnoni M., Sandison M.E., Marius P., and Morgan H., *Bilayer lipid membranes from falling droplets.* Analytical and Bioanalytical Chemistry, 2009. **393**(6-7): p. 1601-1605.

56. Cleveland, P.H. and Koutz, P.J., *Nanoliter dispensing for uHTS using pin tools.* Assay and Drug Development Technologies, 2005. **3**(2): p. 213-225.

57. Hwang W.L., Chen, M., Cronin, B., Holden, M.A. and Bayley, H., *Asymmetric droplet interface bilayers.* Journal of the American Chemical Society, 2008. **130**(18): p. 5878-5879.

58. Bayley, H., et al., *Droplet interface bilayers.* Molecular Biosystems, 2008. **4** (12): p. 1191-1208.

59. Aghdaei, S., et al., *Formation of artificial lipid bilayers using droplet dielectrophoresis.* Lab on a Chip, 2008. **8**(10): p. 1617-1620.

60. Bordi, F. and Cametti, C., *Ion Transport and Electrical Conductivity in Heterogeneous Systems: The Case of Microemulsions*, in *Interfacial Dynamics*, K. Kikola, Editor. 2000, Marcel Dekker, Inc. : New York. p. 541-563.

61. Andreoli, T.E. and Tosteson, D.C., *Effect of Valinomycin on Electrical Properties of Solutions of Red Cell Lipids in Decane.* Journal of General Physiology, 1971. **57**(5): p. 526-538.

62. Poulos J.L., Portonovo, S.A., Bang, H., and Schmidt J.J., *Automatable lipid bilayer formation and ion channel measurement using sessile droplets.* J. Phys. Condens. Matter, 2010. **22**.

63. Heron, A.J., Thompson, J.R., Mason, A.E. and Wallace, M.I., *Direct Detection of Membrane Channels from Gels Using Water-in-Oil Droplet Bilayers.* J. Am. Chem. Soc., 2007. **129**(51): p. 16042–16047.

64. Leptihn S., Thompson, J.R., Ellory J. C., Tucker S. J., and Wallace M. I., *In*

Vitro Reconstitution of Eukaryotic Ion Channels using Droplet Interface Bilayers. J. Am. Chem. Soc., 2011. **133** p. 9370–9375.

65. Wonderlin W.F., Finkel, A., and French R J, *Optimizing planar lipid bilayer single-channel recordings for high resolution with rapid voltage steps.* Biophys. J., 1990. **58**: p. 289-297.

66. Mayer M., Kriebel, Jennah., K., Tosteson M.T., and Whitesides G.M., *Microfabricated Teflon Membranes for Low-Noise Recordings of Ion Channels in Planar Lipid Bilayers.* Biophysical Journal, 2003. **85**: p. 2684-2695.

67. Zagnoni M., Sandison M.E., Marius P., and Morgan H., *Bilayer lipid membranes from falling droplets.* Anal. Bioanal. Chem., 2009. **393** p. 1601-1605.

68. Poulos J L, Jeon, T.J., Damoiseaux, R., Gillespie, E.J., Bradley K.A. and Schmidt J.J., *Ion channel and toxin measurementusing a high throughput lipid membrane platform* Biosens. Bioelectron. , 2009. **24** p. 1806–10.

69. Wonderlin W.F., Finkel, A, and French R.J., *Optimizing planar lipid bilayer single-channel recordings for high resolution with rapid voltage steps.* Biophys. J., 1990. **58**: p. 289-297.

70. Van Buuren, A.R., Marrink, S.J., Berendsen, H.J.C., *A Molecular Dynamics Study of the Decane/Water Interface.* The Journal of Physical Chemistry, 1993. **97**(36): p. 9206-9212.

71. Sanguinetti, M.C. and Jurkiewicz, N.K., *Two components of cardiac delayed rectifier K+ current. Differential sensitivity to block by class III antiarrhythmic agents.* The Journal of general physiology, 1990. **96**(1): p. 195-215.

72. Curran, M.E., et al., *A molecular basis for cardiac arrhythmia: HERG mutations cause long QT syndrome.* Cell, 1995. **80**(5): p. 795-803.

73. Lagrutta, A.A., Trepakova, E.S., and Salata J.J., *The hERG channel and risk of drug-acquired cardiac arrhythmia: an overview.* Current Topics in Medicinal Chemistry, 2008. **8**(13): p. 1102-1112.

74. Hancox, J.C., McPate, M.J., and El Harchi, A., *The hERG potassium channel and hERG screening for drug-induced torsades de pointes.* Pharmacology & therapeutics, 2008. **119**(2): p. 118-132.

75. Viskin, S., *Long QT syndromes and torsade de pointes.* The Lancet, 1999. **354**(9190): p. 1625-1633.

76. Huang, X.P., Mangano, T., Hufeisen, S., Setola, V., Roth, B.L., *Identification of*

human Ether-a-go-go related gene modulators by three screening platforms in an academic drug-discovery setting. Assay and drug development technologies, 2010. **8**(6): p. 727-742.

77. Witchel, H.J., *Emerging trends in ion channel-based assays for predicting the cardiac safety of drugs.* IDrugs: the investigational drugs journal, 2010. **13**(2): p. 90.

78. Zhou, Z., et al., *Properties of HERG channels stably expressed in HEK 293 cells studied at physiological temperature.* Biophysical Journal, 1998. **74**(1): p. 230-241.

79. Schindler, H. and Quast, U., *Functional acetylcholine receptor from Torpedo marmorata in planar membranes.* Proceedings of the National Academy of Sciences, 1980. **77**(5): p. 3052.

80. Schindler, H. and Rosenbusch, J.P., *Matrix protein from Escherichia coli outer membranes forms voltage-controlled channels in lipid bilayers.* Proceedings of the National Academy of Sciences, 1978. **75**(8): p. 3751.

81. Tao, X. and MacKinnon, R., *Functional analysis of Kv1. 2 and paddle chimera Kv channels in planar lipid bilayers.* Journal of molecular biology, 2008. **382**(1): p. 24-33.

82. Leptihn S., Thompson, J.R., Ellory J. C., Tucker S. J., and Wallace M. I., *In vitro reconstitution of eukaryotic ion channels using droplet interface bilayers.* Journal of the American Chemical Society, 2011.

83. El-Arabi, A.M., Salazar, C.J., and Schmidt, J.J. *Ion channel drug potency assay with an artificial bilayer chip.* Lab Chip, 2012.

84. Brohawn, S.G., J. del Marmol, and MacKinnon, R., *Crystal Structure of the Human K2P TRAAK, a Lipid-and Mechano-Sensitive K+ Ion Channel.* Science's STKE, 2012. **335**(6067): p. 436.

85. Poulos J.L., Portonovo, S.A., Bang, H., and Schmidt J.J.,, *Automatable lipid bilayer formation and ion channel measurement using sessile droplets.* Journal of Physics: Condensed Matter, 2010. **22**: p. 454105.

86. Schein, S.J., M. Colombini, and Finkelstein, A., *Reconstitution in planar lipid bilayers of a voltage-dependent anion-selective channel obtained from paramecium mitochondria.* Journal of Membrane Biology, 1976. **30**(1): p. 99-120.

87. Golowasch, J., A. Kirkwood, and Miller, C., *Allosteric effects of Mg2+ on the gating of Ca2+-activated K+ channels from mammalian skeletal muscle.*

Journal of experimental biology, 1986. **124**(1): p. 5-13.

88. Yuan, C., et al., *Bilayer thickness modulates the conductance of the BK channel in model membranes.* Biophysical journal, 2004. **86**(6): p. 3620-3633.

89. Portonovo, S.A., Schmidt, J., *Masking apertures enabling automation and solution exchange in sessile droplet lipid bilayers.* Biomedical Microdevices, 2011: p. 1-5.

90. Chachin, M., et al., *Epinastine, a nonsedating histamine H1 receptor antagonist, has a negligible effect on HERG channel.* European journal of pharmacology, 1999. **374**(3): p. 457-460.

91. Zou, A., Curran, M.E., Keating, M.T., Sanguinetti, M.C., *Single HERG delayed rectifier K+ channels expressed in Xenopus oocytes.* American Journal of Physiology-Heart and Circulatory Physiology, 1997. **272**(3): p. H1309-H1314.

92. Wulff, H., N.A. Castle, and L.A. Pardo, *Voltage-gated potassium channels as therapeutic targets.* Nature Reviews Drug Discovery, 2009. **8**(12): p. 982-1001.

93. Diaz, G.J., et al., *The [3H] dofetilide binding assay is a predictive screening tool for hERG blockade and proarrhythmia: Comparison of intact cell and membrane preparations and effects of altering [K+]o.* Journal of pharmacological and toxicological methods, 2004. **50**(3): p. 187-199.

94. Kiehn, J., Lacerda, A.E., Wible, B., and Brown, A.M., *Molecular physiology and pharmacology of HERG: single-channel currents and block by dofetilide.* Circulation, 1996. **94**(10): p. 2572-2579.

95. Sorota S., Zhang X.S., Margulis M., Tucker K., Priestley T., *Characterization of a hERG screen using the IonWorks HT: comparison to a hERG rubidium efflux screen.* Assay and drug development technologies, 2005. **3**(1): p. 47-57.

96. Ujwal R., Cascio D., Colletier J.P., Faham S., Zhang J., Toro L., Ping P, Abramson J., *The crystal structure of mouse VDAC1 at 2.3 Ã... resolution reveals mechanistic insights into metabolite gating.* Proceedings of the National Academy of Sciences, 2008. **105**(46): p. 17742.

97. Stein, C.A. and Colombini, M., *Specific VDAC inhibitors: phosphorothioate oligonucleotides.* Journal of bioenergetics and biomembranes, 2008. **40**(3): p. 157-162.

98. Orsi, M. and Essex, J.W. *Passive permeation across lipid bilayers: a literature review*, in *Molecular simulations and biomembranes: from biophysics to function* B.P. Sansom MSP, Editor. 2010, RSC Publishing. p. 76-90.

99. Wainhaus, S., Li, C., Cheng, K., and Uss, A. *High-Throughput Screening Using Caco-2 Cell and PAMPA Systems*, in *Drug Absorption Studies*. 2008, Springer. p. 418-429.

100. Kansy, M., Senner, F., and Gubernator, K., *Physicochemical High Throughput Screening: Parallel Artificial Membrane Permeation Assay in the Description of Passive Absorption Processes.* Journal of Medicinal Chemistry, 1998. **41**(7): p. 1007-1010.

101. Faller, B., *Artificial membrane assays to assess permeability.* Current drug metabolism, 2008. **9**(9): p. 886-892.

102. Kuchel, P.W., Ralston, G.B., *Theory and Problems of Biochemistry*. Schaum's Outline. Vol. 7. 1988, New York: McGraw-Hill.

103. Ota, Y., Mishima, S., Maurice, D. M., *Endothelial permeability of the living cornea to fluorescein.* Investigative Ophthalmology, 1974. **13**: p. 945-949.

104. Li, S., Hu, P., Malmstadt, N., *Confocal imaging to quantify passive transport across biomimetic lipid membranes.* Analytical chemistry, 2010. **82**(18): p. 7766–7771.

105. Simon, M.J., Kang, W.H., Gao, S., Banta, S., and Morrison, B., *TAT Is Not Capable of Transcellular Delivery Across an Intact Endothelial Monolayer In Vitro.* Annals of Biomedical Engineering, 2011. **39**: p. 394–401.

106. *Clarke's Isolation and Identification of Drugs*, Moffat, A.C., Editor. 1986, Pharmaceutical Press. p. 421-423.

107. Di, L., et al., *High throughput artificial membrane permeability assay for blood-brain barrier.* European journal of medicinal chemistry, 2003. **38**(3): p. 223-232.